Highly Dispersed Polypropylene/Layered Double Hydroxide Nanocomposites: Preparation, Structure and their Properties

Thesis Submitted to AcSIR for the Award of the Degree of
DOCTOR OF PHILOSOPHY
in Chemical Sciences

By

BAKU NAGENDRA

Registration *No:* 10CC12A39007

Under the guidance of

Dr. E. BHOJE GOWD

CSIR-National Institute for Interdisciplinary Science and Technology (CSIR-NIIST)
Thiruvananthapuram-695 019, Kerala, India

August 2017

DECLARATION

I hereby declare that the matter embodied in the thesis entitled: **"Highly Dispersed Polypropylene/Layered Double Hydroxide Nanocomposites: Preparation, Structure and their Properties"** is the result of the investigations carried out by me at the Materials Science and Technology Division, CSIR-National Institute for Interdisciplinary Science and Technology (CSIR-NIIST), Thiruvananthapuram, under the supervision of Dr. E. Bhoje Gowd and the same has not been submitted elsewhere for any other degree.

In keeping with the general practice of reporting scientific observations, due acknowledgments were made wherever the work described is based on the findings of other investigators.

Baku Nagendra

राष्ट्रीय अंतर्विषयी विज्ञान तथा प्रौद्योगिकी संस्थान
NATIONAL INSTITUTE FOR INTERDISCIPLINARY SCIENCE & TECHNOLOGY

वैज्ञानिक तथा औद्योगिक अनुसंधान परिषद्
Council of Scientific & Industrial Research

इंडस्ट्रियल इस्टेट पि. ओ, पाप्पनंकोड, तिरुवनंतपुरम- 695 019
Industrial Estate P.O., Thiruvananthapuram - 695 019

Dr. E. BHOJE GOWD
Senior Scientist
Materials Science & Technology Division

+91471-2515474
+919048427911

CERTIFICATE

This is to certify that the work incorporated in this Ph.D. thesis entitled **"Highly Dispersed Polypropylene/Layered Double Hydroxide Nanocomposites: Preparation, Structure and their Properties"** *submitted by* ***Mr. Baku Nagendra*** *to Academy of Scientific and Innovative Research (AcSIR), in fulfillment of the requirements for the award of the* ***Degree of Doctor of Philosophy in Chemical Sciences****, embodies original research work under my supervision and guidance at the Materials Science and Technology Division of the CSIR-National Institute for Interdisciplinary Science and Technology (CSIR-NIIST), Thiruvananthapuram. I further certify that this work has not been submitted to any other University or Institution in part or full for the award of any degree or diploma. Research material obtained from other sources has been duly acknowledged in the thesis. Any text, illustration, table, etc., used in the thesis from other sources, have been duly cited and acknowledged.*

Dr. E. Bhoje Gowd
(Thesis Supervisor)

Thiruvananthapuram
August 2017

ACKNOWLEDGEMENTS

First, I express my heartfelt thanks to Dr. E. Bhoje Gowd, my research supervisor. He has been very motivating, encouraging, and enlightening throughout my doctoral research. His patience, flexibility, genuine caring and concern, and the faith in me helped me to grow in my life. Your advice on both research as well as on my personal life have been invaluable.

I am grateful to Dr. A. Ajayaghosh, Director, NIIST, and former Directors Dr. Suresh Das and Dr. Gangan Pratap for providing the necessary facilities and infrastructure to carry out this investigation.

My sincere thanks also goes to Dr. R. Luxmi Varma and Dr. Mangalam S. Nair, present and former AcSIR coordinators and Dr. Narayanan Unni, Dr. U. S. Hareesh, and Dr. Saju Pillai, DAC members for their insightful comments and suggestions.

My gratitude extends to Dr. Andreas Leuteritz, Dr. Uta Reuter and Dr. Petr Formanek at IPF-Dresden, Germany for the MCC and TEM analysis, Dr. T. Narasimhaswamy, CSIR-CLRI for POM measurement, and Prof. Tushar Jana, University of Hyderabad for DMA measurements.

I extend my thanks to Mr. Kiran M, Mr. Robert Philip, Ms. Lucy Paul, Mr. Aswin M, Mr. Vishnu, Dr. George T. M for their timely help in various characterizations.

I'd like to thank Mr. Shaiju P and Mrs. Angel Mary Joseph for their tremendous help and friendship. I couldn't have completed all the required work without you both. You shall always be remembered with a smiling face and a warm and friendly heart. Also, I thank the

Mr. Robbinson C. Jose who played a major role in making me understand many things in the initial stage of Ph.D.

I want to thank present and past group members Dr. S. Nagarajan, Ms. Rejisha, Ms. Rincy, Ms. Deepthi Krishnan, Ms. Sijla Rosely C V, Mr. Sivaprasad, Ms. Praveena, Ms. Jerin K. Pancrecious, and Mr. Amal Raj R. B. for sharing their knowledge and for having a good time in the lab. Also, I thank Dr. J.P. Deepa, Dr. Lekshmi V., Mr. Renjith S., Ms. Neethu K.S, Ms. Reshma L.R, Ms. Molji C., Mr. Manikanda and Ms. Asha Susan Chacko for all the cheerful moments in the lab.

A big "Thank you!" also goes out to all my S7 members, Dr. R. Ramakrishnan, Dr. G. Jaggaiah Naidu, Mr. A. Aashish, Mr. S. Simbu, Mr. S. Arun, Mr. T. Arun, and Mr. Anji Reddy, who made my days at NIIST really enjoyable. The cricket matches, the trips that we enjoyed together, and the daily fun we had made me feel like I am in my native place.

No acknowledgments would be complete without giving thanks to my parents; they've taught me the value of hard work and self-respect. Mom, especially, was a great role model of strength and character. Both have always expressed how proud they are of me. I remember my grandparents, whose role in my life was, and remains, immense. I must acknowledge with tremendous and deep thanks to my partner Gowthami. She has taken care of whatever needed without complaining, so that I could focus on completing my research. Thank you with all my heart and soul.

This thesis would not have been possible without funding from CSIR.

Finally, I thank God, for letting me through all the difficulties.

CONTENTS

NOMENCLATURE

LDH	Layered double hydroxides
O-LDH	Surfactant modified layered double hydroxides
SDBS	Sodium dodecylbenzenesulfonate
SDS	Sodium dodecylsulfate
HMT	Hexamethylenetetramine
SF	Surfactant-free
LM	Layered Materials
BN	Boron nitride
MoS_2	Molybdenum disulfide
MWCNT	Multi-walled carbon nanotubes
AMOST	Aqueous miscible organic solvent treatment
DMF	Dimethylformamide
iPP	Isotactic polypropylene
Đ	Polydispersity index
PNC	Polymer nanocomposites
NCs	Nanocomposites
NA	Nucleating agents
$t_{1/2}$	Crystallization half-time
T_{mc}	Melt-crystallization temperature
T_m	Melting temperature
K	Overall crystallization rate

N	Nucleation density
G	Spherulite growth rate
n	Avrami constant
X_c	Degree of crystallinity
L	Long period
l_a	Amorphous thickness
l_c	Lamellar thickness
ΔH_m	Melting enthalpy
E'	Storage modulus
E''	Loss modulus
tan δ	Loss factor
T_g	Glass transition temperature
$T_{0.5}$	50% Weight loss temperature
HRR	Heat release rate
THR	Total heat released
HRC	Heat release capacity
t_{ig}	Ignition time
LOI	Limited oxygen index
WAXS	Wide-angle X-ray Scattering
SAXS	Small-angle X-ray Scattering
FTIR	Fourier Transform Infrared Spectroscopy
SEM	Scanning Electron Microscopy

TEM	Transmission Electron Microscopy
EDS	Energy dispersive spectrometer
AFM	Atomic force microscopy
POM	Polarized optical microscopy
DSC	Differential Scanning Calorimetry
BET	Brunauer, Emmet and Teller
TGA	Thermogravimetric Analysis
DMA	Dynamic Mechanical Analysis
MCC	Microscale combustion calorimetry
CC	Cone calorimeter
UL-94	Underwriters Laboratories-94

PREFACE

The physical characteristics of polymers are largely improved after the incorporation of the rigid inorganic fillers (graphene, carbon nanotubes, clay, layered double hydroxide (LDH), silica, glass fiber, etc.). It has long been known that the few basic properties including mechanical, gas barrier, flame-retardancy, nucleation and thermal stability are significantly improved, which make these hybrid nanocomposites applicable in numerous material applications. Achieving superior properties of the polymer by reinforced inorganic fillers are expected to be dependent on complete exfoliation and the interaction between the fillers and polymer. Nevertheless, the hydrophobic polymer matrix thermodynamically and kinetically obstructs the distribution of the inorganic additives into it, and always results in aggregated nanocomposites. In 1989, the Toyota research group (Japan), pioneers in the field of nanocomposites, accomplished intercalated nanocomposites which offered the substantial improvement in modulus, without loss in impact resistance. However, preparation methods of exfoliated nanocomposites with surfactant-free LDH fillers remain the key challenge in order to obtain the full potential of properties enhancement. Therefore, it is necessary to develop new approaches to achieve exfoliated polymer nanocomposites.

The following general questions arise while understanding the relationship between structure, morphology, and physical characteristics of the hybrid nanocomposites. What are the thermodynamic driving forces that direct intercalation/exfoliation of LDH? How would lateral dimensions of the fillers affect the

properties of the resultant polymer nanocomposites? Do the intralayer metal constituents of LDH modify the composite's properties? We tried to address some of these questions with the support of experimental evidence in this thesis. In this investigation, we have chosen the surfactant-free synthetic clay (LDH) as reinforcing inorganic filler. Main advantages of LDH over the natural clay are the greater flexibility to tailor the lateral sizes, layer thickness, intralayer metal constituents, gallery anions, etc. The thesis comprises of six chapters, of which Chapter 1 is the introduction to nanocomposites, LDH and the strategies to obtain highly dispersed polymer nanocomposites.

In Chapter 2, a novel solvent-exchange approach has been developed to efficiently exfoliate the hydrophilic LDH in non-polar polypropylene. Larger-sized two-dimensional (2D)-LDH nanoparticles (~3–4 μm) were prepared from the gel form of Mg–Al LDH, and the smaller-sized 2D-nanoparticles (~50–200 nm) were prepared by sonication of as-synthesized LDH particles. The influence of lateral size and the concentration of LDH nanoparticles on the polymer properties were investigated. Incorporation of low loadings of sonicated LDH particles (e.g., 1–2.5 wt %) showed a substantial effect on thermal stability, spherulite size, crystallinity, and crystallization half-time and lamellar morphology of iPP compared to that of nanocomposites with larger LDH particles with same loadings. The better nucleation ability of iPP in the presence of sonicated LDH can be attributed to the high surface area of LDH nanoparticles along with its better dispersibility within the polymer matrix.

The prime focus of chapter 3 is the preparation of three different-sized 2D-LDH (micro, nano, and nanodots), and study their effect on various physical characteristics

of the host iPP matrix. A new method was developed to prepare nanodot-LDH by treating the as-prepared LDH with dilute acid. This method provided directly delaminated LDH sheets with lateral dimensions as low as 10-30 nm and featured a thickness of ~1 nm with the same chemical composition. The incorporation of nanodot LDH showed a remarkable improvement in the polymer properties with only 1 wt % loading. The uniformly dispersed LDH particles have a significant effect on the nucleation ability, thermal stability and mechanical properties of iPP. The nucleation ability of iPP in the presence of nanodot LDH is the best compared to other iPP nanocomposites reported using LDH as fillers in the literature. Furthermore, the microstructure of the iPP nanocomposites was systematically investigated at multiple length scales in the presence of different-sized LDH, which is a key to understand the polymer properties.

Chapter 4 deals with the influence of the LDH intralayer metal constituents on the various properties of iPP/LDH nanocomposites. For that purpose, two-metal LDH and three-metal LDH were synthesized and delaminated using the procedures developed in chapter 2. The sonicated LDH nanoparticles showed a significant increase in the crystallization rate of iPP. However, not much difference in the crystallization rate of iPP was observed in the presence of different types of LDH. The dynamic mechanical analysis results indicated that the storage modulus of iPP was increased significantly with the addition of LDH. The incorporation of different types of LDH showed no influence on the storage modulus of iPP. However, considerable differences were observed in the flame retardancy and thermal stability of iPP with the type of LDH used for the preparation of nanocomposites. Preliminary studies on the flame retardant

properties of iPP/LDH nanocomposites using the microscale combustion calorimetry showed that the HRR was reduced by 39% in iPP/Co-Zn-Al LDH nanocomposite containing 6 wt% LDH, which is higher than that of two-metal-LDH containing nanocomposites iPP/Co-Al LDH (24%) and iPP/Zn-Al LDH (31%). These results demonstrated that the nanocomposites prepared using three-metal LDH showed better thermal and flame retardant properties compared to that of the nanocomposites prepared using two-metal LDH. This difference might be due to the better char formation capability of three-metal LDH compared to that of two-metal LDH.

In chapter 5, LDH, CNT and their hybrid CNT-LDH fillers were incorporated with iPP using a solution blending method to prepare highly dispersed polymer nanocomposites. Through a systematic examination, we found that the CNT dispersed nanocomposites exhibited superior nucleation and temperature-dependent viscoelastic behavior, over the LDH and CNT-LDH filled nanocomposites. Unlike those two physical characteristics (nucleation and dynamic mechanical performance), the hierarchical CNT-LDH filled polymer nanocomposites showed improved flame-retardancy and thermal degradation behavior, even with a small fraction of the filler. Upon addition of the 2 wt% CNT-LDH filler, thermal degradation stability (44 °C) and flame-retardancy (59%) of the iPP has been improved considerably compared to the CNT and LDH reinforced nanocomposites. The LOI values also enhanced significantly, and the maximum improvement was observed for the 10 wt% iPP/CNT-LDH nanocomposites (~26 %). The synergistic effect of CNT and LDH helps in improving the thermal stability and flame-retardancy of the hierarchical iPP/CNT-LDH nanocomposites. The formed hierarchical CNT-LDH jammed networks in polymer matrix act as an effective catalyst

to generate larger amounts of residual carbon char, and it forms a protecting layer over the surface. This protecting layer helps in delaying the heat and flammable gas release and thus makes the iPP/CNT-LDH nanocomposite a potential flame-retardant and thermally stable material.

The sixth chapter summarizes the thesis work, highlighting the influence of lateral size and intralayer metal constituents of LDH on the properties of polypropylene. LDH nanodots were found to exhibit superior properties compared to that of micro-sized and nano-sized LDH. Three-metal LDH showed better flame retardant properties compared to that of the two-metal LDH. Hybrid materials of CNT and LDH showed promising results on the flame retardancy of the polypropylene.

Chapter-1

Introduction: Hybrid Polymer Nanocomposites

1.1. Introduction

IUPAC defines a composite as a material containing multiple phases in which at least one of them is a continuous phase. When the different components (filler and matrix) are mixed, the components will retain their individual identities, and both will directly influence the final properties of the composite.[1, 2] A "nanocomposite" is a composite material with the key difference that at least one of the dimensions of any of the phases will be in the nanometers length scale.[1, 3] These novel materials promise new applications by exploiting the unique synergisms between constituents that only occur when the length scale of the morphology and the critical length associated with the fundamental physics of a given property coincide. We can consider nanoscience and nanotechnology as a revolutionary science in the multidisciplinary areas combining chemistry, physics, material science, electronics and bio sciences.[2, 4-7]

Polymer nanocomposites (PNC), comprising a polymer, which is the major part and reinforcing (rigid phase) material of nanometer range has drawn much attention from both academia and industry, over the few years. In PNC, the combination of two separate phases gives a novel multifunctional polymeric material which retains the inherent advantages of the polymer such as the processability with the added advantages of the rigid inorganic fillers such as enhanced thermal and mechanical stability, flame retardancy, etc.[1, 5, 7-11] PNCs represent an alternative to conventional filled polymers or polymer blends.

As the 21st century unfolds, the development in science and nanotechnology allowed researchers to better understand the structure-property relationship in polymeric composite materials.[3, 5, 12] Commercial polymer nanocomposites were first prepared by Toyota research group by the solution polymerization of caprolactam in the clay galleries. Later on, this product was marketed by UBE Industries and Bayer. Currently, these nylon 6-based nanocomposites are used to make belts for Toyota car engines and also for the production of packaging films.[4, 13]

Different Fillers used in Polymer Nanocomposites: Depending on the dimensions of the particles are in the nanometer range, particles can be categorized into three types. When all the dimensions are in the order of nanometers, they are called zero dimensional (0D) nanoparticles, such as fullerene nanoparticles, nanoclusters, etc. If two dimensions of the particles are in the nanometer range and the third one is larger, it is called one-dimensional (1D) nanotubes or nanowhiskers, which usually form an elongated structure, for example, carbon nanotubes and carbon nanofibers.[7, 14, 15] On the other hand, if only one dimension is in the order of nanometer range, it is called two-dimensional (2D) nanomaterials.[16, 17] In this case the particles are present in the form of sheets of few nanometer thick to hundreds to thousands nanometer long, for example, graphene.[16, 18] All these types of inorganic fillers have been utilized by researchers and the various thermal, mechanical and other impacts of these on the polymer properties were understood.[5, 10]

Among the nanofillers, the 2D nanofillers stands as a peculiar one, which can alter the polymer properties even when added in very small quantity.[10, 14, 17, 18] In these materials, the thicknesses of the sheets will be in the nanometer length scale, whereas the lateral dimensions will vary from nanometers to micrometers. When these nanometer thick sheets are uniformly dispersed into a polymer matrix, it is found that the enhanced surface area of these materials drastically alters the polymer physical properties.[10, 17] Graphene is the most studied 2D material, containing a one atom thick layer of carbon atoms, which when incorporated into a polymer, increases its mechanical and thermal stability along with the increase in thermal and electrical conductivity.[16, 18] Some other examples of 2D materials are boron nitride (BN),

molybdenum disulfide (MoS_2), MXene, layered silicates, layered double hydroxides, etc.[6, 17-23]

Layered Double Hydroxide (LDH), synthetic clay, in its bulk form is not a 2D material, since this contains stacked lamellas of hundreds of layers, but can be converted to 2D material of ~1 nm thickness by different delamination approaches.[24-26] LDH has received considerable attention as multifunctional filler in the polymer industries in the last few decades, especially due to the flexibility to tune the lateral sizes, layer thickness, intralayer metal composition ratio, gallery anions, etc.[6, 27-29]

Large varieties of polymers such as polyolefins [polyethylene, polypropylene, poly(ethylene-*co*-vinyl acetate) (EVA), ethylene propylene(dienemethylene) (EPDM) and poly (1-butene), vinyl polymers [poly(methyl methacrylate) (PMMA), poly(styrene) (PS), poly(ethylene vinyl alcohol) (PVA), poly(vinylidene fluoride) (PVDF)], condensation (step) polymers like [nylon-6, poly(1-caprolactone) (PCL), poly(ethylene terephthalate), polyurethane (PU), epoxy polymer resins (EPR), polysulfone (PS), poly(lactic acid)] and specialty polymers [N-heterocyclic polymers like polypyrrole (PPY), polyaniline (PANI)] have been used for the preparation of polymer nanocomposites with different LDH.[6, 25, 30, 31] However, LDH is suitable only for few categories of the polymers including polyolefins and some of the vinyl polymers, which can significantly enhance the overall performance.[32-35] On the other hand, for some other polymers, for example, polyesters and polyamides, the addition of LDH causes no effect or sometimes even negative effects on the polymer properties like thermal stability, crystallization etc.[31, 36-38]

1.2. Isotactic Polypropylene (iPP)

Polypropylene was discovered in the year 1950.[39, 40] Structurally, PP is a vinyl polymer, with a repeating unit of $-[CH_2\text{-}CH(CH_3)]_n-$, and it is prepared by the polymerization of high-purity propylene gas in the presence of a Ziegler-Natta catalyst. By controlling the stereoregularity, it is feasible to generate atactic, syndiotactic and isotactic PP. Particularly, a lot of work has been done with the iPP in the field of material science, and it was established like a commodity thermoplastic material. The commercial importance of iPP is due to many aspects like their physical characteristics,

low material cost, high production rate, availability, etc. The general physical characteristics of iPP are tabulated in (Table 1.1).[41]

Table 1.1: Physical characteristics of polypropylene (isotactic).[41-43]

S.No	Physical characteristics	Value
1.	Glass transition temperature (T_g)	-10 to 10 °C
2.	Melting temperature (T_m)	160-175 °C
3.	Softening point	140-160 °C
4.	Melt crystallization temperature (T_{mc})	105-120 °C
5.	Density	0.89-0.92 g/cm^3
6.	Young's Modulus	1300 -1800 N/mm^2 (at room temperature)
7.	Melt Flow Index (MFI)	3-35 g/10 min.
8.	Decomposition temperature	350-450 °C
9.	Limiting oxygen index (LOI)	16-17.5 (%)
10.	Heat of combustion	44 (kJ/g)
11.	Moisture regain	<0.1 (%)

The commercial importance of iPP arises from its solid-state organization or structural feature which makes superior physical characteristics. It is important to note that iPP exhibits complex polymorphic behavior with five different forms: α (monoclinic), β (trigonal), γ (orthorhombic), δ-phase and smectic phase.[43] These forms are extremely sensitive to the external factors such as processing conditions and foreign additives. Different crystalline phases of iPP lead to dissimilar mechanical and optical properties. The α-phase is the best known and most stable form of the commercial grades of iPP. It is found mostly in melt crystallized specimens, especially with the addition of α nucleating agents (NA).[42] Even though iPP has widespread applications, the limited impact strength, low T_g (-10 to 10 °C), poor crystallization rate and high flammability nature reduces its broader utilization as an engineering plastic.[11, 14, 44, 45] To improve certain physical properties and to meet the requirements of specific

applications a wide number of nanofillers have been incorporated into the matrix of iPP.[7, 11, 14]

1.3. Layered Double Hydroxides (LDH)

LDH are clay like multilayered materials that exhibit unique physical and chemical characteristics, similar to those of the natural clay minerals. They usually comprise of inorganic lamellar compounds with the high capacity for anion intercalation. It has been known for the last 150 years, since the discovery of the mineral hydrotalcite.[46-48] It was synthesized 100 years later by Feitknechtin et al. for the first time and they determined the stoichiometry of hydrotalcite $[Mg_6Al_2(OH)_2]CO_3{\cdot}4H_2O$.[49-51] Later, Allmann et al. explained the structural features of LDH by employing single crystal X-ray diffraction technique. [48, 52]

Structure of Layered Double Hydroxides

The basic layered structure of LDH is comparable to that of the brucite $[Mg(OH)_2]$ structure. In a brucite layer, each magnesium ion is octahedrally surrounded by six hydroxide ions. These octahedral units form infinite layers by edge-sharing with the hydroxide ions sitting perpendicular to the plane to form the two-dimensional layer. The structure of hydrotalcite was obtained by the substitution of a fraction of divalent cations in a brucite structure by trivalent cations.

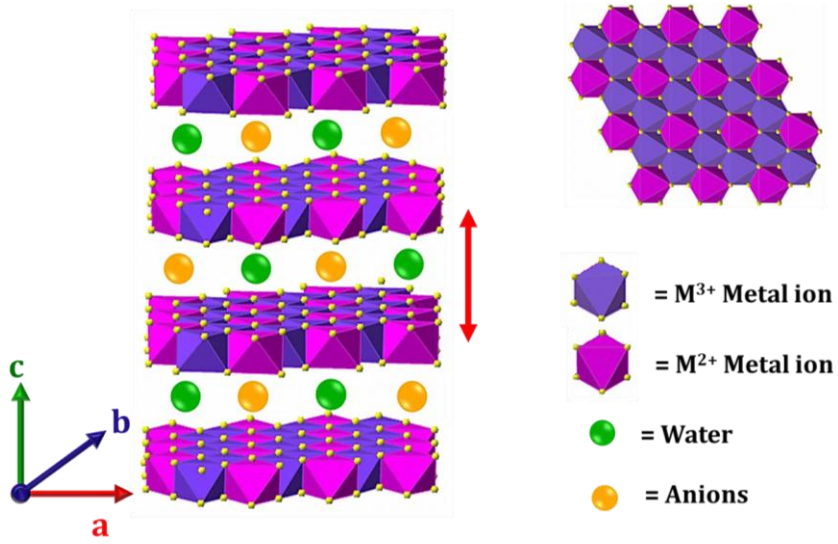

Figure 1.1. Three directional structure of layered double hydroxide (LDH).

The substitution is made in such a way that the layers attain a net positive charge, which is compensated by the intercalated anions and water molecules between the layers in the gallery space. The LDH structure results from the stacking of brucite-like layers containing extra positive charge due to the partial substitution of M^{2+} by M^{3+}. This excess positive charge is balanced by weakly bounded exchangeable anions, which is located in the interlayer region through hydrogen bonding along with the water molecules.[25, 26, 53, 54]

LDH general formula: $[M^{(II)}_{1-x} M^{(III)}_{x}(OH)_2]^{x+}[A^{n-}_{x/n}]^{x-}.mH_2O$ [25, 53]

The above-mentioned formula describes the chemical composition of LDH; where M(II) and M(III), represents the divalent (Co^{2+}, Zn^{2+}, Mg^{2+}, Ni^{2+}, etc.,) and trivalent (Ga^{3+}, Fe^{3+}, Al^{3+}, etc.,) metal ions, respectively. "A" is the interlayer anion with charge n, x is the fraction of the divalent cations to trivalent cations and m is the number of water molecules. The value of x lies in the range 0.2 - 0.35, and if the values are outside this range, that will give compounds with different structures. The identity and the relative proportions of the di- and trivalent cations with ionic radius in the range of 0.50 to 0.74 Å atomic radius, as well as the interlayer ions can be varied, which can give a large variety of materials. The M^{2+} ions occupy alternate layers of octahedral sites while OH^- ions are hexagonally close packed in which the metal ions are coordinated to OH^- ions to form indefinite 2D layers. The net positive charge present on the basal hydroxide layers is compensated by the intercalation of A^{n-} ions into the interlayer along with water molecules. The basal spacing in brucite structure is about 0.48 nm, whereas the LDH exhibits basal spacing about 0.77 nm, attributed to the existence of the anions and water molecules in the gallery space.[24, 53]

1.4. Strategies for the Preparation of LDH

For obtaining the LDH, several key parameters must be considered, e.g., the cation substitution ratios of M^{2+} by M^{3+}, the atomic radius of the cations (0.5-0.76 Å), nature of cation and gallery anion, solution pH, etc. In addition to this, the following factors such as concentration, base strength (strong or weak base), the rate of addition of one solution over the other, stirring rate, final pH of the resulting suspension, pH during the

addition of base, reaction time and temperature, etc. have to be controlled. All these parameters influence the lateral size, symmetry, layer thickness, crystallinity, and gallery anion of the final LDH.[27, 47, 53]

Numerous strategies have been developed for the synthesis of LDH in the past two decades. Those approaches are majorly divided into two classifications: direct and indirect synthesis.[27, 47]

1.4.1. Direct Synthesis: This includes coprecipitation or salt-base approach, hydrothermal synthesis, induced hydrolysis, sol-gel, salt-oxide, and electrochemical preparation.[27, 47, 55]

Coprecipitation Method: The LDH preparation by coprecipitation method at constant pH is the most commonly used approach, which can provide phase pure LDH in acceptable product yields. In this approach, mixed metal salts containing both M^{2+} and M^{3+} are firstly taken in a reaction vessel. The basic (NaOH or KOH or NH_3) solution is continuously added to keep the pH constant (pH=10-12). Frequently, the coprecipitation method is carried out at room temperature, in the presence of strong bases such as NaOH, KOH or NH_3. On the other hand, in the presence of weak bases (such as urea, HMT), the reaction is performed at higher temperatures (60-125 °C). Even though it is a slow hydrolysis process, it can produce highly crystalline, phase pure LDH compared to strong bases.

Hydrothermal Synthesis Method: Hydrothermal method usually involves heating the sample in gold or silver capsule or stainless steel under the high pressure ranging from 10 to 150 MPa at temperatures above 120°C. The high pressure and temperature treatment results in the formation of highly crystalline and uniform particle sized LDH.

Sol-Gel Method: The sol-gel method is based on the hydrolysis and condensation of the molecular precursors. This method involves the hydrolysis of the desired metal precursors such as inorganic salts or metal organic compounds in the aqueous solution or organic solvent at ambient conditions to produce polymeric or particulate sol. Insoluble salts are hydrolyzed either by supplying heat to the sol mixture or by using an appropriate solvent. An appropriate amount of acid or base can be added to the sol mixture during hydrolysis to facilitate precipitation.

1.4.2. Indirect Synthesis: This method involves simple anion exchange, reconstitution of calcined material, and anion exchange using double phase with salt formation within surfactants, etc.[47, 55]

Regeneration Method: This method is based on the "memory effect" of some of the LDH. The LDH with carbonate anion is the most often used precursor, due to its behavior during calcination. Calcination is performed at the proper temperature to break the hydroxyl groups partially from lamellae and convert interlamellar anion into volatile, forming a double oxyhydroxide. After calcination, a solution containing the anion of interest is added, regenerating the LDH by hydrolysis with the new intercalated anion. Generally, pH is raised during the regeneration process, so it must be corrected to avoid hydroxyl groups occupying the interlayer space.

1.4.3. Surfactant Modification of LDH: LDH is hydrophilic in nature and is considered unsuitable for hosting non-polar organic macromolecules without prior surface treatment. Interlayer anions can be exchanged with organic anions to obtain organophilic LDH, which can expand interlayer spacing and more readily produces a polymer/LDH nanocomposite by intercalation or exfoliation.[6] Traditional anion exchange approach was used for LDH surface modification. According to Leroux et al. the anion exchange capacity (AEC) depends on many parameters including metallic cation ratio, molecular mass, size of the anion, etc.[23] Therefore, it is possible to intercalate a wide variety of anionic surfactants with different sizes. The sodium based surfactants such as acetate, lactate, dodecyl sulfate, sodium dodecyl benzene sulphonate and oleate are traditionally used to expand the *d*-spacing from 0.75 to 3.5 nm. Generally, the LDH-nitrate form is commonly used for the ion exchange reactions; however, it is more difficult in the case of LDH-carbonate form.[6, 24, 25]

1.4.4. Structure and Morphology of LDH

The LDH structure formation, relative crystallinity, surfactant modification as well as basal plane distances can be examined by X-ray powder diffraction (XRD).[53] XRD shows 00n order peaks related to the lamellae stacking sequence. Other than the 00n peaks, higher 2θ reflections are considered to be the non-harmonic related to the in

plane structure. For LDH, diffraction peak indexing is done by comparing with hydrotalcite diffraction pattern. To determine LDH gallery anionic species orientation, interlayer baseline spacing values from XRD data are compared with anion sizes. Interlayer distances can be calculated from the 2θ values by Bragg's equation ($n\lambda = 2d\sin\theta$).[24] The presence of LDH gallery anion species can be easily identified with the help of FTIR. Generally, inorganic anion species can be found in the fingerprint region (500-1500 cm^{-1}), whereas the organic anions exhibit peaks in both fingerprint and functional group regions. A common broadband can be found in all the LDH in the region 3800-2500 cm^{-1}, which is the characteristic peak of O-H stretching of hydroxyl groups in the lamellae structure and water molecules in the gallery.[24] The morphological features of LDH such as size, shape and thickness can be varied with respect to the preparation method and chemical composition, and those changes can easily understand by microscopic techniques such as scanning electron microscopy (SEM), transmission electron microscopy (TEM) and atomic force microscopy (AFM).[6, 24]

1.5. General Delamination Approaches for Layered Materials (LM) in Liquid Phase

Liquid phase delamination or exfoliation of layered materials is an interesting route for producing thin platelets with a thickness of a few atomic layers.[16, 17, 24] The LM consist of two-dimensional (2D) nanosheets with strong covalent and metallic bindings within the individual layer and weak out of plane (c-axis) noncovalent interaction forces.[17, 56] Such LM can be converted to thin nanomaterial by shearing or mechanical agitation method, and the process is called "exfoliation" or "delamination".[17, 18, 57, 58] The exfoliated nanomaterials exhibit extraordinary physical and chemical properties, which include accessible surface area, tunable electronic band gap, photo physical properties, etc., unlike their bulk precursors.[16-18, 20] The synthesis of nanosized 2D-LM can be classified into two categories: (1) bottom-up and (2) top-down.[6, 17] Among these two methods, the "top-down" approach is the widely used one since it is simple and scalable. Therefore, it is important to discuss general delamination approaches of LMs by the top-down approach in detail. The top-down approach is again subdivided as (a)

intercalation (b) ion exchange and (c) direct sonication approaches, as shown in Figure 1.2.[17, 56]

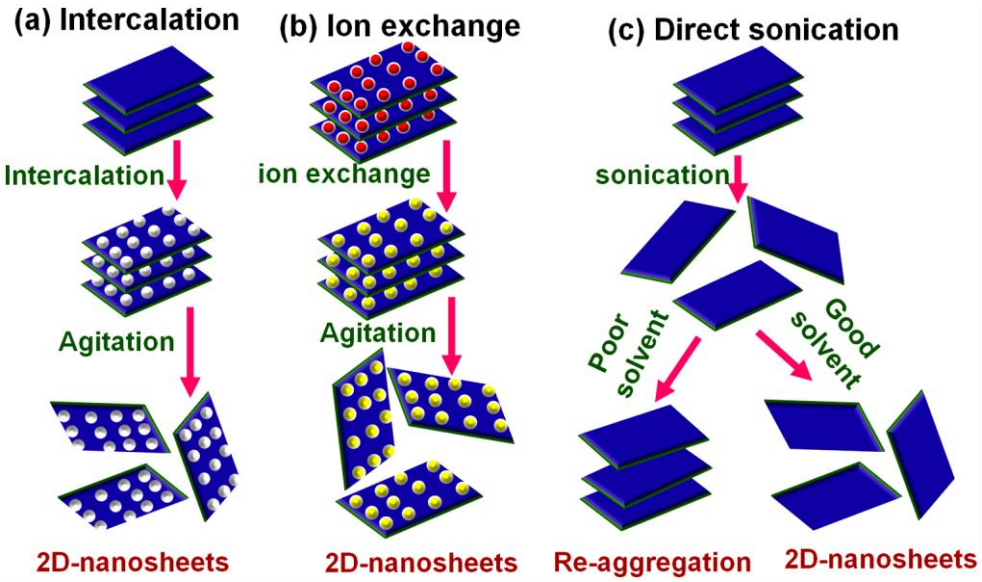

Figure 1.2. Schematic representation of the liquid phase exfoliation of various layered materials (a) intercalation (b) ion exchange (c) direct sonication assisted delamination.

(a) Intercalation: Ions are intercalated between the layers in a liquid environment by swelling the crystal and weakening the interlayer attraction. Then, agitation is applied, (such as shear, ultrasonication, or thermal) which can completely separate the layers, resulting in an exfoliated dispersion.

(b) Ion Exchange: Some layered compounds contain ions between the layers to balance the surface charge on the layers. These ions (red spheres in Figure 1.2b) can be exchanged in a liquid environment with other, often larger ions (yellow spheres in Figure 1.2). As in intercalation, agitation results in an exfoliated dispersion.

(c) Sonication Assisted Exfoliation: The layered material is sonicated in an appropriate solvent, resulting in delaminated nanosheets. The "good" solvents are those with appropriate surface energy, where the exfoliated nanosheets are stabilized for the long duration. Reaggregation and sedimentation will occur rapidly, in the presence of "bad" solvents. Therefore, the solvent selection is one of the key aspects to stabilize the 2D nanosheets in the liquid medium.

1.6. Liquid Phase Exfoliation and Exfoliation Mechanism of LDH

The process of LDH delamination or exfoliation method comes under the ion exchange approach, as we discussed in the general LM delamination approaches.[6, 25] Exfoliation of LDH is an interesting route for generating positively charged thin platelets with the thickness of a few atomic layers, which can be used as multifunctional additives for polymers. However, achieving 2D-LDH nanosheets is extremely difficult unlike any of the other lamellar layered materials. This is due to the high charge density and the high anion content, which results in strong interlayer electrostatic interactions between the sheets. In addition, the hydrophilic nature and extensive interlamellar H-bonding networks also lead to a tight stacking of the lamellae. Therefore, to successfully delaminate LDH into nanosheets, extensive research has been conducted in the past two decades.[6, 17, 24, 25, 59] The exfoliation of the LDH is classified into three generations on the basis of the delamination environment as discussed below.

Generation-I (From 1999 to 2004): For the first time complete delamination of LDH was reported by Adachi-Pagano et al. in 1999.[60] In their study, they demonstrated the total delamination of the Zn–Al LDH-DDS in butanol solvent. The prime requirement of LDH surfactant modification is to introduce aliphatic tails of DDS which simultaneously enlarges interlayer distance and weakens the brucite interlayer forces. Mechanical agitation of such modified LDH in a highly polar solvent leads to the delamination of LDH. The detailed exfoliation mechanism will be discussed in the later section. Later many reports have appeared with other solvents including water, methanol, ethanol, propanol, octanol, etc.[6]

Generation-II (From 2004 to 2012): In 2005, Li et al. developed a single step approach for the liquid phase exfoliation of the LDH.[61] In their study Mg-Al LDH-NO_3 was used instead of surfactant intercalated LDH and they successfully exfoliated LDH in formamide solvent for the first time. Subsequently, single step approach has been expanded to many other LDH, with different metal constituents (divalent or trivalent) and gallery inorganic anions. Liu et al. studied the delamination of Co-Al LDH intercalated with a variety of inorganic gallery anions including NO_3^-, Cl^-, ClO_4^-, CO_3^{2-}, SO_4^{2-}, PO_4^{3-}, and they found that most of this intercalated LDH exhibited a delamination

behavior in formamide.[24] Among them, LDH in the nitrate form was found to have the best delamination yields.[6, 24]

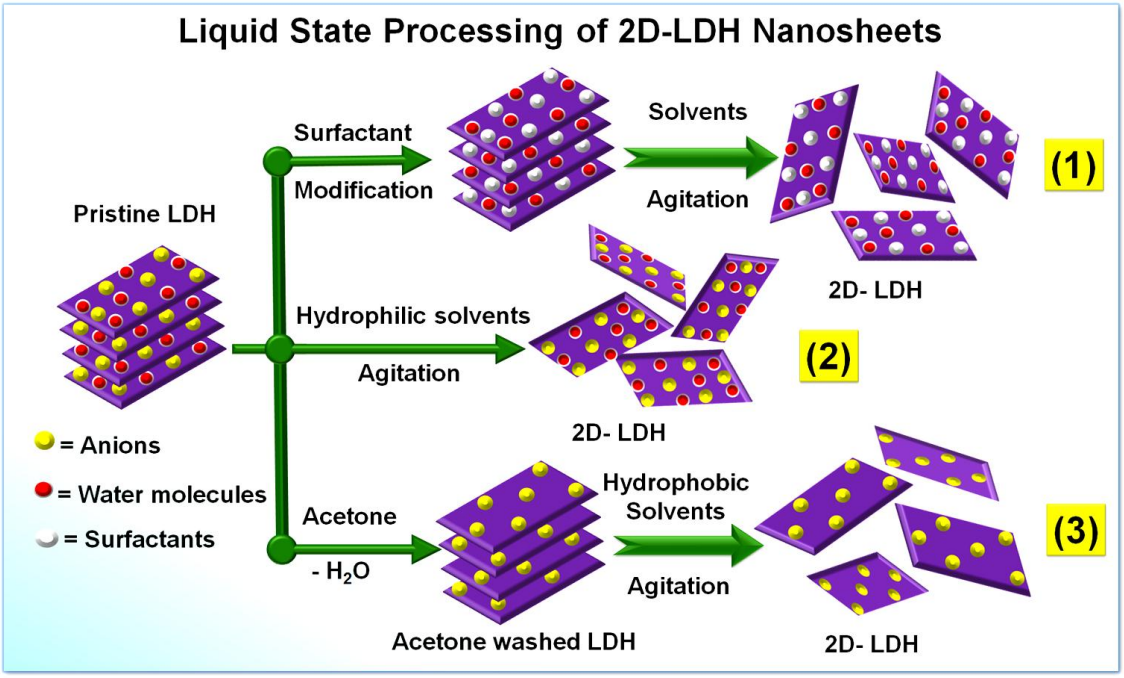

Figure 1.3. Schematic illustration of different LDH delamination processes.

Generation-III (From 2012 to till date): The first two generations were mainly focused on the use of polar hydrophilic solvents, whose applications were limited to hydrophilic medium. In order to extend it to the hydrophobic medium (non-polar medium); current generation is mainly focusing on the hydrophobic solvent assisted LDH delamination. Recently, O'Hare and co-workers developed a novel solvent exchange approach that is the aqueous miscible organic solvent treatment (AMOST), in which the freshly prepared LDH was repeatedly washed with acetone as aqueous miscible organic solvent followed by dispersion in hydrophobic xylene solvent.[33, 62] The modified solvent exchange treatment helps to remove the water molecules, and the surface gets modified into hydrophobic, which leads to stable dispersion of LDH in hydrophobic solvents.

Mechanism for Delamination of LDH

The LDH delamination is likely to happen in two stages as shown in proposed schematic illustration: swelling (stage-1) followed by exfoliation (stage-2). When a certain amount of formamide solvent is added to LDH, it replaces some of the water molecules instantaneously, and produces a highly swollen phase with a large gallery distance, as shown in Figure 1.4. The main driving force for the replacement of the water is that the formamide solvent molecules are able to form strong hydrogen bonds with LDH. Apparently, DMF solvent may break the intra and intermolecular H-bonding network among the hydroxyl slabs, the interlayer water molecules, and anions. As a result, it can readily penetrate into the LDH gallery and produces a loosely packed and swollen phase. The mechanical agitation or ultrasonic treatment of the swollen phase results in the exfoliation of LDH.[24, 26, 61, 63]

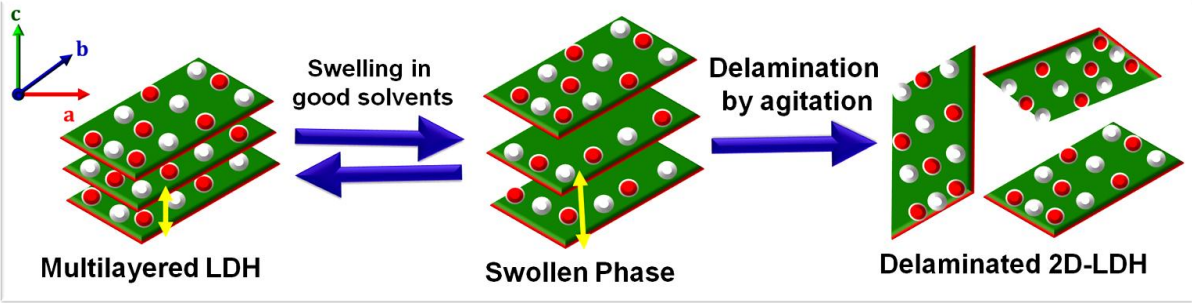

Figure 1.4. Schematic illustration of the liquid phase exfoliation of the LDH in nonpolar solvents.

1.7. Hybrid Polymer/LDH Nanocomposites

Development of polymeric nanocomposites towards specific application is an important projection in industry and research sectors for the last two decades.[64] On material development side it is needed to achieve the specific properties like mechanical stability, flame retardancy, gas permeability, thermal and electrical conductivity, UV stability etc.[7-9, 11, 13, 14, 64] Compared to natural clays, LDH has better structural homogeneity, freedom to tailor several varieties of compounds with different geometries using different metal compositions and the ability to tune the properties while synthesis for the specific application.[6, 28, 31, 65-67] The properties of reinforced LDH nanocomposites are decided by the crystalline geometry of layers along with the

different intercalated anions and interactions of the interlayer anions with polymeric chain.[31, 65, 67] Also the performance of the final composites is greatly affected by the dispersion of the nanometer thick layers within the host matrix.[33, 65]

1.7.1. Different Strategies for the Preparation of Polymer/LDH Nanocomposites

1.7.1.1. Polymer/Surfactant Modified LDH Nanocomposites

Depending on the availability of raw materials (LDH, polymer or monomer), LDH can be incorporated into the polymer matrix by four major approaches: (a) *in situ* polymerization (b) melt-processing (c) solution blending, and (d) pre-exfoliation followed by mixing.[1, 13, 25]

(a) *In situ* Polymerization: In this approach, LDH is directly added into a monomer solution or monomer and solvent mixture, which leads to the swelling of the LDH. Polymerization can be initiated either by heating or UV-light irradiation or appropriate initiator addition. Tanaka et al. for the first time (in 1989), synthesized the acrylate anions (monomer) intercalated Mg–Al LDH, with the purpose of preparing the polymer/LDHs nanocomposites.[68] The monomer intercalated LDH was preheated above 80 °C in the presence of an initiator, thereby the intercalated acrylate anions got polymerized to form LDH/polyacrylate nanocomposite. Later, a similar approach has been employed to synthesize different type of LDH/polymers nanocomposites. Qiu et al. used initiator-modified LDH for the preparation of exfoliated LDH/polystyrene nanocomposites, by an in situ ATRP technique.[69] In some other reports, the emulsion polymerization technique was employed for the synthesis of homogenously dispersed Zn-Al LDH/polystyrene nanocomposites, in the presence of surfactants (N-lauroyl-glutamate) and hexadecane mixture.[6]

(b) Melt Processing: This approach involves high-temperature treatment and shear effect. The polymer and filler are mixed above the softening point of the polymer. The greater advantages of melt compounding approach over either of the *in situ* polymerization or polymer solution intercalation are the environmental friendliness and cost-effectiveness. Moreover, it is a very simple and industrially viable method for the bulk scale production. However, getting the completely exfoliated nanocomposites by melt mixing approach is always difficult, compared to any other methods since the

LDH are having strong electrostatic interaction between the layers and gallery anions and hydrophilic nature.[8]

(c) Solution Blending: In the solvent based approach, a solvent that has the capability to dissolve the selected polymer and swell the layered material rapidly is used. Initially, the layered materials are swollen in the solvent followed by adding the polymer or polymer solution and subjected to appropriate heating with continuous stirring, which results in the formation of highly dispersed nanocomposites. The solvent based approach was often used for water soluble polymers such as PVA, PEO, etc. Later it has been extended to the other polymers also which are soluble in solvents such as toluene, xylene, chloroform, tetrahydrofuran (THF), etc.

Qu and co-workers were the first to report a series of exfoliated polymer/LDH nanocomposites, such as PE-g-MA/Mg–Al LDH, LLDPE/Zn–Al LDH, and PMMA/Mg–Al LDH nanocomposites in the presence of the xylene.[69-71] However, the LDH surface and polymer backbone were functionalized with the surfactants and hydrophilic functional groups, respectively. That surface modification led to the better adhesion between the polymer and LDH. Complete delamination of the LDH is possible with this technique by considering a few key aspects like solvent parameters, reducing the LDH content, refluxing time, and precipitation rate.[25, 70]

(d) Pre-exfoliation Followed by Dispersion into Polymer: In this approach, the initial step involves the pre-exfoliation of multilayered material which is followed by mixing of the polymer to form a well dispersed polymer/filler nanocomposites. Since the layered fillers are completely exfoliated, the "pre-exfoliation followed by dispersion into polymer" always end up with the real polymer/filler nanocomposites, unlike any other synthesis approaches.[6, 25] With the growth of the LDH exfoliation technologies, numerous approaches have been developed for the preparation of polymer/LDH nanocomposites by pre-exfoliated LDH nanosheets. For the first time, O'Leary et al. reported that the Mg–Al LDH-DDS exfoliated in acrylate monomers medium under high-speed stirring, followed by polymerization of the acrylate monomers/LDH suspensions to give the exfoliated polymer/LDH nanocomposites.[72] Later, Li et al. used a similar approach for the synthesis of PMMA/Mg–Al LDH nanocomposite.[73]

1.7.1.2. Polymer/Surfactant-Free LDH Nanocomposites

A large number of approaches have been reported for the preparation of exfoliated nanocomposites, mainly in the context of surfactant modified LDH. However, high level of surfactant loadings could lead to negative impact on costs, processability and also possible to inferior thermal properties of the polymer nanocomposites.[12] The end-use applications of polymer nanocomposites would be greatly expanded with surfactant-free materials.

Properties of polymer nanocomposites strongly depend on the degree of dispersion of LDH in the polymer matrices. Preparation of highly exfoliated polymer nanocomposites using LDH is a difficult approach since the thermodynamic and kinetic barriers inhibit the dispersion of hydrophilic inorganic nanoparticles in hydrophobic polymer matrices and stronger electrostatic interlayer interactions between the LDH platelets.

Preparation of exfoliated polymer nanocomposites using surfactant-free LDH (SF-LDH) is seldom studied. Delamination of SF-LDH in the powder form is a major challenge, which has slowed down their commercial exploitation. Recently, Wang et al.[62] reported a novel solvent exchange approach to obtain the delaminated dry powders. However, applications of such delaminated powders are still in its early stage only. On the other hand, there are only a few reports on the exfoliation of the LDH and the polymer/LDH exfoliated nanocomposites using SF-LDH by solvent mixing method.[33, 74-76] Recently, O'Hare and co-workers developed AMOST method where the freshly prepared wet LDH was repeatedly washed with acetone followed by dispersion of LDH in hydrophobic xylene solvent.[33, 62] The major advantage of this modified is that it helps in the simultaneous removal of the water molecules and surface modification of hydrophilic LDH to hydrophobic, which leads to a stable dispersion in polar hydrophobic solvents. Such prepared LDH suspension was used to synthesize homogenously dispersed PP/SF-LDH nanocomposites.[33]

1.7.2. Structure and Morphology of Hybrid Polymer/LDH Nanocomposites

In general, layered materials have the layer thickness in the order of few nanometers with very high aspect ratio. The lower filler loadings help in the uniform dispersion throughout the polymer matrix without any aggregation, whereas it is difficult to achieve a good dispersion in larger filler loadings. Depending upon the interfacial interactions between the polymer and filler, and their thermodynamic parameters, the layered fillers exist in the polymer matrix in four different morphologies (Figure 1.5). Those are (a) aggregated, (b) intercalated, (c) exfoliated, and (d) intercalated and flocculated nanocomposites.[1, 25] The morphology of these four nanocomposites can easily be understood by considering the basal plane distance of the dispersed layered filler. The "basal plane spacing" is nothing but the distance between planes in the unit layer to another plane in the next unit layer.[1]

(a) Aggregated Nanocomposites: If the polymer chains cannot enter the galleries, the layered basal plane remains unchanged, and the composite is called "aggregated or conventional" nanocomposites.

(b) Intercalated Nanocomposites: In the case of the intercalated nanocomposites, the insertion of polymer chains takes place into the gallery of the layers, and it causes an enlarged basal plane distance, without disturbing their crystallographic character.

(c) Exfoliated Nanocomposites: In an exfoliated nanocomposite, the individual layers of the 2D material push apart to create a disordered morphology, and the layer to layer distance depends on the amount of filler loadings. Usually, the exfoliated nanocomposites have been observed in the nanocomposites with lower loadings, however, it is difficult to accomplish in bulk filler loadings.

(d) Intercalated and Flocculated Nanocomposites: Recently Ray et al. observed a new type of morphology in nanocomposites which come under the category of the intercalated nanocomposites, and termed it as "intercalated and flocculated" nanocomposites.[13] Basically, it appeared similar to the intercalated morphology; however, they have a considerable difference in the morphology as well as properties. The polymer chains intercalated to two or more layered materials (clay or LDH) form a bridge like morphology through hydroxylated edge to edge interaction (through

noncovalent interactions), whereas the intercalated nanocomposites shows an individual intercalated multilayer, which can be readily distinguished by microscopic technology, however it is more difficult with the X-ray measurement.

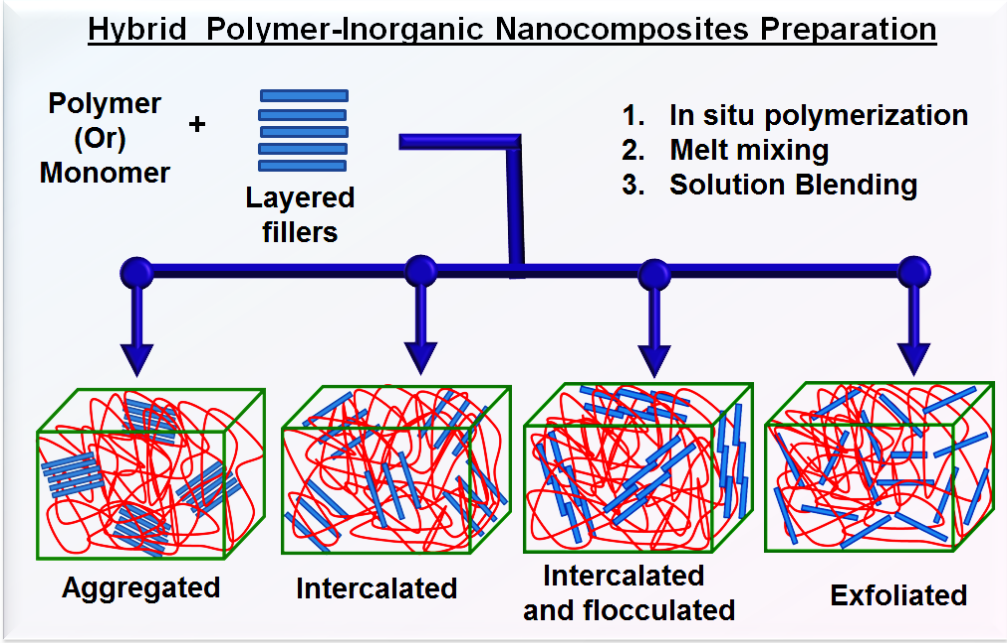

Figure 1.5. Schematic representation of four different thermodynamically favorable morphologies of polymer nanocomposites.

Among the above mentioned four types of nanocomposites, the exfoliated nanocomposites receive greater interest since the homogenous dispersion of the layered filler in polymer matrix results in unexpected properties compared to the other types of nanocomposites. Nevertheless, layered fillers (like LDH) have a high charge density and strong interlayer electrostatic interaction, which makes it much more difficult to achieve exfoliated nanocomposites.

1.7.3. Techniques used for the Characterization of Nanocomposites

WAXD and TEM characterization techniques have been used to understand and establish the structure and morphology of polymer nanocomposites. Both WAXD and TEM are essential tools for evaluating nanocomposite structure.[13] However, TEM is time-intensive and gives only qualitative information, whereas the WAXD measurements allow the quantification of charges in the interlayer spacing. By observing the position, symmetry, and intensity of the basal reflections (00n) from the

distributed layered materials, the nanocomposite structure can be easily understood like whether it is intercalated or exfoliated. Typically, if the basal plane reflections are shifting towards the lower (2θ) angle and retain their symmetry of diffraction peaks, then they are called 'intercalated' nanocomposites. If the basal planes completely disappear or exceed more than 6-8 nm with weak diffraction plane, they are called "exfoliated" nanocomposites. On the other hand, the intercalated-flocculated structured nanocomposites are more difficult to understand by WAXD technique; however, it can be readily distinguished by TEM analysis.[8, 13, 25]

1.7.4. Physical Characteristics of Hybrid Polymer/LDH Nanocomposites

The inclusion of exfoliated single or few layered LDH in hydrophobic polymers alters the crystallization behavior, mechanical and thermal properties, flammability behavior, etc. of the host polymer.[30, 33, 65] The following section will describe the different properties (crystallization, mechanical, thermal and flammability) that can be modified in the presence of different fillers, especially LDH, in detail.

1.7.4.1. Crystallization and Crystallization Kinetics:

Polymer crystallization has been extensively studied ever since the concept of the chain folding was introduced by Storks in 1938 and later validated independently by Keller and Eppe, in 1957.[77-79] Crystallization in polymers is a process in which the transitions from disordered amorphous phase into more ordered crystalline phase happens, from either melt or solution state. Crystallization is favored by a regular arrangement of the polymer chains giving the structure a high degree of symmetry. For example, isotactic and syndiotactic polypropylene with their side groups arranged in a regular fashion gives a semicrystalline polymer, whereas the atactic form of these polymers, in which the side groups are arranged randomly, always results in amorphous structure.[80, 81]

Crystallization of long chain polymer molecules from its melt state starts with the chain folding followed by the formation of ordered regions called lamellae.[78, 82] These lamellae will grow radially in all direction to form the spherical aggregates called spherulites. The spherulites will be consisting of the highly ordered lamellar regions

separated by the random amorphous regions.[81, 82] The dimensions of spherulites range from micrometers to millimeters, which are dependent on many parameters such as the chemical structure of the polymer chain and the crystallization conditions like cooling rate, crystallization temperature, the content of the nucleating agent, etc. Spherulites can be readily observed by polarized light microscopy, and Bunn and Alcock were the first to recognize the formation of spherulites for polymers in their study on branched polyethylene.[83, 84]

Melt crystallization can be divided into two categories namely, isothermal crystallization where the solidification or crystallization takes place at a constant temperature and nonisothermal crystallization where the crystallization happens when cooling from the melt at a constant cooling rate.[11, 14] Crystallization is considered to occur in two steps, which is usually preceded by homogeneous nucleation, heterogeneous nucleation, or self-nucleation, followed by growth of the crystal with time.[14, 82] There are two basic nucleation processes: first, there is the birth of the new solid phase or nucleus within the melt, this is called primary nucleation; then follows the process of crystal growth which requires nucleation at the growing interface and this is called secondary nucleation. The primary nucleation can be initiated by several ways. It is called homogeneous nucleation when it involves a spontaneous aggregation of polymer chains in a reversible way up to the point where a critical size is reached; beyond this point, the addition of chains is irreversible and crystal starts to grow. Homogeneous nucleation occurs in the absence of a second phase and requires a large degree of supercooling. Primary nucleation is called heterogeneous nucleation when it involves the aggregation of polymer chains at the interface of a foreign phase such as impurities or a purposely added nucleating agent.[80-82, 85] The addition of nucleating agents increases the rate of nucleation and leads to the formation of a larger number of smaller sized spherulites. This modification can improve several physical properties of the polymer.[85, 86] Heterogeneous nucleation requires a small degree of supercooling.

The rate of crystallization of polymers is a very important property from the industrial point of view since this affects the production time of thermoplastic goods.[11, 14, 45, 82] The research and development of nucleating agents, which are incorporated into

thermoplastic polymers during processing, have been mainly industry driven and directed towards the improvement of the thermal, mechanical and optical properties of the polymer involved and to reduce production costs through cycle time efficiency. A great effort has been devoted to this during the last few decades, and this is still an area of substantial scientific and commercial interest.[11, 13, 14, 45] Table 1.2 summarizes the variety of inorganic and organic nucleating agents, and their classification on the basis of dimensions of the filler.

Table 1.2. Change in the melt-crystallization peak temperature (T_{mc}), and thermal degradation temperature ($T_{0.5}$) for different iPP nanocomposites.

S.No	Dimension of the filler	Nano filler type (inorganic or organic)	Filler size (nm or μm)	Filler volume (%)	ΔT_{mc} (°C)	$\Delta T_{0.5}$ (°C) (N_2 gas)	Ref.
1.	**0D**	Si_3N_4	~40 nm	0.1-2	3-4.5	-	[87]
2.		ZnO	~60 nm	0.3-5	3-14	-	[88]
3.		Ai_2O_3	45 nm	1.5-5	2-3.5	-	[89]
4.		CaO	~40 nm	2-10	-4-10.5		[90]
5.		SiO_2	~80 nm	0.2-5	-2-11	-	[91]
6.		POSS	-	3-9	4-6	-	[92]
7.		Carbon black	~125 nm	0.2-1	2-3	-	[93]
8.		Fullerene	~80 nm	1-1.2	~14	-	[94]
9.		Fullerene like WS_2 nanoparticles	~110 nm	8	22	19	[95]

10.	**1D**	SWCNT	-	0.2-2 0.6-1.2 0.8	12-16 6-10 11	- - -	96 97 98
11.		MWCNT	-	0.2-2	9-12	-	96
12.		MoS_2 nanotubes	~80 nm	2	11	44	15
13.		Hierarchical Glass Fiber- WS_2 particles	~15 nm	4	22	25	99
14.	**2D**	Graphene	--	0.1-2 0.5-1	4-8 9-11	- -	100 101
15.		Clay	~300 nm	2.5-7.5	4-6.5	-	102
16.	**1D & 2D**	**Commercial and other nucleating agents**					
		(a) Sodium Benzoate	~400 nm	1	9	-	103
		(b) HPN	~400 nm	1	22	-	103
		(c) DMDBS	~15 nm	0.2	17.5	-	45
		(d) PTBBA	"	0.2	19	-	"
		(e) BA	"	0.2	14	-	"
		(f) PA	"	0.2	6.5	-	"
		(g) Ga- PTBBA	"	0.2	16.5	-	"
		(h) Zr- PTBBA	"	0.2	8.4	-	"

17.	**2D & 3D**	**LDH**					
		(a) SF-Mg-Al LDH	~300 nm	1-12	3.5-5.4	43-61	[32]
		(b) SF-Mg-Al LDH	~ 350 nm	1-5	12-14.5	-	[104]
		(c) SF-Mg–Al LDH	~100 nm	1-16	7-9	5-50	[35]
		(d) Mg–Al LDH-Borate	~100 nm	1-30	-	-35-25	[105]
		(e) Mg_3Al-LDH	~60 nm	0.5-12	8-14.5	15-44	[33]
		(f) O-CoAl-LDH	~1.5 μm	1.5-6	-	0	[106]
		(g) Mg_3-Al LDH-X	~ 300 nm	9	10-13	-5-44	[107]
		(h) Mg_3-Al LDH	~ 250 nm	13-28.6	4-8	-2-61	[28]
		(i) Mg-Zn-Al LDH	-	2-4	-	4-8	[108]

The following section gives the general factors which control the crystallization rate and morphology and general crystallization terms.

Following are the important parameters which are impacting the crystallization behavior:[11, 14, 82]

- Molecular structure and molecular mass of the components
- Type and degree of dispersion of the phases in the molten stage
- Crystallization conditions (e.g.: cooling and heating rate)
- Composite ratios
- Nature of the interactions in components (composite mixture)
- Melt state history
- Crystallization environment (e.g.: solvent, humidity, etc.)

Some of the following factors influence the crystalline morphology development, resulting in changes of crystallization parameters such as:[81, 82]

- Overall crystallization rate (K)
- Spherulite growth rate (G)
- Semicrystalline polymer morphology (e.g.: size, shape, and texture of the spherulites)
- Nucleation density (N)
- Total degree of crystallinity (X_c)

Thermal Parameters Related to the Crystallization of Polymers

Equilibrium Melting Temperature T°_m: The equilibrium melting temperature T°_m is defined as the melting temperature of an infinite stack of extended chain crystals, large in directions perpendicular to the chain axis and where the chain ends have established an equilibrium state of pairing. This is one of the most important thermodynamic properties of crystallizable chain polymers, as it is the reference temperature from which the driving force for crystallization is defined. The change in Gibbs free energy ΔG per unit mass at T°_m is zero. This is the general condition that determines the melting point of any substance.

Thus, the temperature response of linear polymers can be divided into three distinctly separate segments:

Above T_m: In this segment, the polymer remains as a melt or liquid whose viscosity is dependent on the molecular weight and temperature of observation.

Between T_m and T_g: This domain may range between near 100% crystalline and near 100% amorphous chain molecular clusters depending on the polymer structural regularity and experimental conditions. The amorphous part behaves much like supercooled liquid in this segment. The overall physical behavior of the polymer in this intermediate segment is much like rubber.

Below T_g: Polymers below T_g is more like glass, which is hard and rigid, with a specified coefficient of thermal expansion. These glassy polymers are closer to a crystalline solid

than to a liquid in their behavior in terms of mechanical properties. With respect to molecular order, however, this glass more closely resembles the liquid. There is no difference between linear and cross linked polymer below T_g. The T_g depends on the rate of cooling.

Crystallization Kinetics

During crystallization from the bulk, polymers form lamellae, which in turn are organized into spherulites or their predecessor structures, hedrites. This section is concerned with the rates of crystallization under various conditions and the theories that provide not only an insight into the molecular mechanisms but also considerable predictive power.[81, 82]

The rate of radial growth of the spherulites is linear in time and the growth rate goes through a maximum as the temperature of crystallization is lowered. These several experimental findings form the basis for theories of polymer crystallization kinetics. The first one is based on the work of Avrami, where the formulations intended for metallurgy were adapted to the needs of polymer science.[109] There is one intermediate model which was proposed by Hoffman-Weeks to understand the T°_{m} of polymeric mixture which later used in Hoffman-Lauritzen model to predict secondary nucleation growth during crystallization of polymer. The second theory was developed by Hoffman and Lauritzen who suggested the kinetic nucleation theory of chain folding, which provides an overall understanding of how lamellar structures establish from the melt.[110, 111] However, out of these two theories first Avrami model theory is a simple and has the power to predict molecular mechanisms of polymer crystallization, and it has been extensively employed model theory.[11, 14]

Avrami Isothermal Crystallization Kinetic Model: The Avrami approach is often used to characterize crystallization under laboratory conditions to predict crystallization during processing. The study of the crystallization process is based on the evolution of the crystalline fraction of the polymer, as a function of the time in isothermal regime or as a function of the temperature under dynamic constant rates. When a polymer crystallizes, the extent of the phase transformation depends on the

crystallizing species and the experimental conditions. The isothermal crystallization kinetics generally analyzed by a classical Avrami equation as given fellow.[81, 82, 109]

$$1 - X(t) = \exp(-Kt^n) \qquad (1.1)$$

Where $X(t)$ is the relative crystallinity, n is the Avrami exponent (dependent on the nature of nucleation and crystal growth geometry). Both n and K depend on the nucleation and growth mechanisms of spherulites. In order to deal conveniently with an operation, eq. (1) is usually rewritten as the double logarithmic form as follows

$$\ln[-ln(1 - X_t)] = \ln K + n \ln(t) \qquad (1.2)$$

The k and n values could be directly obtained from the slope and intercept of the best-fit line as shown Figure 1.6. In most cases, n exhibits a noninteger value between 1 and 4 and is attributed to the mixed growth of spherulites and two stage crystallization.[109]

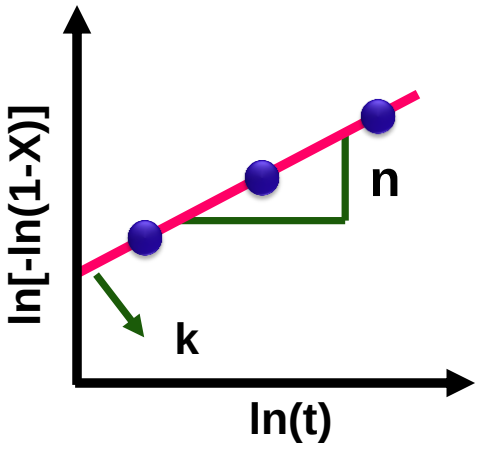

Figure 1.6. Schematic representation of the Avrami plot.[109]

Table 1.3. Avrami exponent (n)[81, 82, 109]

Avrami exponent (n)	**Dimension of crystal growth**
4	3 dimension (spheres shape)
3.5	
3	
2.5	2 dimension (discs shape)
2	
1.5	1 dimension (rods shape)
1	

kt^n is the volume of crystallized polymer, which is determined by considering the two cases: whether preexisting nuclei are present or not. If the nuclei are predetermined and crystallization happens at once on cooling the polymer to the present temperature, it is termed as heterogeneous nucleation, and if there is sporadic nucleation of spherical crystal it is named as homogeneous nucleation. In most of the polymer nanocomposites the secondary nucleation behavior is observed, since the

dispersed filler behaves like a preexisted nucleating centers which promote the overall crystallization rate of the polymer.[14]

1.7.4.2. Mechanical Properties

Understanding the viscoelastic behavior of the nanocomposites in variable-temperature conditions has a significant importance for providing insights for any practical applications such as polymer processing, lubrication, etc.[13, 81, 112] The rigid inorganic filler dispersed polymer nanocomposites exhibit peculiar viscoelastic behaviors which are rarely present in the pure polymer. According to Khare et al. in the presence of inorganic additives, polymer chains get spatial confinement, which increases the mechanical properties significantly.[113]

The mechanical properties of nanocomposites are usually characterized by a variety of parameters, which include Young´s modulus, storage modulus, tensile strength, impact strength, hardness, softening point, etc.[1, 8, 11] Dynamic mechanical analysis (DMA) measures the response of a given material to an oscillatory deformation (here in tension–torsion mode) as a function of temperature. DMA results are composed of three parameters: (a) the storage modulus G' (b) the loss modulus G'' and (c) tan δ (G''/G'). The tan δ is used for determining the occurrence of molecular mobility of polymers, such as T_g.[1, 5]

One of the main reasons for adding fillers to polymers is to increase the modulus or stiffness via reinforcement mechanisms described by theories for composites. Properly dispersed and aligned LDH platelets have proven to be very effective for increasing the stiffness of the host polymer.[13, 112] It was observed in many reports that by the incorporation of LDH into the polypropylene matrix, a remarkable increase in stiffness and a decrease in tan δ owing to reinforcement effect of rigid LDH have been observed.[30, 35] The enhancement in storage modulus and loss modulus was more prominent below the T_g of polymer, whereas behind that a progressive reduction was observed.[11]

The tan δ curves for PP nanocomposites have been shown three major molecular relaxations: one at -10 to 10 °C temperature range associated with the glass–rubber relaxation of the amorphous portion. Another broad peak appeared between 50 to 100

°C is related to the crystalline phase relaxation (α). These two molecular relaxations were observed frequently in many reports.[11, 15, 99] Another molecular relaxation was observed by McCrum and co-workers in the lower temperature region (at -80 °C) which was assigned to be the gamma phase (γ) molecular relaxation.[114]

1.7.4.3. Thermal Stability

In general, it has been widely accepted that the dispersion of LDH or any other nanometer-sized inorganic particles into a polymer enhances the thermal degradation stability of the matrix, by inhibiting the formation and evolution of volatile byproducts during the decomposition process. However, the addition of LDH might not always favor the improvement in thermal stability, and sometimes can promote the earlier polymer degradation.[38, 106] The degradation temperatures observed for the polymer/LDH nanocomposites are related to the type of different metal constituents, gallery anions, size, concentration, the state of filler distribution, and their interactions with the reactive groups in the polymer.[27, 30, 35, 108] Table 1.2 compares the thermal stability improvements observed via the incorporation of LDH, determined by thermogravimetric analysis (TGA), by analyzing the difference between the initial degradation temperature of the nanocomposite and that of the neat matrix (ΔT_i), at the temperatures for 50% weight loss (ΔT_{50}).

1.7.4.4. Flammability Behavior

Most of the commercially available low-cost polyolefins such as polypropylene, polyethylene, etc. come under the category of highly flammable materials, which obstructs its use in various end products. The combustion of polymers is driven by a thermally induced decomposition (pyrolysis) phenomenon of the solid polymer into smaller fragments, which then volatilize; mix with oxygen in the atmosphere, and combust further with the evolution of toxic gases. This combustion also releases more heat, which radiates onto the unburned polymer, thereby leading to the extended pyrolysis and combustion until a lack of heat/fuel/oxygen causes the fire to extinguish. Thermoplastic polymers have a tendency to drip and flow under fire conditions, which can lead to additional mechanisms of flame spread or propagation whereas thermoset

polymers tend not to drip and flow and instead produce pyrolysis gases from the surface of the sample directly into the condensed phase.[65, 66, 115, 116]

Tackling the problems associated with flammability of the commodity polymers is very much important from the industrial point of view since these are widely used for various applications like packaging materials, building materials, transportation, thin films, bottles, etc. Various additives and fillers like halogenated compounds, phosphorous containing compounds, inorganic nanofillers, etc. were utilized to reduce the flammability of polymers like PP, PE, PS, etc.[65, 66, 115, 117]

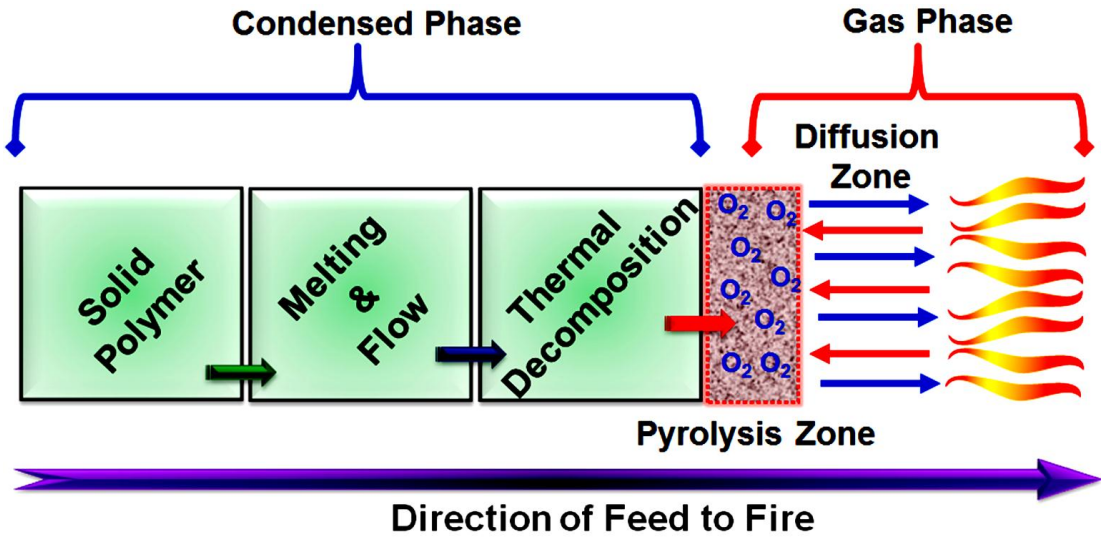

Figure 1.7. Schematic illustration of polymer decomposition and combustion behavior.

Depending on the mechanism of flame retardancy, the available flame retardant additives can be categorized into three groups as shown below.[115]

(a) Gas Phase Flame Retardants (e.g. halogen, phosphorus): These materials reduce the heat released in the gas phase from combustion by inhibiting the exothermic oxidation reaction in the flame through scavenging reactive free radicals and thus decreasing the energy feedback to the polymer matrix. Even though halogenated compounds are good flame retardants, they are toxic and carcinogenic and raise serious environmental and health concerns.

(b) Endothermic Flame Retardants (e.g. metal hydroxides such as magnesium hydroxide (MDH) and aluminiumhydroxide (ATH), carbonates) These materials

function in the gas phase and condensed phase by releasing non-flammable gases (H_2O, CO_2) which is an endothermic reaction absorbing energy from the ignition source. The released water vapours can dilute the fuel and cool the polymer. The lower substrate temperature slows down the pyrolysis rate. These materials also leave behind a ceramic-like residue, which acts as an insulating layer on the surface and protects the underlying polymer from further decomposition.

(c) Char-Forming Flame Retardants (e.g. intumescents, nanocomposites) This category of materials operate in the condensed phase by preventing fuel release through binding up fuel as non-pyrolyzable carbon (char), thereby providing thermal insulation for underlying polymer through the formation of char protection layers. Typically, such an intumescent system is composed of three major components: an acid source, a carbon source, and a blowing agent.

An acceptable flame retardant additive for a polymer should have the following features:[41, 117]

- It should be thermally stable up to the normal polymer processing conditions (~300 °C)
- Good compatibility with polymers and it should not have leach out and migratory properties
- The additive should retain its flame retardant behavior when incorporated into polymer matrix
- It should also reduce the evolution of any toxic gases and smoke during burning process

Nanofillers as Flame Retardants

Polymer nanocomposites have motivated considerable interests in the development of flame retardant polymeric materials because the addition of rigid inorganic nanofillers not only provides fire retardant properties to the materials but also, does not change the other properties of the host matrix or even enhance some of them, such as mechanical properties of the resultant polymer nanocomposites at a relatively low loadings.[65, 66, 115]

Table 1.4. Summary of the different category of flame retardant additives.[41, 65, 66, 115, 117-119]

Different category of flame retardants	**Examples**	
Halogenated compounds	Decabromodiphenyl ether, Tetrabromo bisphenol A, Bis(2,3-dibromopropylether) Tetrabromo bisphenol A, 1,2-ethylene bis(tetrabromophthalimide), Hexabromocyclododecane, Tris (tribromoneopentyl) phosphate	
Phosphorus-based compounds	Bisphenol A Diphosphate, Triphenylphosphate, Resorcinol Diphosphate, 9,10-dihydro-9-oxa-10-phosphaphenanthrene-10-oxide (DOPO), Ammonium Polyphosphate	
Nitrogenous based compounds	Melamine, triazine, urea (phosphate) and guanidine	
Mineral based flame retardants filler	**Natural**	Aluminum hydroxides ($Al(OH)_3$), cobalt hydroxide ($Co(OH)_2$) magnesium hydroxides ($Mg(OH)_2$), nickel hydroxide ($Ni(OH)_2$), magnesium carbonate ($MgCO_3^{2-}$), clays (montmorillonite, hectorite, and saponite)
	Synthetic (LDH based)	Ca-Al LDH, Co-Al LDH, Cu-Al LDH, Mg-Al LDH, Mg-Fe LDH, Ni-AL LDH, Ni-Fe LDH, Zn-Al LDH, Zn-Fe LDH, Mg-Zn-Al LDH; most of the cases LDH gallery was intercalated with variety of the inorganic and organic anions.
Inorganic flame retardants	POSS, mesoporous SiO_2, graphene, CNT, carbon fibers, carbon block, MoS_2, borates, glass fibers,	

Depending on the elemental constitution and other characteristics of the nanofillers, these hybrid polymer inorganic systems may follow any one or more of the

above-mentioned flame retardancy mechanisms.[31, 65-67, 108] Figure 1.8 shows the general mechanism of flame retardancy of polymers in the presence of external additives.

LDH as Flame Retardant Nanofiller: LDH, which possess a unique lamellar structure, are proved to be effective flame retardant additives to polyolefins, and also to other polymers. LDH offer the possibility of tuning the lateral sizes, layer thickness, intralayer metal composition ratio, gallery anions, etc. and thereby tune the flame retardancy also.[31, 34, 65, 67, 108] Dispersion of LDH in the host matrix and compatibility of LDH with the polymer can also seriously affect the heat release rate of the polymer matrix. It is observed that only the exfoliated nanosheets with homogeneous dispersion in the polymer matrix can increase the flame retardancy effectively. Although a complete understanding of the mechanism of LDH based nanocomposites is not yet reported, it is supposed to be a combination of all the three types of above-mentioned mechanisms.[119] During thermal decomposition, LDH will lose the interlayer H_2O, decomposition of the intercalated anions (e.g. CO_3^{2-}) and it forms metal oxide char residues.[65, 115]

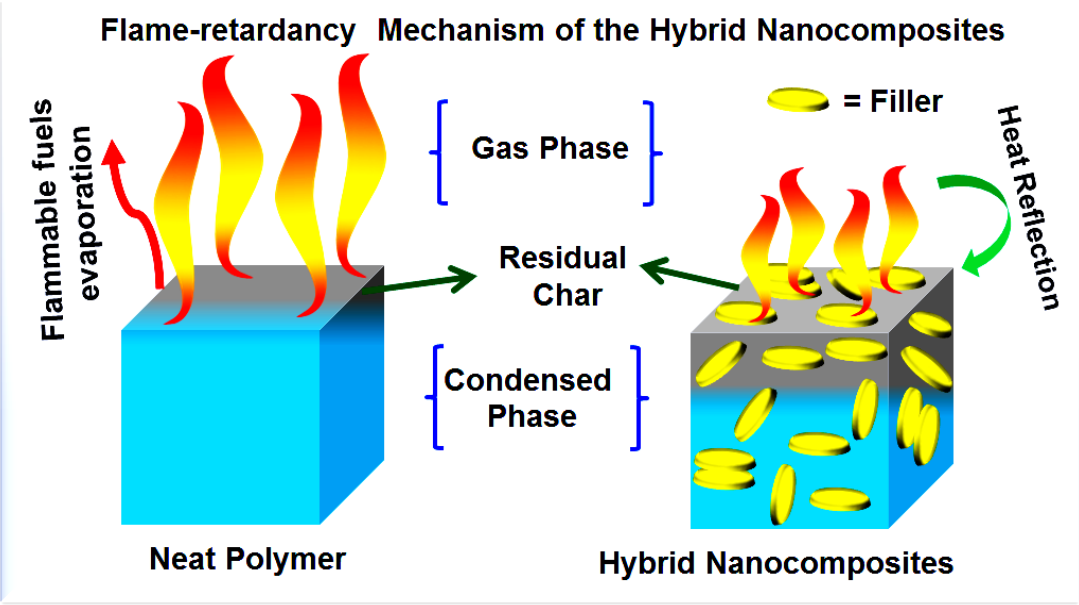

Figure 1.8. Schematic image representing the flame retardant mechanism in hybrid polymer nanocomposites.

The effects of these processes will reduce fuel available for combustion, which will lower the heat release and eventually stop the combustion. When there is not enough fuel to propagate the reaction, the formation of an expanded carbonaceous char

Table 1.5. Summary of different anion modified LDHs added to polymers and their flame retardancy behavior.

S.No	Type of LDH	Gallery anions	Polymer	Filler amount (%)	Reduction in pHRR (%)	Ref.
1.	Co-Al LDH	DBS	MA-g-PP	6	30	106
2.	Mg-Al LDH	DBS	MA-g-PP	4.8	29	120
3.	Mg_3Al LDH Zn_2Al LDH Zn_2Al LDH	Borate " "	PP " "	6 6 30	24 30 69.5	105
4.	Mg-Al LDH	NO_3^- DBS AR88-dye AY36-dye	MA-g-PP	5	11 11 22 33	121
5.	Mg-Al LDH	Spherical like Plate like Flower like	PP	23	57.9 60.7 54.8	28
6.	MgZnAl-LDH	DBS + ammonium polyphosphate	PP	20	76	108
7.	Mg-Al LDH	DBS	LDPE	20	57	122
8.	Zn-Al LDH	Oliate	PE	10	60	37
9.	Zn-Al LDH	Cl^-, CO_3^{2-}, NO_3^-, SO_4^{2-}	HDPE	40	24 41 48 54	29

10.	Ni-Al LDH	CNT	PP	5	10	[123]
11.	Zn-Al LDH	$CuMoO_4$	PP	5	40	[124]
12.	Mg-Al LDH	CNT	PP	20	46	[34]

is promoted. This char formation protects the bulk polymer from the exposure to air, which reduces the heat release during the combustion and suppresses the smoke production. In summary, the flame retardant mechanism of LDHs can be attributed to the combination of the following three functions: (1) Heat absorption, (2) Gas dilution, and (3) Char formation. Literature is enriched with LDH as flame retardant additives to a variety of polymers and the Table below summarizes (Table 1.5) the flame retardancy efficiency of LDHs with different metal constituents on various polymers. Figure 1.9 displays the datasheets showing the number of research publications on flame retardancy and LDH based flame retardancy.

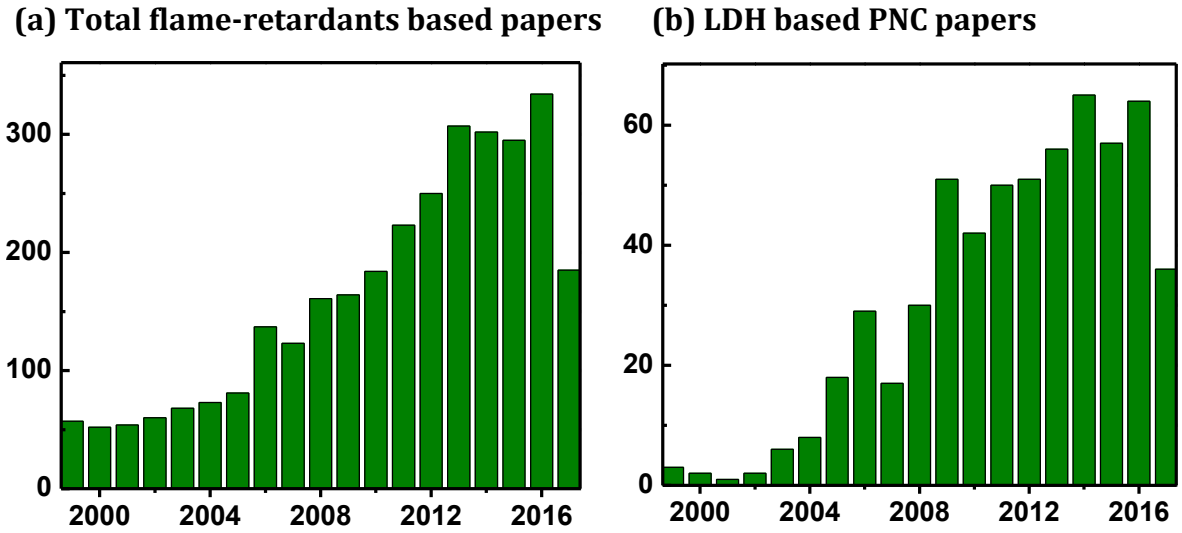

Figure 1.9. Number of publications per year (1999–2017) with the keyword of (a) flame retardants polymer based papers (b) LDH based polymer nanocomposites" (Source: Web of Science and data collected on: August 2017).

Techniques and Indices for Determining Flame Retardancy Performance

Mainly four techniques are used to evaluate the flame retardancy of a polymer; microscale combustion calorimetry (MCC), limiting oxygen index (LOI), cone calorimeter (CC) and UL-94.[65]

Microscale Combustion Calorimetry (**MCC):** MCC, also known as pyrolysis combustion flow calorimetry, is a convenient and fast method for laboratory evaluation of the flame retardant properties with small amounts of material. It is based on a TGA-like degradation of the polymer in nitrogen, followed by combustion of the gases produced in air. The parameters include the heat release rate (HRR), heat release capacity (HRC) and temperature of degradation.

Cone Calorimeter (CC): Cone calorimeter is the most effective technique for the laboratory evaluation of the flame retardant properties of polymers which measure the HRR and peak heat release rate (PHRR). A highly flame-retardant system normally shows a low PHRR value. Another important parameter is total heat released (THR), which represents the sum of heat released until the flame is extinguished. Besides these, average specific extinction area (ASEA), a measure of smoke, average mass loss rate (AMLR) and the time to ignition (t_{ig}, also known as TTI) are also measured using this technique.

Limiting Oxygen Index (LOI): The fraction of oxygen in a nitrogen–oxygen mixture required to support combustion is measured in this technique to understand the flammability behavior of the polymer. LOI is tested based on ASTM D2863, the latest version being D2863-87. The higher number indicates more difficulty for combustion to occur. LOI value is expressed as a number indicating the percentage of oxygen required for self-sustained combustion of any materials but does not provide any useful information about the burning behavior. A good flame retardant material should have an LOI value greater than 26.

Underwriters Laboratories-94 (UL-94): It is one of the most widely used performance standards for a plastic material used to evaluate the extinguishing ability of the material after it is ignited. UL-94 testing is carried out by following two standards: one is the vertical burn test (UL-94 V), and the other is the horizontal burn test (UL-94 HB). This standard is divided into five parts: HB, V-2, V-1, V-0 and 5 V. UL-94 V gives useful information regarding the dripping behavior of the nanocomposites. The dripping of the burnt melt directly influences the spread of flame through the

secondary flame during real life burning situations. A good fire retardant material should reach the UL-94 V-0 rating and should not show any dripping during the test.

1.8. References

1 B. Chen, J. R. G. Evans, H. C. Greenwell, P. Boulet, P. V. Coveney, A. A. Bowden and A. Whiting, *Chem Soc Rev* **37:**568-594 (2008).

2 H. Zou, S. Wu and J. Shen, *Chem Rev* **108:**3893-3957 (2008).

3 J. W. Cho and D. R. Paul, *Polymer* **42:**1083-1094 (2001).

4 Y. Kojima, A. Usuki, M. Kawasumi, A. Okada, Y. Fukushima, T. Kurauchi and O. Kamigaito, *J Mater Res* **8:**1185-1189 (1993).

5 S. K. Kumar, B. C. Benicewicz, R. A. Vaia and K. I. Winey, *Macromolecules* **50:**714-731 (2017).

6 Q. Wang and D. O'Hare, *Chem Rev* **112:**4124-4155 (2012).

7 N. G. Sahoo, S. Rana, J. W. Cho, L. Li and S. H. Chan, *Prog Polym Sci* **35:**837-867 (2010).

8 D. R. Paul and L. M. Robeson, *Polymer* **49:**3187-3204 (2008).

9 J. R. Potts, D. R. Dreyer, C. W. Bielawski and R. S. Ruoff, *Polymer* **52:**5-25 (2011).

10 H. Kim, A. A. Abdala and C. W. Macosko, *Macromolecules* **43:**6515-6530 (2010).

11 M. Naffakh, A. M. Díez-Pascual, C. Marco, G. J. Ellis and M. A. Gómez-Fatou, *Prog Polym Sci* **38:**1163-1231 (2013).

12 M. Z. Rong, M. Q. Zhang, Y. X. Zheng, H. M. Zeng, R. Walter and K. Friedrich, *Polymer* **42:**167-183 (2001).

13 S. Sinha Ray and M. Okamoto, *Prog Polym Sci* **28:**1539-1641 (2003).

14 J.-Z. Xu, G.-J. Zhong, B. S. Hsiao, Q. Fu and Z.-M. Li, *Prog Polym Sci* **39:**555-593 (2014).

15 M. Naffakh, M. Remskar, C. Marco, M. A. Gomez-Fatou and I. Jimenez, *J Mater Chem* **21:**3574-3578 (2011).

16 K. S. Novoselov, D. Jiang, F. Schedin, T. J. Booth, V. V. Khotkevich, S. V. Morozov and A. K. Geim, *Proc Natl Acad Sci U S A* **102:**10451-10453 (2005).

17 V. Nicolosi, M. Chhowalla, M. G. Kanatzidis, M. S. Strano and J. N. Coleman, *Science* **340:**(2013).

18 K. R. Paton, E. Varrla, C. Backes, R. J. Smith, U. Khan, A. O'Neill, et al., *Nat Mater* **13:**624-630 (2014).

19 M. Naguib, V. N. Mochalin, M. W. Barsoum and Y. Gogotsi, *Adv Mater (Weinheim, Ger)* **26:**992-1005 (2014).

20 J. N. Coleman, M. Lotya, A. O'Neill, S. D. Bergin, P. J. King, U. Khan, et al., *Science* **331:**568-571 (2011).

21 M. Alexandre and P. Dubois, *Mater Sci Eng R-Rep* **28:**1-63 (2000).

22 W.-L. Song, P. Wang, L. Cao, A. Anderson, M. J. Meziani, A. J. Farr and Y.-P. Sun, *Angew Chem Int Ed* **51:**6498-6501 (2012).

23 F. Leroux and J.-P. Besse, *Chem Mater* **13:**3507-3515 (2001).

24 Z. Liu, R. Ma, M. Osada, N. Iyi, Y. Ebina, K. Takada and T. Sasaki, *J Am Chem Soc* **128:**4872-4880 (2006).

25 F. Leroux, M. Adachi-Pagano, M. Intissar, S. Chauviere, C. Forano and J.-P. Besse, *J Mater Chem* **11:**105-112 (2001).

26 R. Ma, Z. Liu, L. Li, N. Iyi and T. Sasaki, *J Mater Chem* **16:**3809-3813 (2006).

27 K. Okamoto, N. Iyi and T. Sasaki, *Appl Clay Sci* **37:**23-31 (2007).

28 L. Qiu, Y. Gao, X. Yan, J. Guo, A. Umar, Z. Guo and Q. Wang, *RSC Adv* **5:**51900-51911 (2015).

29 Y. Gao, Q. Wang, J. Wang, L. Huang, X. Yan, X. Zhang, Q. He, Z. Xing and Z. Guo, *ACS Appl Mater Interfaces* **6:**5094-5104 (2014).

30 D. Basu, A. Das, K. W. Stöckelhuber, U. Wagenknecht and G. Heinrich, *Prog Polym Sci* **39:**594-626 (2014).

31 E. N. Kalali, X. Wang and D.-Y. Wang, *J Mater Chem A* **3:**6819-6826 (2015).

32 J.-H. Yang, W. Zhang, H. Ryu, J.-H. Lee, D.-H. Park, J. Y. Choi, A. Vinu, A. A. Elzatahry and J.-H. Choy, *J Mater Chem A* **3:**22730-22738 (2015).

33 Q. Wang, X. Zhang, J. Zhu, Z. Guo and D. O'Hare, *Chem Commun* **48:**7450-7452 (2012).

34 Y. Gao, Y. Zhang, G. R. Williams, D. O'Hare and Q. Wang**6:**35502 (2016).

35 Q. Wang, X. Zhang, C. J. Wang, J. Zhu, Z. Guo and D. O'Hare, *J Mater Chem* **22:**19113-19121 (2012).

36 C. Li, J. Wan, E. N. Kalali, H. Fan and D.-Y. Wang, *J Mater Chem A* **3:**3471-3479 (2015).

37 C. Manzi-Nshuti, P. Songtipya, E. Manias, M. M. Jimenez-Gasco, J. M. Hossenlopp and C. A. Wilkie, *Polymer* **50:**3564-3574 (2009).

38 D.-Y. Wang, A. Leuteritz, Y.-Z. Wang, U. Wagenknecht and G. Heinrich, *Polym Degrad Stab* **95:**2474-2480 (2010).

39 G. Natta, P. Pino, P. Corradini, F. Danusso, E. Mantica, G. Mazzanti and G. Moraglio, *J Am Chem Soc* **77:**1708-1710 (1955).

40 J. K. Stille, *Chem Rev* **58:**541-580 (1958).

41 S. Zhang and A. R. Horrocks, *Prog Polym Sci* **28:**1517-1538 (2003).

42 S. Valdo Meille and S. Bruckner, *Nature* **340:**455-457 (1989).

43 A. T. Jones, J. M. Aizlewood and D. R. Beckett, *Makromol Chem* **75:**134-158 (1964).

44 M. R. Mani, R. Chellaswamy, Y. N. Marathe and V. K. Pillai, *Macromolecules* **49:**2197-2205 (2016).

45 M. R. Mani, R. Chellaswamy, Y. N. Marathe and V. K. Pillai, *Chem Commun* **51:**10026-10029 (2015).

46 M. Kawamura, T. Irie, T. Shiraishi and K. Tokunaga, *J Soc Chem Industry, Jap* **60:**162-165 (1957).

47 L. P. F. Benício, R. A. Silva, J. A. Lopes, D. Eulálio, R. M. M. d. Santos, L. A. d. Aquino, L. Vergütz, R. F. Novais, L. M. d. Costa, F. G. Pinto and J. Tronto, *Revista Brasileira de Ciência do Solo* **39:**1-13 (2015).

48 V. K. Agrawal and G. C. Trigunayat, *Acta Crystallogr Sect B* **24:**971-972 (1968).

49 W. Feitknecht and F. Held, *Helv Chim Acta* **27:**1480-1495 (1944).

50 W. Feitknecht and M. Gerber, *Helv Chim Acta* **25:**131-137 (1942).

51 W. Feitknecht, *Helv Chim Acta* **18:**28-40 (1935).

52 R. Allmann, *Acta Crystallogr Sect B* **24:**972-977 (1968).

53 Z. Ping Xu, P. Braterman and F. Yarberry, Layered Double Hydroxides (Ldhs), in *Handbook of Layered Materials*. CRC Press (2004).

54 W. Pies and A. Weiss, b2262, II.2.3.4 Simple hydroxide chlorides with H2O, NH3, in *Key Element: O Part 2*, ed by K. H. Hellwege and A. M. Hellwege. Springer Berlin Heidelberg, Berlin, Heidelberg, pp. 93-99 (1980).

55 A. Jaiswal, R. K. Gautam and M. C. Chattopadhyaya, Layered Double Hydroxides and the Environment: An Overview, in *Advanced Materials for Agriculture, Food, and Environmental Safety*. John Wiley & Sons, Inc., pp. 1-26 (2014).

56 J. M. Tour, *Nat Mater* **13:**545-546 (2014).

57 M. Chhowalla, H. S. Shin, G. Eda, L.-J. Li, K. P. Loh and H. Zhang, *Nat Chem* **5:**263-275 (2013).

58 M. R. Lukatskaya, O. Mashtalir, C. E. Ren, Y. Dall'Agnese, P. Rozier, P. L. Taberna, M. Naguib, P. Simon, M. W. Barsoum and Y. Gogotsi, *Science* **341:**1502-1505 (2013).

59 T. Hibino and W. Jones, *J Mater Chem* **11:**1321-1323 (2001).

60 M. Adachi-Pagano, C. Forano and J.-P. Besse, *Chem Commun* 91-92 (2000).

61 L. Li, R. Ma, Y. Ebina, N. Iyi and T. Sasaki, *Chem Mater* **17:**4386-4391 (2005).

62 Q. Wang and D. O'Hare, *Chem Commun* **49:**6301-6303 (2013).

63 R. Ma, Z. Liu, K. Takada, N. Iyi, Y. Bando and T. Sasaki, *J Am Chem Soc* **129:**5257-5263 (2007).

64 P. Kiliaris and C. D. Papaspyrides, *Prog Polym Sci* **35:**902-958 (2010).

65 Y. Gao, J. Wu, Q. Wang, C. A. Wilkie and D. O'Hare, *J Mater Chem A* **2:**10996-11016 (2014).

66 Z. Matusinovic and C. A. Wilkie, *J Mater Chem* **22:**18701-18704 (2012).

67 P.-J. Wang, X.-P. Hu, D.-J. Liao, Y. Wen, T. R. Hull, F. Miao and Q.-T. Zhang, *Ind Eng Chem Res* **56:**920-932 (2017).

68 M. Tanaka, I. Y. Park, K. Kuroda and C. Kato, *Bull Chem Soc Jpn* **62:**3442-3445 (1989).

69 L. Qiu, W. Chen and B. Qu, *Colloid Polym Sci* **283:**1241-1245 (2005).

70 W. Chen and B. Qu, *Chem Mater* **15:**3208-3213 (2003).

71 L. Qiu, W. Chen and B. Qu, *Polym Degrad Stab* **87:**433-440 (2005).

72 S. O'Leary, D. O'Hare and G. Seeley, *Chem Commun* 1506-1507 (2002).

73 B. Li, Y. Hu, J. Liu, Z. Chen and W. Fan, *Colloid Polym Sci* **281:**998-1001 (2003).

74 B. Nagendra, C. V. S. Rosely, A. Leuteritz, U. Reuter and E. B. Gowd, *ACS Omega* **2:**20-31 (2017).

75 B. Nagendra, K. Mohan and E. Bhoje Gowd, *ACS Appl Mater Interfaces* **7:**12399-12410 (2015).

76 B. Nagendra, A. Das, A. Leuteritz and E. B. Gowd, *Polym Int* **65:**299-307 (2016).

77 K. H. Storks, *J Am Chem Soc* **60:**1753-1761 (1938).

78 A. Keller, *Philos Mag* **2:**1171-1175 (1957).

79 R. Eppe, E. W. Fischer and H. A. Stuart, *J Polym Sci* **34:**721-740 (1959).

80 L. H. Sperling, *Introduction to Physical Polymer Science*, Wiley (2015).

81 F. Auriemma, G. C. Alfonso and C. De Rosa, *Polymer Crystallization II: From Chain Microstructure to Processing*, Springer International Publishing (2017).

82 E. Piorkowska and G. C. Rutledge, *Handbook of Polymer Crystallization*, Wiley (2013).

83 C. W. Bunn and T. C. Alcock, *Transactions of the Faraday Society* **41:**317-325 (1945).

84 C. W. Bunn, *Discussions of the Faraday Society* **5:**132-144 (1949).

85 S. Z. D. Cheng and B. Lotz, *Philosophical Transactions of the Royal Society of London Series A: Mathematical, Physical and Engineering Sciences* **361:**517-537 (2003).

86 B. Lotz and S. Z. D. Cheng, *Polym J* **40:**891-899 (2008).

87 W. Hao, W. Yang, H. Cai and Y. Huang, *Polym Test* **29:**527-533 (2010).

88 J. Tang, Y. Wang, H. Liu and L. A. Belfiore, *Polymer* **45:**2081-2091 (2004).

89 H. Zhao and R. K. Y. Li, *J Polym Sci, Part B: Polym Phys* **43:**3652-3664 (2005).

90 Z. Lin, Z. Huang, Y. Zhang, K. Mai and H. Zeng, *J Appl Polym Sci* **91:**2443-2453 (2004).

91 S. Jain, H. Goossens, M. van Duin and P. Lemstra, *Polymer* **46:**8805-8818 (2005).

92 M. Pracella, D. Chionna, A. Fina, D. Tabuani, A. Frache and G. Camino, *Macromol Symp* **234:**59-67 (2006).

93 M. A. L. Manchado, L. Valentini, J. Biagiotti and J. M. Kenny, *Carbon* **43:**1499-1505 (2005).

94 D. Wan, Z. Zhang, Y. Wang, H. Xing, Z. Jiang and T. Tang, *Soft Matter* **7:**5290-5299 (2011).

95 M. Naffakh, C. Marco and G. Ellis, *J Phys Chem B* **115:**10836-10843 (2011).

96 H. E. Miltner, N. Grossiord, K. Lu, J. Loos, C. E. Koning and B. Van Mele, *Macromolecules* **41:**5753-5762 (2008).

97 B. P. Grady, F. Pompeo, R. L. Shambaugh and D. E. Resasco, *J Phys Chem B* **106:**5852-5858 (2002).

98 A. R. Bhattacharyya, T. V. Sreekumar, T. Liu, S. Kumar, L. M. Ericson, R. H. Hauge and R. E. Smalley, *Polymer* **44:**2373-2377 (2003).

99 A. M. Díez-Pascual and M. Naffakh, *ACS Appl Mater Interfaces* **5:**9691-9700 (2013).

100 S. Zhao, F. Chen, C. Zhao, Y. Huang, J.-Y. Dong and C. C. Han, *Polymer* **54:**3680-3690 (2013).

101 J.-Z. Xu, Y.-Y. Liang, H.-D. Huang, G.-J. Zhong, J. Lei, C. Chen and Z.-M. Li, *J Polym Res* **19:**1-7 (2012).

102 P. H. Nam, P. Maiti, M. Okamoto, T. Kotaka, N. Hasegawa and A. Usuki, *Polymer* **42:**9633-9640 (2001).

103 A. W. Phillips, A. Bhatia, P.-w. Zhu and G. Edward, *Macromolecules* **44:**3517-3528 (2011).

104 S. P. Lonkar, S. Morlat-Therias, N. Caperaa, F. Leroux, J. L. Gardette and R. P. Singh, *Polymer* **50:**1505-1515 (2009).

105 Q. Wang, J. P. Undrell, Y. Gao, G. Cai, J.-C. Buffet, C. A. Wilkie and D. O'Hare, *Macromolecules* **46:**6145-6150 (2013).

106 D.-Y. Wang, A. Das, F. R. Costa, A. Leuteritz, Y.-Z. Wang, U. Wagenknecht and G. Heinrich, *Langmuir* **26:**14162-14169 (2010).

107 Y. Gao, J. Wu, Z. Zhang, R. Jin, X. Zhang, X. Yan, A. Umar, Z. Guo and Q. Wang, *J Mater Chem A* **1:**9928-9934 (2013).

108 X. Wang, Y. Sporer, A. Leuteritz, I. Kuehnert, U. Wagenknecht, G. Heinrich and D.-Y. Wang, *RSC Adv* **5:**78979-78985 (2015).

109 M. Avrami, *J Chem Phys* **8:**212-224 (1940).

110 J. D. Hoffman, J. I. Lauritzen, E. Passaglia, G. S. Ross, L. J. Frolen and J. J. Weeks, *Kolloid-Zeitschrift und Zeitschrift für Polymere* **231:**564-592 (1969).

111 J. I. L. Jr. and J. D. Hoffman, *J Appl Phys* **44:**4340-4352 (1973).

112 M. Gahleitner, *Prog Polym Sci* **26:**895-944 (2001).

113 R. Khare, J. J. de Pablo and A. Yethiraj, *Macromolecules* **29:**7910-7918 (1996).

114 N. G. McCrum, C. P. Buckley and C. B. Bucknall, *Solutions Manual to Accompany Principles of Polymer Engineering*, Oxford University Press (2000).

115 A. B. Morgan and J. W. Gilman, *Fire Mater* **37:**259-279 (2013).

116 C. Huggett, *Fire Mater* **4:**61-65 (1980).

117 A. Dasari, Z.-Z. Yu, G.-P. Cai and Y.-W. Mai, *Prog Polym Sci* **38:**1357-1387 (2013).

118 M. L. Janssens, *Fire Technology* **27:**234-249 (1991).

119 T. Kashiwagi, F. Du, J. F. Douglas, K. I. Winey, R. H. Harris and J. R. Shields, *Nat Mater* **4:**928-933 (2005).

120 D.-Y. Wang, A. Leuteritz, B. Kutlu, M. A. d. Landwehr, D. Jehnichen, U. Wagenknecht and G. Heinrich, *J Alloys Compd* **509:**3497-3501 (2011).

121 N.-J. Kang, D.-Y. Wang, B. Kutlu, P.-C. Zhao, A. Leuteritz, U. Wagenknecht and G. Heinrich, *ACS Appl Mater Interfaces* **5:**8991-8997 (2013).

122 F. R. Costa, U. Wagenknecht and G. Heinrich, *Polym Degrad Stab* **92:**1813-1823 (2007).

123 D. Baoxian and F. Zhengping, *Nanotechnology* **21:**315603 (2010).

124 B. Wang, K. Zhou, B. Wang, Z. Gui and Y. Hu, *Ind Eng Chem Res* **53:**12355-12362 (2014).

Chapter-2

Polypropylene/Layered Double Hydroxide (LDH) Nanocomposites: Influence of LDH Particle Size on the Crystallization Behavior of Polypropylene

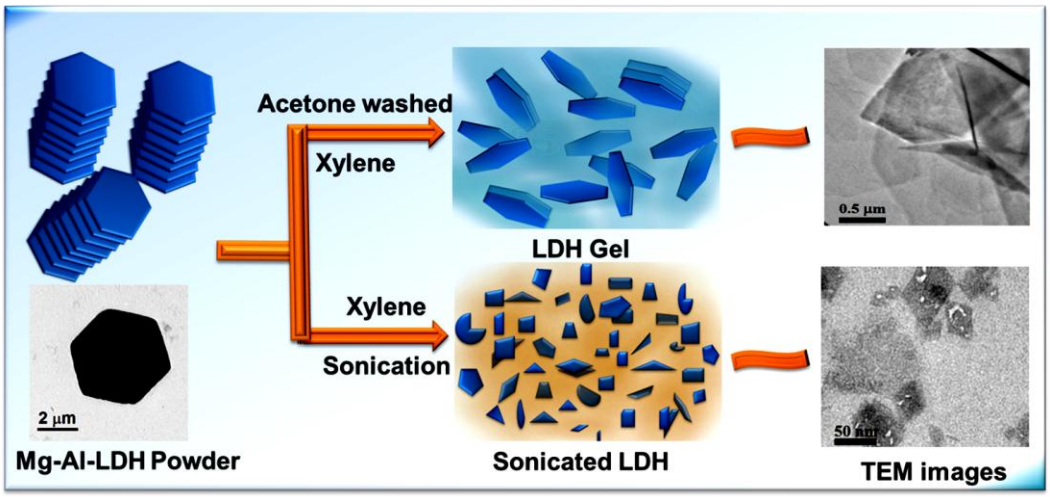

2.1. Abstract

Highly dispersed iPP nanocomposites were prepared by incorporating two different sized Mg-Al LDH nanoparticles with different loadings from 1 to 10 wt% using a modified solvent mixing method. Larger sized LDH nanoparticles (~3-4µm) were prepared from the gel form of Mg-Al LDH and the smaller sized nanoparticles (~50-200 nm) were prepared by sonication of as-synthesized LDH particles. Such obtained LDH nanoparticles were carefully characterized using Wide-angle X-ray diffraction (WAXD), transmission electron microscopy and scanning electron microscopy. WAXD and atomic force microscopy results indicate that the LDH nanoparticles were highly dispersed in iPP matrix. The influence of LDH nanoparticles size and concentration on the thermal stability, spherulitic morphology, melting behavior, isothermal crystallization kinetics and lamellar structure of iPP were investigated. Incorporation of low loadings of sonicated LDH

particles (e.g. 1-2.5 wt%) show substantial effect on thermal stability, spherulite size, crystallinity and crystallization half-time and lamellar morphology of iPP compared to the pure iPP and that of nanocomposites with larger LDH particles with same loadings. The better nucleation ability of iPP in presence of sonicated LDH can be attributed to the high surface area of LDH nanoparticles along with its better dispersibility within the polymer matrix. The incorporation of LDH nanoparticles doesn't change the crystallization growth mechanism and crystal structure of iPP.

2.2. Introduction

Polymer based nanocomposites filled with nanosized stiff particles have evolved and attracted great interests from both in industry and academia during the last two decades.[1-5] A range of layered materials of varying dimensions have been used as nanofillers, but the most commercial importance is engaged with layered materials such as clays and related phyllo-silicates.[2, 6,7] Performance of polymer nanocomposites strongly depends on the degree of dispersion and aspect ratio of layered materials in the polymer matrices. In particular, exfoliation of layered materials in polymer matrices has been shown to improve the flame retardancy, optical, thermal, rheological and mechanical properties of base polymer.[1-7] In most cases, layered materials are surface-modified with organic compounds for improving the dispersion in the polymer matrix.

Lately, LDH are considered as a new emerging class of nanofillers for the preparation of multifunctional polymer/LDH nanocomposites.[1, 5, 8, 9] LDH layers are 0.48-0.49 nm thick, and their lateral dimensions can be varied between few nm and several μm by adjusting the synthetic conditions.[10-13] Important feature of these materials is tremendous flexibility in tuning the composition of both inorganic layers as well as balancing anions in the interlayer space.[1] Preparation of highly exfoliated polymer nanocomposites using LDH is always a great challenge because of the stronger electrostatic interlayer interactions due to their higher charge density. To date, variety of polymer systems were used in nanocomposites preparation with LDH, which include polyethylene[14-16], polypropylene[17-20], polyamides[21, 22], polystyrene[23], polylactic acid[24, 25], poly(methyl methacrylate)[26], poly(vinyl chloride)[27], etc. In most of these nanocomposites, either the LDH was modified with the organic compounds (surfactants) or the polymer itself was

modified to facilitate the miscibility between the hydrophobic polymer and the hydrophilic LDH to achieve intercalated or exfoliated nanocomposites.[1, 9, 14-20] However, these modifications could lead to additional steps in the preparation of nanocomposites, unwanted change in the polymer characteristics and possible degradation of organic modifiers upon the processing of these nanocomposites.[14] The end-use applications of polymer nanocomposites would be greatly expanded with surfactant-free materials. Varieties of LDH have been used in the preparation of nanocomposites with polymers, which include Co-Al LDH,[19] Mg-Al LDH,[17, 18] Zn-Al LDH,[16, 28] etc. In the present study, Mg-Al LDH was chosen because of its white colour and its resemblances with the commonly used fire retardant metal hydroxides.

Few reports are available in the literature to demonstrate the exfoliation of the LDH and the preparation of exfoliated polymer/LDH nanocomposites using surfactant-free LDH.[18, 28-30] The pioneering group of Dermot O'Hare has reported an aqueous miscible organic solvent treatment (AMOST) method for the preparation of stable dispersions of surfactant free LDH in nonpolar solvents and the subsequent preparation of exfoliated polypropylene/LDH nanocomposites (PP) by solution mixing.[18, 28, 31] The advantage of AMOST method is the conversion of the hydrophilic LDH layers to hydrophobic, so that the miscibility can be achieved between the LDH and hydrophobic polymer.

In semicrystalline polymer nanocomposites, the dispersed nanofillers can induce the structural and morphological changes of the polymer matrix and therefore control the various properties of the nanocomposites. The study on crystallization of polymer nanocomposites is of great technical importance, in view of the fact that the nanofillers alter the crystallization behavior and the extent of crystallinity that in turn depends on the processing conditions. A number of studies were aimed to elucidate the influence of nanosized filler on the crystallization behavior of semicrystalline polymers.[3, 32, 33] iPP is one of those most widely used thermoplastic polymers in the polymer industry because of its easy processability and good balance between properties and cost. In spite of extensive studies on the crystallization behavior of iPP in presence of various nanofillers such as layered silicates[34, 35], carbon nanotubes[36, 37] and graphene[38], a limited attention has been given on iPP/LDH nanocomposites. Lonkar et al. studied the crystallization

behavior of iPP in presence of organically modified LDH and found that LDH could alter the type of nucleation, growth and geometry of PP crystals.[20, 39] However, to our knowledge, no studies have been conducted on the crystallization behavior of iPP in presence of unmodified LDH.

In the present study, we prepared iPP/Mg-Al LDH nanocomposites by two different methods using unmodified LDH. In first method, the gel form of Mg-Al LDH was directly dispersed in iPP solution to prepare highly dispersed nanocomposites. In another method, for the first time, sonicated LDH was used for the preparation of highly dispersed nanocomposites. Sonication of LDH for longer duration leads to the formation of hydrophobic surfaces, which enable them to be highly dispersible in non-polar polymer solutions. This study also aims at unravelling the influence of unmodified LDH and its particle size on the crystallization behavior of iPP using differential scanning calorimetry and polarized optical microscopy. It was found that, iPP/LDH nanocomposites containing smaller sized LDH nanoparticles (~50-200 nm) showed better thermal stability and nucleation ability compared to that of iPP/LDH nanocomposites containing larger sized LDH nanoparticles (~3-4 μm) with same loading.

2.3. Results and Discussion

2.3.1. Synthesis and Characterization of Mg-Al LDH

The Mg-Al LDH used in this study was synthesized by co-precipitation method under ambient atmospheric conditions.[40] The powder X-ray diffraction patterns confirmed the formation of LDH structure, exhibiting sharp reflections corresponding to the (00n) planes (Figure 2.1a). The SEM (Figure 2.1b) and TEM (Figures 2.2a) images show the stacked hexagonal platelets with a mean lateral size of 3.5 μm. As-prepared LDH platelets had a dark contrast, indicating the presence of several layers of hexagonal platelets in a single particle. The energy-dispersive X-ray spectra (EDS) confirmed the composition of the as-prepared Mg-Al LDH (Figure 2.2b). The dominant oxygen peak in EDS indicates the presence of water molecules within the layers of the LDH platelets. FTIR spectrum of the Mg-Al LDH also confirmed the presence of CO_3^{2-}, NO_3^- and water molecules (Figure 2.3a). The characteristic band for interlayer carbonate (CO_3^{2-}) and interlayer nitrate (NO_3^-) were observed at 1356 cm^{-1} and 1382 cm^{-1}, respectively. Urea, which was used as

base to prepare LDH, readily undergoes hydrolysis in presence of water at 100 °C to give ammonium carbonate. Such obtained ammonium carbonate further converted into ammonia and hydrogen carbonate.[41] These conditions favored the formation of CO_3^{2-} along with the NO_3^-. The broad band at 3444 cm^{-1} is due to the O-H stretching of the metal hydroxide layer and interlayer H_2O molecules. Another band centered at 1607 cm^{-1} is assigned to be the interlayer water (H_2O) molecule.

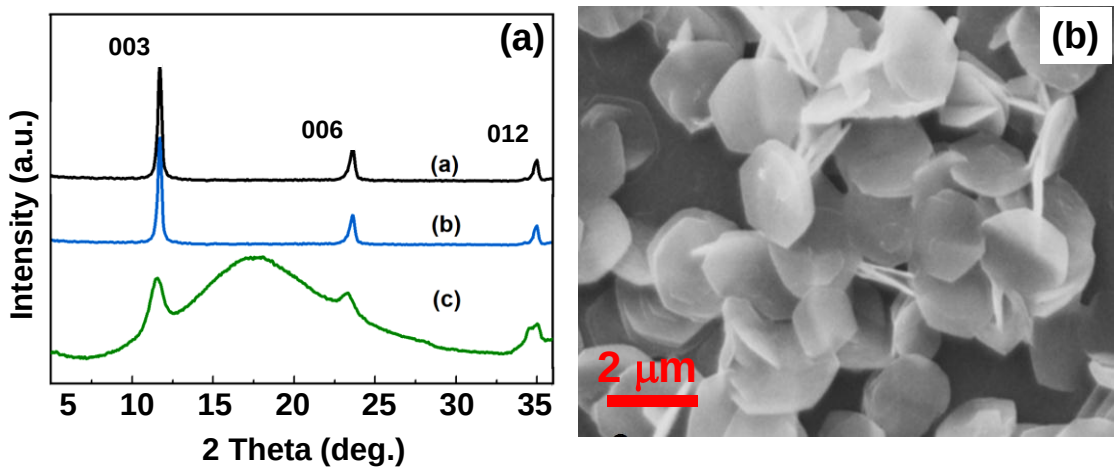

Figure 2.1. Powder X-ray diffraction patterns of (a) as-prepared Mg-Al LDH, sonicated LDH and Mg-Al LDH gel, (b) SEM image of as-prepared Mg-Al LDH.

2.3.2. Swelling and Exfoliation of Mg-Al LDH

O'Hare and co-workers reported that treatment of as-prepared LDH by aqueous miscible organic solvent converts the hydrophilic LDH to hydrophobic.[18] Herein, we adopted their method to prepare the dispersions of LDH in non-polar solvents like xylene. Further storage of such dispersion resulted in a transparent gel-like aggregate (Figure 2.3b). Figure 2.1a shows the powder X-ray pattern of gel-like aggregate. The 00n reflections are somewhat broad and low in intensity, which may be due to stacking disorder of LDH platelets in the swollen state. A broad amorphous-like halo was also observed at $2\theta \sim 17.5°$ due to the scattering of xylene. It is also important to mention here that X-ray measurements of gels were made in the open capillaries, where there was a possibility for solvent evaporation during the X-ray measurement.

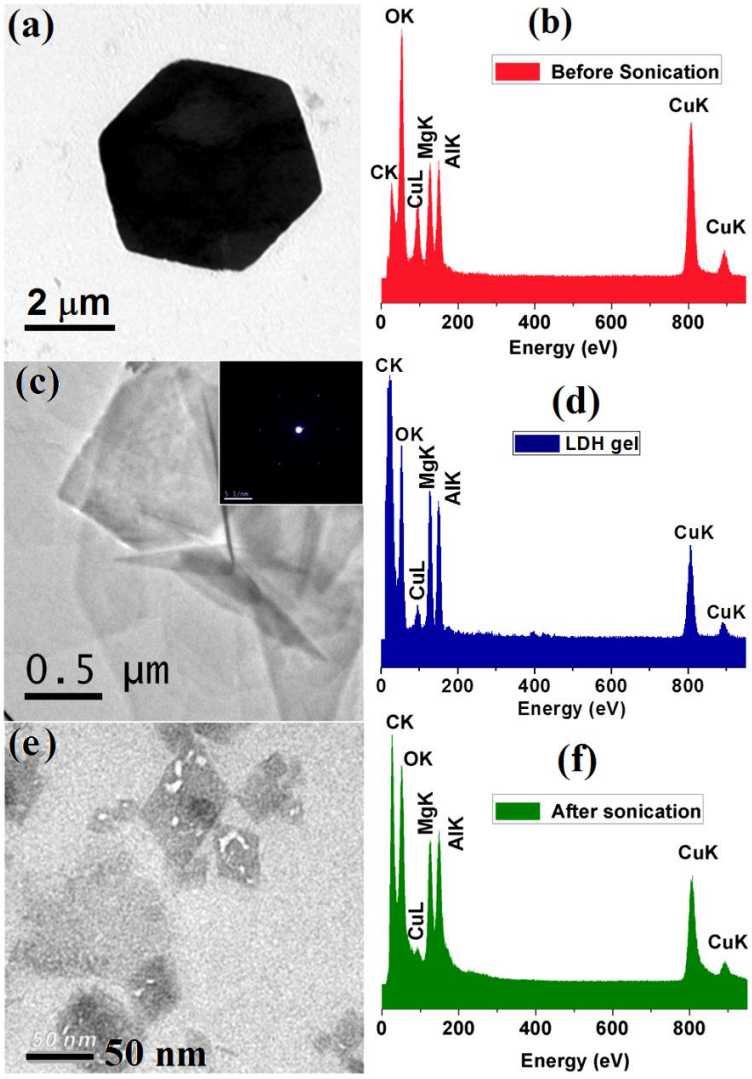

Figure 2.2. TEM images of (a & b) as-prepared Mg-Al LDH and corresponding EDS spectrum, (c & d) delaminated Mg-Al LDH and corresponding EDS spectrum. Inset is the Selected Area Electron Diffraction (SAED) pattern of delaminated Mg-Al LDH, (e & f) sonicated LDH and corresponding EDS spectrum.

TEM image of Mg-Al LDH gel dispersed in xylene clearly showed the delamination of LDH platelets to single-layer nanosheets (Figure 2.2c). Due to the thin nature of exfoliated single-layer nanosheets, contrast of single-layer is very weak. The selected area electron diffraction (SAED) (inset of Figure 2.2c) shows hexagonally arranged spots, indicating that the delaminated nanosheets are single crystalline.[40] The corresponding EDS (Figure 2.2d) shows the drastic reduction in the oxygen peak compared to their bulk LDH structure, indicating the removal of interlayer H_2O molecules from the stacked structure. The surface area measured for LDH gel (after drying) was 200 ± 5 m^2/g. Liquid exfoliation of LDH is known for quite some time, and it has emerged as a process in producing the novel two-

dimensional materials.[29, 42, 43] Wu et al., demonstrated the gel formation in LDH-NO_3 in formamide without incorporation of surfactants.[44] However, their procedure did not work for carbonate containing LDH as carbonate is a much stronger hydrotalcite-builder than nitrate. Very recently, Song et al., used anion exchange process to increase the inter-layer spacing and subsequently delaminated the bulk LDH to single-layer nanosheets.[29] In the present study, by taking the advantage of AMOST method, we successfully exfoliated the bulk Mg-Al LDH to single-layer nanosheets.

2.3.3. Sonication of Mg-Al LDH

Ultrasonic vibration (sonication) has been used in the fabrication of two-dimensional nanosheets such as graphene, transition metal oxides, and transition metal dichalcogenides from bulk layered materials in liquid.[43, 45, 46] In the present study, we used sonication method to prepare stable dispersions of LDH in non-polar solvents. Figure 2.1a shows the powder X-ray diffraction pattern of sonicated LDH powder. The sharp reflections corresponding to the (00n) planes indicate the retention of crystal structure upon the sonication. No traces of impurities were observed in sonicated LDH powders. The TEM (Figure 2.2e) of the sonicated sample show the broken platelets of LDH layers and the lateral size reduced to few tens of nanometers. The corresponding energy-dispersive X-ray spectrum shown in Figure 2.2f is consistent with the EDS spectrum of bulk LDH. However, a noteworthy change was observed upon the sonication, i.e., the oxygen peak decreased in intensity drastically indicating the removal of water molecules from bulk LDH. During sonication, water molecules present within the LDH layers are replaced by xylene molecules, weakening the interlayer attraction. Then, further sonication can completely take apart the layers, resulting in an exfoliated dispersion. Simultaneously, the LDH layers are broken into small fragments in the sonication process. The surface area measured for sonicated LDH powder was 710 ± 5 m^2/g. Qu and co-workers observed the breakage of organically modified Zn-Al LDH platelets in xylene with refluxing time.[47]

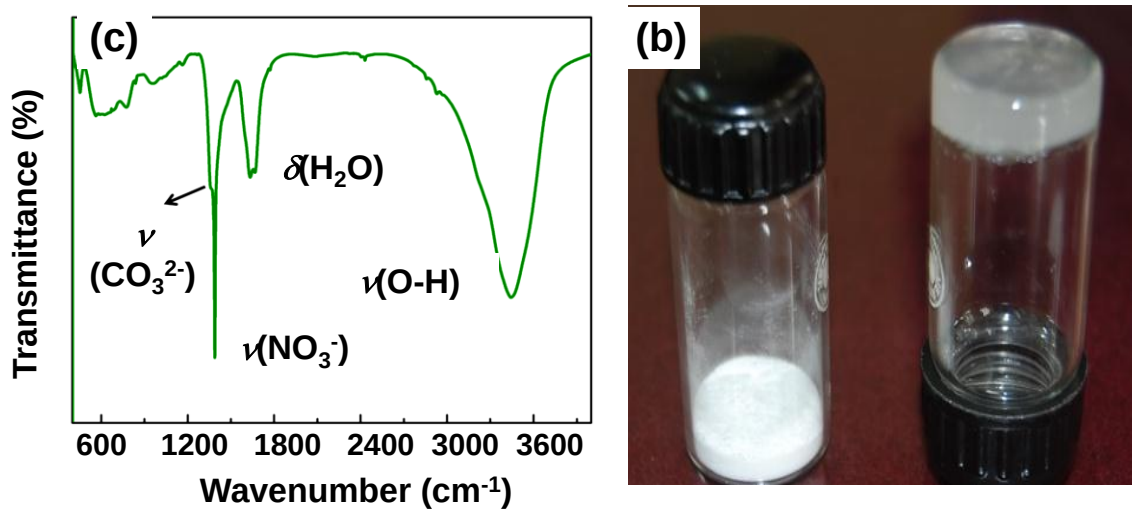

Figure 2.3. (a) FTIR spectrum of as-synthesized Mg-Al LDH, and (d) Photographs of Mg-Al LDH powder and LDH gel formed in xylene.

2.3.4. Synthesis, Structure and Morphology of iPP/Mg-Al LDH Nanocomposites

Figure 2.4 shows the schematic illustration of the method used for the preparation of highly dispersed iPP nanocomposites by two different methods using Mg-Al LDH. In first method, a transparent gel-like aggregate of Mg-Al LDH was directly added to the iPP solution. Treatment of as-prepared LDH with acetone followed by dispersion in xylene helps in the removal of interlayer H_2O molecules from the stacked LDH structure. The swollen LDH platelets were readily dispersed to single-layer nanosheets in the polymer solution to obtain the highly dispersed nanocomposites. In another method, sonicated Mg-Al LDH (broken LDH fragments) was added to iPP solution to obtain highly dispersed nanocomposites. As mentioned in the preceding section, replacement of water molecules with organic solvents weakens the interaction between the Mg-Al LDH platelets, which helps in delamination of these platelets when dispersed in iPP solution. The resultant solution was poured into ethanol. The precipitate was filtered, washed with excess ethanol and dried under vacuum overnight. In order to compare the properties of iPP and iPP/LDH nanocomposites under the similar conditions, pristine iPP powder was also prepared under similar treatment.

Figure 2.5 shows the X-ray diffraction patterns of Mg-Al LDH, iPP and its nanocomposites containing different amounts of LDH. Unlike other reported

iPP/LDH nanocomposites, the reflections corresponding to the (00n) planes of LDH are not observed in both the nanocomposites (prepared using LDH gel and sonicated LDH).[18, 48] Such disappearance of LDH reflections is due to the loss of periodicity of the LDH. These results suggest that Mg-Al LDH platelets are exfoliated and well dispersed in the polymer matrix.

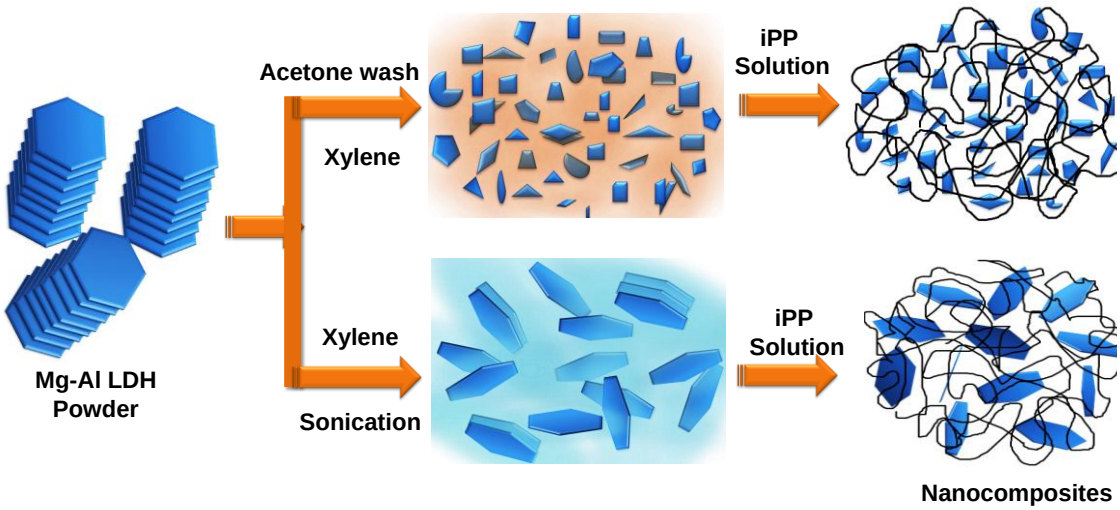

Figure 2.4. Schematic illustration of the polymer nanocomposite preparation based on iPP and Mg-Al LDH.

IPP and nanocomposites are crystallized isothermally at 130 °C after melting at 200 °C under strictly controlled conditions to understand the influence of LDH on polymorphic behavior of iPP as we mentioned in experimental section. Both iPP and iPP/LDH nanocomposites show reflections at 2θ = 14.2°, 17.0°, 18.7°, 21.3°, and 22.1° corresponding to the monoclinic α form of iPP (Figure 2.5.).[49] No change in the polymorphism of iPP was observed in the presence of LDH platelets. Table 2.1 shows the degree of crystallinity of iPP matrix in the iPP/LDH nanocomposites. The degree of crystallinity was calculated as the ratio of the area under the crystalline peaks to the total area under the X-ray scattering curve. It can be clearly seen that the nanocomposites prepared using LDH gel showed less crystallinity (~57%) compared to the nanocomposites prepared using sonicated LDH (~65%). The low crystallinity of the nanocomposites using LDH gel is due to the fact that the crystalline lamellar growth of iPP might be hindered to some extent in presence of larger LDH particles having lateral size 2-3 μm.

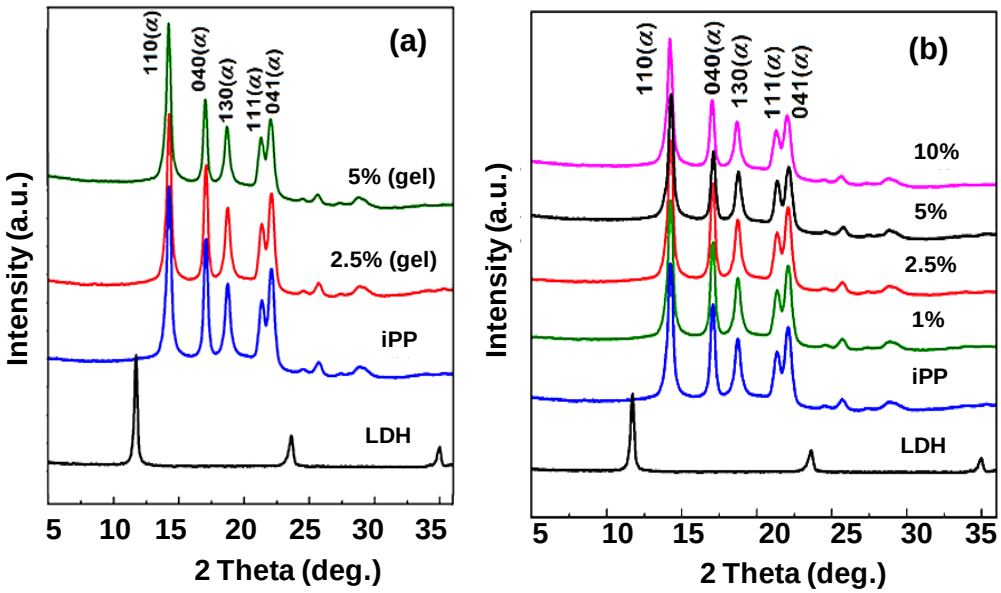

Figure 2.5. Powder X-ray diffraction data for (a) iPP nanocomposites prepared by using LDH gel and (b) iPP nanocomposites prepared by using sonicated LDH. For the purpose of comparison, powder X-ray diffraction data iPP and LDH are shown in both (a) and (b).

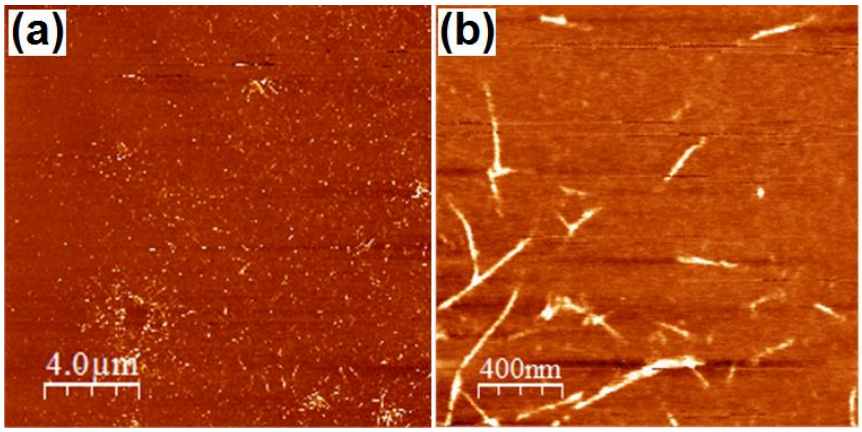

Figure 2.6. AFM images of iPP nanocomposite film containing 10 wt% of sonicated LDH (a) 20 x 20 μm (b) 2 x 2 μm.

The dispersion of LDH particles in iPP matrix was further confirmed by AFM measurements. Nanocomposite thin film was prepared by melt pressing the powder samples in between the coverslips. Figure 2.6 shows the AFM phase images of 10 wt% of sonicated LDH containing nanocomposite film. It is obvious from the figure that nanosized LDH platelets with few nm thickness and few hundreds of nm length are homogeneously dispersed in the iPP matrix. It is worth mentioning here that the breadth of the nanoparticles/nanodots appears much larger in AFM image than the true values due to the AFM tip surface convolution effect.[50, 51]

Table 2.1: Degree of crystallinity, average number of spherulites and average diameter of the spherulites calculated after melt crystallization at 130 °C, 50% weight loss temperature for iPP and its nanocomposites.

Sample	% of X_c by WAXS (± 0.5)	Average number of spherulites counted on an area of 2.13×10^{-2} m^2	Average diameter of spherulites (μm)	$T_{0.5}$ (°C) (± 1)
iPP	65	26	40.0	411
iPP-LDH Gel (2.5%)	59	26	35.0	434
iPP-LDH Gel (5%)	57	60	20.0	431
iPP- Sonicated LDH (1%)	65	600	8.0	448
iPP- Sonicated LDH (2.5%)	64	520	8.0	439
iPP- Sonicated LDH (5%)	63	560	8.0	433
iPP- Sonicated LDH (10%)	66	320	12.0	430

2.3.5. Thermal Degradation Behavior of iPP/Mg-Al LDH Nanocomposites

The influence of nanocomposites preparation method and various loadings of LDH on the thermal stability of iPP were investigated by TGA under nitrogen atmosphere. The corresponding TGA thermograms are shown in Figure 2.7. The 50% weight loss temperature ($T_{0.5}$) measured for various samples are summarized in Table 2.1. All the nanocomposite samples showed higher thermal stability than that of the pure iPP. Nanocomposites prepared using the gel form of LDH showed lower thermal stability than that of the nanocomposites prepared using same wt% of sonicated LDH. However, significant differences are seen in thermal stability of nanocomposites prepared using different wt% of sonicated LDH. The nanocomposite prepared with 1 wt% of sonicated LDH showed better thermal stability than the other nanocomposites. The $T_{0.5}$ increases from 411 °C for pure iPP to 448 °C with 1 wt% of sonicated LDH, and then gradually decreased to 430 °C (10 wt% of sonicated LDH) with the increase in wt% of sonicated LDH loadings. O'Hare and co-workers reported 9 wt% LDH as optimal loading for the nanocomposites prepared using acetone washed LDH.[18] In another study, the same group showed higher thermal stability for iPP at 1 wt% LDH loadings in surfactant-modified Mg-

Al LDH/PP nanocomposites synthesized by microemulsion method.[17] Based on the results obtained in this chapter for the LDH gel samples and the literature data, we are speculating here that the radicals generated during degradation were trapped by the well dispersed LDH nanoparticles.[17, 18] Lower loadings of sonicated LDH might be dispersed well in iPP matrix compared to excessive loadings, and probably is the reason why $T_{0.5}$ is higher for lower LDH loadings in nanocomposites prepared using sonicated LDH. It is also worth mentioning here that the nanocomposites prepared using gel form of LDH has less number of dispersed particles compare to that of nanocomposites prepared by sonicated LDH with equivalent amounts of LDH loadings. It might be the reason for lower thermal stability of nanocomposites containing gel form of LDH compared to that of nanocomposites with sonicated LDH.

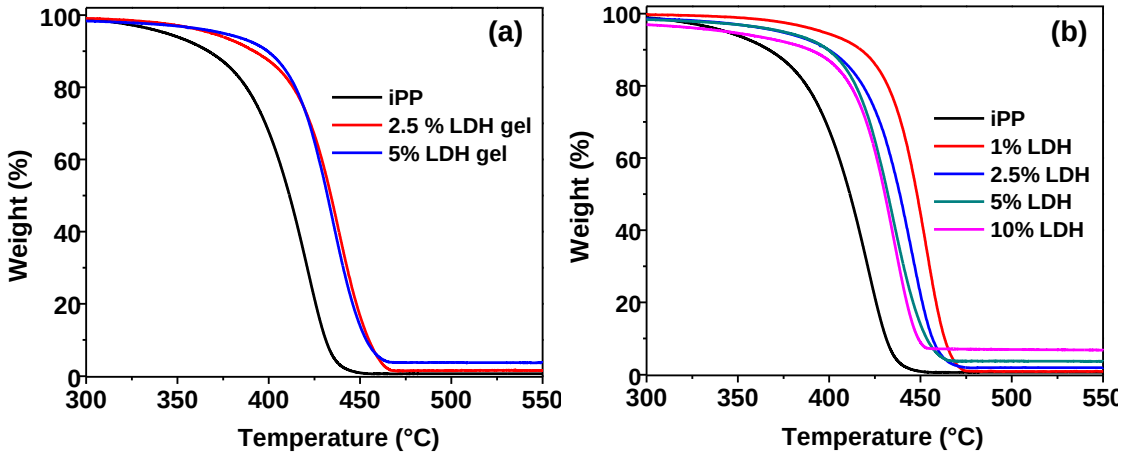

Figure 2.7. TGA thermograms for (a) iPP/LDH gel nanocomposites and (b) iPP/sonicated LDH nanocomposites.

2.3.6. Crystallization Behavior of iPP/Mg-Al LDH Nanocomposites

Figure 2.8 shows the POM images of iPP and its nanocomposites prepared using both sonicated LDH and gel form of LDH after isothermal crystallization at 130 °C. Under the given conditions (samples melted at 200 °C for 3 min then rapidly cooled to isothermal crystallization temperature 130 °C for 30 min), pure iPP crystallized into larger spherulites with an average diameter of ~40 μm. Due to the slow crystallization rate, these spherulites grow slowly and collide with each other (Fig. 2.8a). Upon the addition of sonicated LDH, the nucleation density increased and the diameter of the spherulites reduced significantly (Fig. 2.8b-d and Table 2.1). The uniform size of the spherulites in iPP/LDH nanocomposites (1 wt%

sonicated LDH) suggest that highly dispersed LDH platelets act as nucleation sites and barricade iPP spherulite growth. On further increasing the sonicated LDH loadings, the diffuse Maltese cross patterns were observed. On the other hand, when the gel form of LDH was used, the spherulites are imperfect, and the sizes are slightly smaller than that of pure iPP (Fig. 2.8e & 2.8f and Table 2.1). The texture of these spherulites is different from that of the pure iPP. The presence of larger LDH particles hinders the polymer chain diffusion and resulted in imperfect spherulites. It is also worth mentioning here that the nanocomposites prepared with the gel form of LDH showed lower crystallinity compared to that of pure iPP or other nanocomposites. It was also observed that the size of the spherulites decreased with the increase in LDH content in nanocomposites prepared using the gel form of LDH. By comparing the effect of preparation method of nanocomposites on the crystalline morphology of iPP, it is apparent that sonicated LDH method provides the largest number of nuclei due to the better dispersion of LDH platelets in iPP matrix.

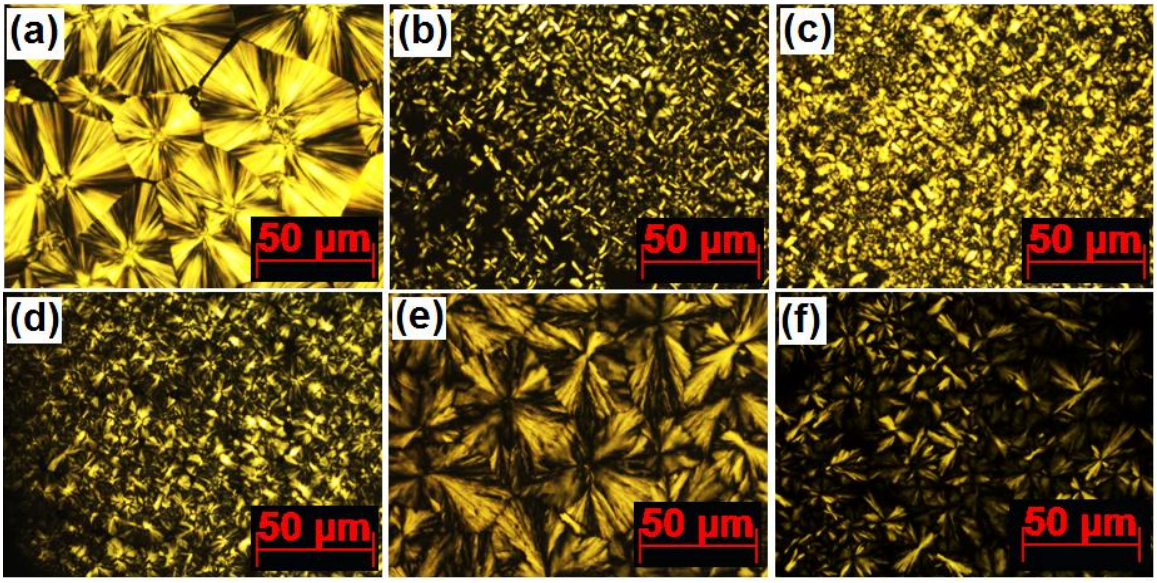

Figure 2.8. Polarized optical micrographs of pure iPP and its nanocomposites crystallized isothermally at 130°C. (a) iPP, (b) iPP/1 wt% sonicated LDH, (c) iPP/5 wt% sonicated LDH, (d) iPP/10 wt% sonicated LDH, (e) iPP/2.5 wt% of LDH gel and (f) iPP/5 wt% of LDH gel.

The effect of LDH on the isothermal melt crystallization kinetics of iPP was studied using DSC. The thermal program employed for the isothermal crystallization is depicted in Figure 2.9a. Figure 2.9(b & c) shows the DSC thermograms of pure iPP and its nanocomposites crystallized at 130 °C. The

relative crystallinity (X_t) at a given crystallization time was calculated from the DSC exotherms and the plots of X_t against crystallization time for all the samples are shown in Figure 2.10.

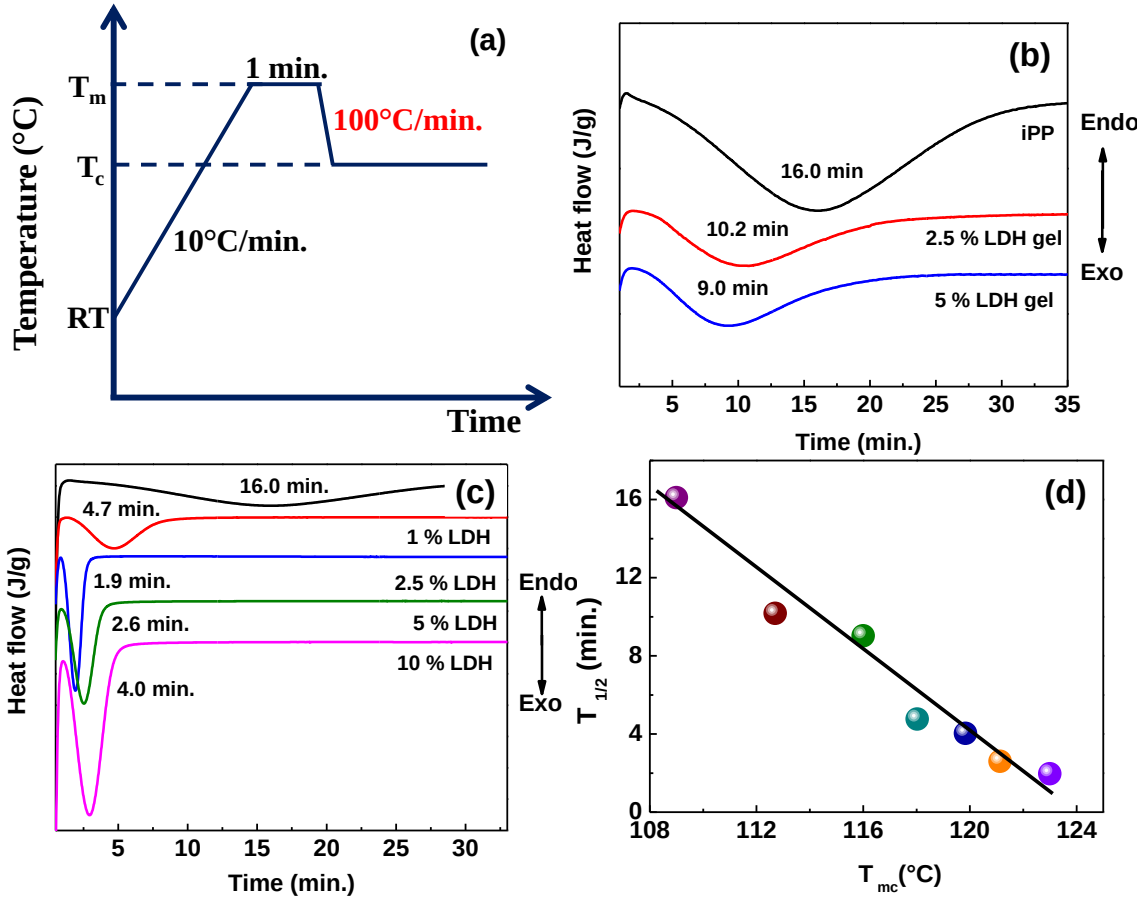

Figure 2.9. (a) Thermal programme used for the isothermal crystallization, crystallization isotherms obtained at 130 °C for pure iPP and its nanocomposites (b) iPP/LDH gel nanocomposites, (c) iPP/sonicated LDH nanocomposites and (d) crystallization half-time (measured at isothermal crystallization temperature 130°C) versus melt crystallization temperature (measured non-isothermally during melt cooling at 10°C/min).

It is obvious that all these curves exhibit a sigmoid dependence on time. The crystallization half-time ($t_{1/2}$), which is defined as a half period from the onset of crystallization to the end of crystallization, measured for various samples are summarized in Table 2.2. The crystallization half-time of pure iPP was 16.1 min. When the LDH was introduced into IPP, the crystallization half-time was decreased for all the nanocomposites irrespective of the preparation method. Both the induction time and the width of the exotherm decreased, reflecting an enhancement in the crystallization rate of iPP in presence of LDH particles.

However, significant differences have been observed in the crystallization rate of nanocomposites prepared by different methods. When the gel form of LDH was added into iPP, the crystallization half-time decreased moderately with the increase of LDH content. On the other hand, when the sonicated LDH was added into iPP, the crystallization rate was greatly enhanced, demonstrating the high nucleation ability of sonicated LDH particles. As the sonicated LDH loadings increase, the crystallization half-time first decreases from 16.1 min for pure iPP to 1.9 min with 2.5 wt% of sonicated LDH. Further increase in the LDH content, the crystallization half-time was increased to 4 min with 10 wt% of sonicated LDH. These results suggested that 2.5 wt% of sonicated LDH is the optimal loading for the effective crystallization of iPP due to its better dispersion in iPP matrix. As observed in the AFM image shown in Figure 2.6, higher loadings of LDH shows some agglomerates and it might be responsible for the slower crystallization of iPP with higher loadings. The better nucleation ability of iPP in presence of sonicated LDH might be due to the high surface area of broken LDH platelets along with its better dispersibility within the polymer matrix.

Isothermal crystallization kinetics for pure iPP and its nanocomposites were analyzed using Avrami equation according to the dependence of $X(t)$ on the crystallization time (t).[52, 53]

$$\mathbf{1 - X(t) = \exp(-Kt^n)} \qquad \mathbf{(2.1)}$$

Where $X(t)$ is the relative crystallinity, n is the Avrami exponent (which is dependent on the nature of nucleation and crystal growth geometry), and K is the overall isothermal crystallization rate constant connected with both nucleation and crystal growth contributions. The linear form of eq 2.1 can be expressed by taking a logarithmic transformation:

$$\mathbf{\ln[-ln(1 - X_t)] = \ln K + n \ln(t)} \qquad \mathbf{(2.2)}$$

By plotting $\ln[-ln(1 - X_t)]$ *versus* $\ln(t)$, the Avrami parameters (n and K) may be directly obtained from the slope and the intercept, respectively, from the early linear segment. Figure 2.11 shows such plots for pure iPP and its nanocomposites prepared by using LDH gel and sonicated LDH. Table 2.2 summarizes the Avrami constants estimated for various samples crystallized at 130°C. The n value of pure iPP was ~2.6, which was comparable to the literature values.[54, 55]

This *n* value might be attributed to a heterogeneous nucleation followed by diffusion controlled spherulite growth (mixed two-dimensional (2D) and three-dimensional (3D) crystal growth). The nanocomposites prepared using the gel form of LDH showed *n* value similar to the pure iPP suggesting that the delaminated LDH platelets did not change the crystallization mechanism of iPP. On

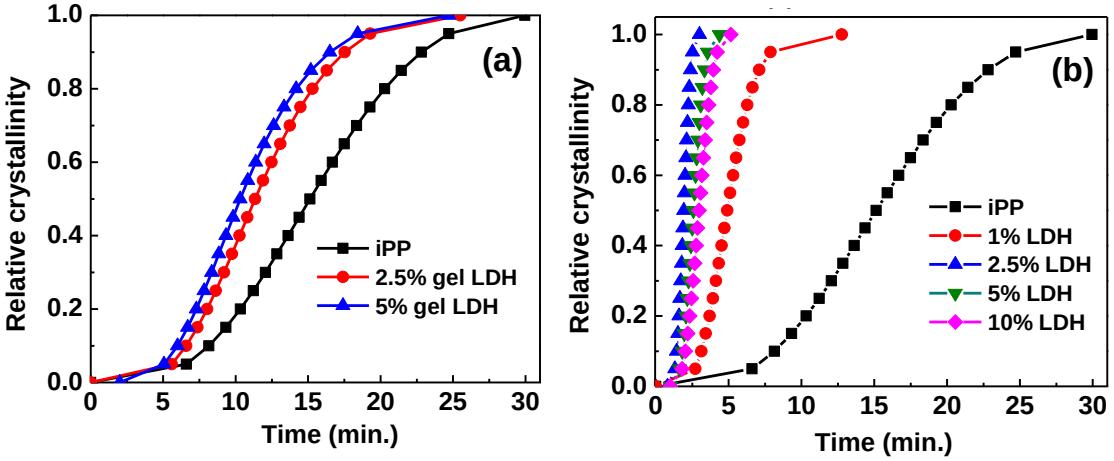

Figure 2.10. Variation in relative crystallinity with crystallization time for pure iPP and its nanocomposites crystallized isothermally at 130 °C (a) iPP/LDH gel nanocomposites and (b) iPP/sonicated LDH nanocomposites.

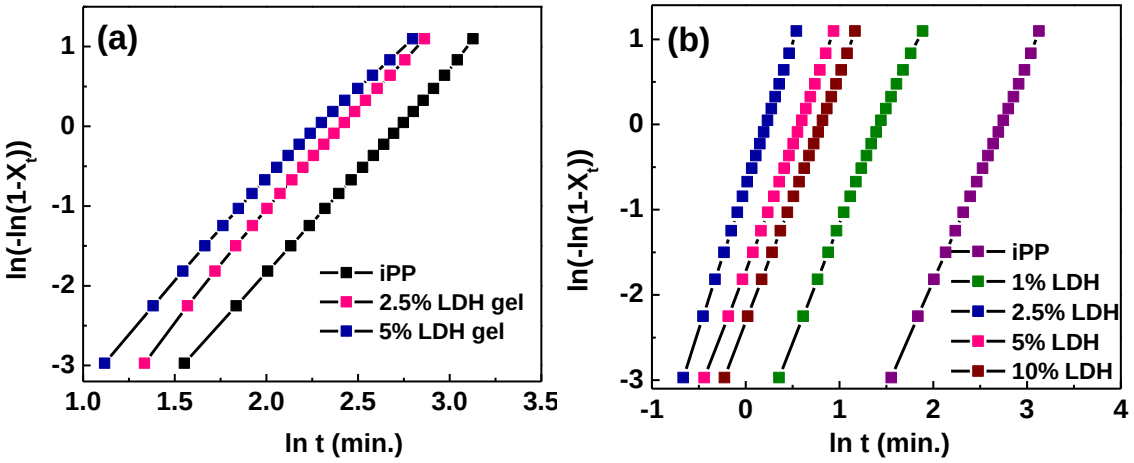

Figure 2.11. Plots of $\ln[-ln(1-X_t)]$ *versus* ln (*t*) for pure iPP and its nanocomposites crystallized isothermally at 130°C. (a) iPP/LDH gel nanocomposites, and (b) iPP/sonicated LDH nanocomposites.

The other hand, the *n* value fluctuates within the range of 2.8-3.4 for the nanocomposites prepared using sonicated LDH, also indicating the same crystallization mechanism. The *n* value around three is typical for a rapidly nucleating system undergoing 3D crystal growth. The DSC results discussed here are very much consistent with iPP spherulitic morphology, which was shown in Figure 2.8.

First DSC cooling thermograms from the melt of the corresponding samples are shown in Figure 2.12. The melt crystallization temperature (T_{mc}) is often used to measure the crystallization rate of semicrystalline polymers. Table 2.2. summarizes the T_{mc} values obtained for iPP and various nanocomposites. Figure 2.9d shows a plot of crystallization half-time *versus* T_{mc}. The linear behavior shows the consistency in the crystallization rate of iPP and its nanocomposites by isothermal and non-isothermal crystallization methods. Similar conclusions as those made in the preceding section may be drawn about the effect of LDH on the crystallization rate of iPP.

Table 2.2: Crystallization half-time, melt crystallization temperature, melting temperature and Avrami constant of iPP and its nanocomposites.

	$t_{1/2}$ (min.) at 130 °C (± 0.2)	T_{mc} °C (± 0.3)	T_m °C (± 0.5)	Avrami Constant (n) (± 0.05)
iPP	16.1	109	165.1	2.6
iPP-LDH Gel (2.5%)	10.3	112.7	151.4	2.6
iPP-LDH Gel (5%)	9.3	116	151.4	2.5
iPP- Sonicated LDH (1%)	4.7	118.0	158.7	2.8
iPP- Sonicated LDH (2.5%)	2.0	123	163.8	3.4
iPP- Sonicated LDH (5%)	2.7	121.1	160.7	3.0
iPP- Sonicated LDH (10%)	3.9	119.8	163.5	2.9

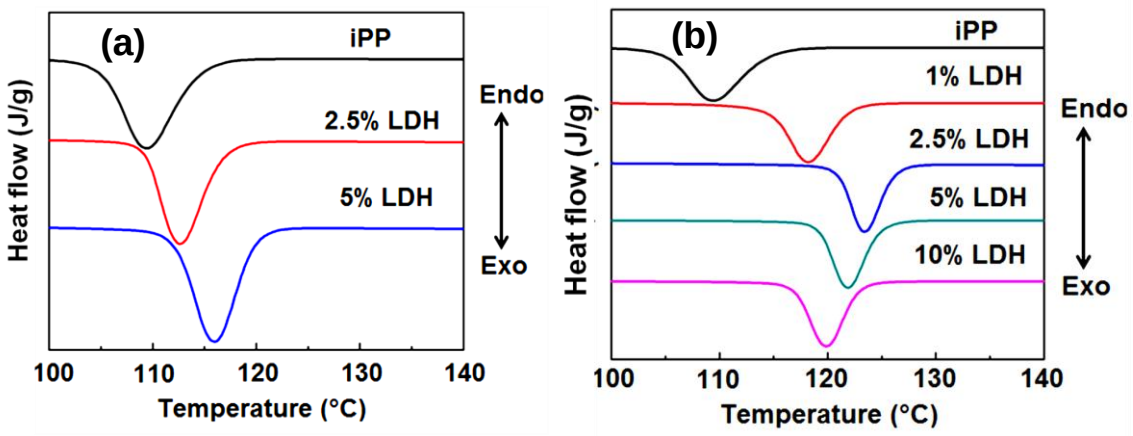

Figure 2.12. DSC cooling thermograms of iPP and its nanocomposites crystallized non-isothermally after melting at temperature 200 °C for 2 min. (a) iPP/LDH gel nanocomposites using and (b) iPP/sonicated LDH nanocomposites.

2.3.7. Melting Behavior of iPP/Mg-Al LDH Nanocomposites

The influence of LDH particles size and concentration on the melting behavior of iPP were studied by heating the isothermally crystallized iPP samples at a heating rate of 10 °C/min. Figure 2.13 shows the melting thermograms of iPP and its nanocomposites containing different sized LDH particles (prepared by the gel form of LDH and sonicated LDH). Clearly, the size of LDH has a dramatic impact on the melting behavior of iPP.

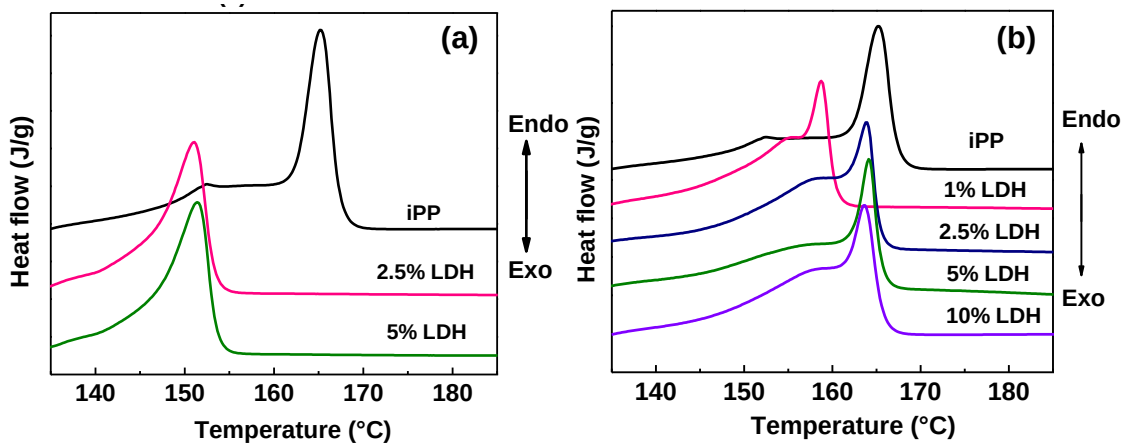

Figure 2.13. DSC melting thermograms for pure iPP and its nanocomposites crystallized isothermally at 130 °C. (a) iPP/LDH gel nanocomposites, and (b) iPP/sonicated LDH nanocomposites.

The melting temperatures of various samples are summarized in Table 2.2. Pure iPP shows double melting behavior with a dominant peak at 165.1 °C. X-ray diffractograms obtained for these samples ruled out the possibility of different crystalline polymorph, which is not the reason for double melting behavior in this situation. As already pointed out in literature, double melting peaks are the result of partial melting followed by recrystallization during heating. It means in pristine iPP, the shoulder peak might corresponds to the melting of crystals that formed at isothermal crystallization temperature (130 °C) and upon heating the sample recrystallized and melted at high melting temperature peak (165.1 °C). With the addition of larger sized particles (prepared using the gel form of LDH), the melting temperature of iPP decreased drastically to 151.4 °C. In these samples, high melting temperature peak was absent due to the presence of larger LDH particles. These larger particles hinder the polymer chain diffusion and recrystallization during heating. As a result a single large endotherm was observed in nanocomposites prepared using the gel form of LDH. On the other hand, the nanocomposites

prepared using the sonicated LDH showed melting behavior similar to that of pure iPP. These results confirmed that the lateral size of the LDH particles play an important role in controlling the recrystallization of polymer chains during heating. All the nanocomposite samples containing sonicated LDH particles showed double melting peaks as a result of partial melting followed by recrystallization during heating. The shoulder peak presented at lower temperature for pure iPP shifts to the higher temperature upon the addition of sonicated LDH particles, which might be due to the changes in crystallite thickness and its distribution. In this way, it was found that the size of LDH and its dispersion in the polymer matrix can significantly affect the melting behavior of iPP.

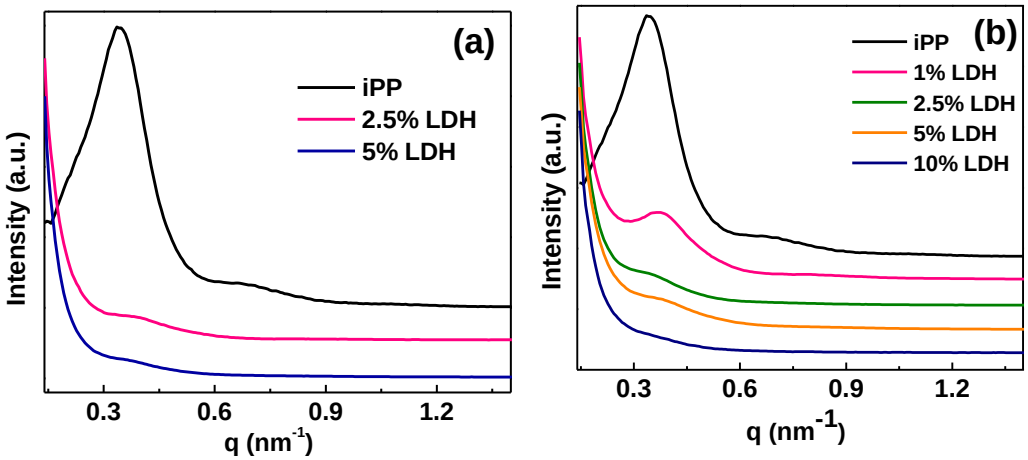

Figure 2.14. Small-angle X-ray scattering profiles of pure iPP and its nanocomposites crystallized isothermally at 130°C. (a) iPP/LDH gel nanocomposites and (b) iPP/sonicated LDH nanocomposites.

The SAXS intensities for both pure iPP and the nanocomposites prepared by using the gel form of LDH and sonicated LDH are shown in Figures 2.14. Pure iPP sample shows first maxima (q_1) at (0.37 nm^{-1}) attributed to the alternating crystalline and amorphous microstructure of the lamellae. Additional scattering peaks are seen for pure iPP at higher q indicating the regular stacking of lamellar structures. The integer ratio between the scattering peaks is characteristic of a periodic lamellar structure.[36, 56] On the other hand, nanocomposite samples show a weak peak in the q range (0.35-0.45 nm^{-1}) corresponding to the iPP lamellar morphology. As discussed in the preceding section, the nanocomposites have comparable levels of degree of crystallinity, but the contrast of the SAXS peak is weak for nanocomposites. It should be noted here that the SAXS measurements were performed in the transmission geometry and some of the X-ray radiation was

absorbed by highly dispersed LDH particles in nanocomposites. It is also obvious from Figure 2.14. that the intensity of the SAXS peak was further reduced with the increase in LDH loadings. Another noteworthy change is the strong scattering intensity at low *q* in nanocomposites, which can be attributed to the scattering of well-dispersed LDH particles within the iPP matrix.

2.4. Conclusions

In this work, highly dispersed iPP nanocomposites having different sized Mg-Al LDH nanoparticles were synthesized using the modified solvent mixing method. The sonication of LDH in xylene enables the modification of LDH surfaces to hydrophobic and simultaneously the LDH layers are broken into small fragments. The dispersion of LDH nanoparticles within the iPP matrix was confirmed by WAXD and atomic force microscopy, which is an indicative of compatibility of LDH nanoparticles with the iPP matrix. We have found that sonicated LDH nanoparticles dramatically improves the thermal stability, nucleation ability and crystallization rate of iPP at very low LDH loadings compared to that of nanocomposites with larger LDH particles with the same concentration. This might be due to the high surface area smaller LDH nanoparticles and its better dispersibility within the polymer matrix. The incorporation of LDH nanoparticles did not change the crystallization growth mechanism and crystal structure of iPP.

2.5. Experimental Section

Synthesis of Mg-Al LDH: Synthesis of Mg-Al LDH was carried out in a two-neck round bottom flask equipped with a reflux condenser under the ambient atmospheric conditions by the co-precipitation method. Magnesium nitrate ($Mg(NO_3)_2{\cdot}6H_2O$), aluminium nitrate ($Al(NO_3)_3{\cdot}9H_2O$), and urea were dissolved in Millipore water in the ratio 2:1:7 to give the final concentrations of 10, 5, and 35 mM, respectively. Then, the mixture was refluxed at 100 °C under continuous stirring for 24 hours. Finally, the precipitate was washed with hot Millipore water to remove the unreacted reactants if any and vacuum dried at 60 °C for 24 hours. Similarly, the experiment was repeated in argon (Ar) atmosphere to verify the influence of the reaction environment on the morphology of LDH (data not shown here).

LDH Gel Preparation: Vacuum dried Mg-Al LDH was re-dispersed in acetone and stirred the dispersion at ambient temperature for 1 hour. Then the precipitate was filtered and repeatedly washed with acetone. Such obtained LDH powder was dispersed in xylene and stirred it for 12 hours at ambient temperature. The resulting colloidal suspension was stable at room temperature for few minutes and after that LDH slowly settled down as sediment. Decanting of the excess xylene leads to the formation of a transparent gel (Figure 2.3b).

Sonication of LDH: As prepared LDH dry powder was dispersed in xylene and sonicated for 4 days using an ultrasonic sonication bath at room temperature. Enough care was taken to avoid the temperature increase during sonication. The resulting suspension was stable at room temperature for few hours.

Preparation of Polypropylene/Mg-Al LDH Nanocomposites: iPP used in this study had a weight average of 120000 g/mol with a polydispersity index ($Đ$) of 4.5. The nanocomposites of iPP/Mg-Al LDH were prepared by two different routes using solution blending method. In one case, nanocomposites of iPP/Mg-Al LDH with different compositions (0, 2.5, and 5 % LDH) were obtained using the gel form of LDH. In this case, 10 g of iPP was dissolved in 100 mL of xylene in a round bottom flask at 150 °C with continuous stirring under argon atmosphere. After the complete dissolution of iPP, the required amount of Mg-Al LDH xylene gel was added to the flask under continuous stirring. In another case, the dispersion of LDH in xylene was prepared by sonication of required amount of LDH for 4 days. Such sonicated LDH dispersion was added to the required amount of iPP solution in a round bottom flask at 150 °C with continuous stirring under argon atmosphere. Amount of LDH was adjusted to different weight % to prepare nanocomposites with different LDH contents (0, 1, 2.5, 5, and 10 % LDH). The resultant solution was refluxed at 150 °C for 24 hrs for the homogeneous dispersion of LDH platelets in iPP solution. The polymer solution was poured into 100 mL of ethanol. The precipitate was filtered, washed with ethanol several times and dried in a vacuum oven at 100 °C for 24 h.

2.6. Characterization

Wide-angle and Small-angle X-ray Scattering (WAXS/SAXS): WAXS/SAXS measurements were carried out on XEUSS SAXS/WAXS system using a

Genixmicrosource from Xenocs operated at 50 kV and 0.6 mA. The Cu Kα radiation (λ = 1.54 Å) was collimated with FOX2D mirror and two pairs of scatter less slits from Xenocs. The 2D-patterns were recorded on a Mar345 image plate and processed using Fit2D software. All the measurements were made in the transmission mode. The sample to detector distance, which was calibrated with silver behenate standard, was 1044 mm for SAXS and 214.5 mm for WAXS, respectively. All the samples were crystallized under controlled conditions to understand the effect of LDH on the crystallization behavior of iPP. Samples were melted at 200 °C in DSC for approximately 5 min to remove the previous thermal history and are rapidly quenched to the isothermal crystallization temperature (130 °C). Samples were allowed to crystallize at 130 °C for 1 h (Figure 2.9a). Such prepared samples were used for SAXS and WAXS analysis.

Surface Area Analysis: The specific surface area was measured using the Brunauer, Emmet and Teller (BET) surface area analyzer (Micrometrics TriStar 3000 V6.05A). Surface areas were measured from the Nitrogen adsorption using the multi-point method after degassing the LDH powders at 150 °C for 2 hr.

Fourier Transform Infrared Spectroscopy (FTIR): The infrared spectra were measured with a Perkin-Elmer series FT-IR spectrometer-2 over the wavenumber range of 4000 – 400 cm^{-1}. The powder sample was mixed with KBr and pressed in the form of pellets. The FTIR spectra were collected with 32 scans and a resolution of 1 cm^{-1}.

Scanning Electron Microscopy (SEM): Surface morphology of the LDH was investigated using SEM (Zeiss EVO 18 cryo SEM) with an accelerating voltage of 20 kV. LDH suspensions in water were deposited over a glass cover slip, which is pasted onto carbon-coated grid and imaged after natural drying at room temperature.

Transmission Electron Microscopy (TEM): TEM images were recorded on a JEOL 2010 transmission electron microscope operating at 300 kV. As-prepared LDH particles were dispersed in water and directly deposited on a carbon-coated copper grid. In another case, after acetone treatment/sonication, LDH samples were dispersed in xylene and deposited on a carbon-coated copper grid. All the grids were dried for 2 days and imaged under transmission electron microscope.

The elemental constitution of the materials was determined on an energy dispersive spectrometer (Technai G^2 30LaB_6, ST with EDS).

Thermogravimetric Analysis (TGA): The TGA thermograms were recorded in the heating process by using thermo gravimetric analysis TA Q50 under nitrogen gas atmosphere at a rate of 10 °C/min.

Differential Scanning Calorimetry (DSC): The crystallization and melting behavior of all samples were measured using a differential scanning calorimeter (Perkin Elmer Pyris 6 DSC). The melt crystallization temperature (T_{mc}) was measured for iPP and iPP/LDH nanocomposites. In this case, sample was first heated from room temperature to 200 °C (above melting temperature of iPP) at a rate of 10 °C/min, where it was held for 1 min to erase the thermal history of the sample, then cooled at a rate of 10 °C/min to room temperature to measure the T_{mc}. All the samples were reheated to 200 °C to measure the melting temperature. In another set of experiments, crystallization half-time was measured at isothermal crystallization temperature. The thermal program employed for the isothermal crystallization is depicted in Figure 2.9a. Molten samples were rapidly cooled to a desired crystallization temperature (T_c) i.e. 130 °C at a rate of 100 °C/min, and kept for 60 min for the isothermal crystallization. All the DSC experiments were conducted under nitrogen atmosphere.

Polarized Optical Microscopy (POM): A polarized optical microscope (Universal polarizing microscope ZPU01, Carl Zeiss Inc.) equipped with a Linkam hot stage was used to monitor the spherulites. Average spherulite size was measured manually using Image J software. This size corresponds to the average equatorial diameter of the spherulite. The thin-film specimens were prepared by melting the samples at 200 °C for 1 min and then rapidly cooled to the crystallization temperature.

Atomic Force Microscopy (AFM): Atomic force microscopy (Digital Instruments, Inc., Santa Barbara) (AFM) imaging was performed using a Dimension 3100 and a CP microscope (Park Scientific Instrument, Inc) in the tapping mode.

2.7. References

1 Q. Wang and D. O'Hare, *Chem Rev* **112:**4124-4155 (2012).

2 S. Sinha Ray and M. Okamoto, *Prog Polym Sci* **28:**1539-1641 (2003).

3 H. Kim, A. A. Abdala and C. W. Macosko, *Macromolecules* **43:**6515-6530 (2010).

4 F. Leroux, M. Adachi-Pagano, M. Intissar, S. Chauviere, C. Forano and J.-P. Besse, *J Mater Chem* **11:**105-112 (2001).

5 D. Basu, A. Das, K. W. Stöckelhuber, U. Wagenknecht and G. Heinrich, *Prog Polym Sci* **39:**594-626 (2014).

6 R. A. Vaia and E. P. Giannelis, *MRS Bulletin* **26:**394-401 (2001).

7 X. Fu and S. Qutubuddin, *Polymer* **42:**807-813 (2001).

8 F. Leroux and J.-P. Besse, *Chem Mater* **13:**3507-3515 (2001).

9 F. Costa, M. Saphiannikova, U. Wagenknecht and G. Heinrich, Layered Double Hydroxide Based Polymer Nanocomposites, in *Wax Crystal Control · Nanocomposites · Stimuli-Responsive Polymers*. Springer Berlin Heidelberg, pp. 101-168 (2008).

10 M. Meyn, K. Beneke and G. Lagaly, *Inorg Chem* **29:**5201-5207 (1990).

11 M. Borja and P. K. Dutta, *J Phys Chem* **96:**5434-5444 (1992).

12 Y. Zhao, F. Li, R. Zhang, D. G. Evans and X. Duan, *Chem Mater* **14:**4286-4291 (2002).

13 M. Ogawa and H. Kaiho, *Langmuir* **18:**4240-4242 (2002).

14 W. Chen and B. Qu, *Chem Mater* **15:**3208-3213 (2003).

15 W. Chen, L. Feng and B. Qu, *Chem Mater* **16:**368-370 (2004).

16 W. Chen and B. Qu, *J Mater Chem* **14:**1705-1710 (2004).

17 Q. Wang, X. Zhang, C. J. Wang, J. Zhu, Z. Guo and D. O'Hare, *J Mater Chem* **22:**19113-19121 (2012).

18 Q. Wang, X. Zhang, J. Zhu, Z. Guo and D. O'Hare, *Chem Commun* **48:**7450-7452 (2012).

19 D.-Y. Wang, A. Das, F. R. Costa, A. Leuteritz, Y.-Z. Wang, U. Wagenknecht and G. Heinrich, *Langmuir* **26:**14162-14169 (2010).

20 S. P. Lonkar, S. Morlat-Therias, N. Caperaa, F. Leroux, J. L. Gardette and R. P. Singh, *Polymer* **50:**1505-1515 (2009).

21 M. Zammarano, S. Bellayer, J. W. Gilman, M. Franceschi, F. L. Beyer, R. H. Harris and S. Meriani, *Polymer* **47:**652-662 (2006).

22 H. Peng, W. C. Tjiu, L. Shen, S. Huang, C. He and T. Liu, *Compos Sci Technol* **69:**991-996 (2009).

23 A. Illaik, C. Taviot-Guého, J. Lavis, S. Commereuc, V. Verney and F. Leroux, *Chem Mater* **20:**4854-4860 (2008).

24 P. Pan, B. Zhu, T. Dong and Y. Inoue, *J Polym Sci, Part B: Polym Phys* **46:**2222-2233 (2008).

25 D.-Y. Wang, A. Leuteritz, Y.-Z. Wang, U. Wagenknecht and G. Heinrich, *Polym Degrad Stab* **95:**2474-2480 (2010).

26 C. Manzi-Nshuti, D. Wang, J. M. Hossenlopp and C. A. Wilkie, *J Mater Chem* **18:**3091-3102 (2008).

27 H. Zhu, W. Wang and T. Liu, *J Appl Polym Sci* **122:**273-281 (2011).

28 Q. Wang, J. P. Undrell, Y. Gao, G. Cai, J.-C. Buffet, C. A. Wilkie and D. O'Hare, *Macromolecules* **46:**6145-6150 (2013).

29 F. Song and X. Hu, *Nat Commun* **5:**(2014).

30 Q. Wang and D. O'Hare, *Chem Commun* **49:**6301-6303 (2013).

31 M. Yang, O. McDermott, J.-C. Buffet and D. O'Hare, *RSC Adv* **4:**51676-51682 (2014).

32 T. D. Fornes and D. R. Paul, *Polymer* **44:**3945-3961 (2003).

33 L. Li, C. Y. Li and C. Ni, *J Am Chem Soc* **128:**1692-1699 (2006).

34 P. Maiti, P. H. Nam, M. Okamoto, N. Hasegawa and A. Usuki, *Macromolecules* **35:**2042-2049 (2002).

35 P. H. Nam, P. Maiti, M. Okamoto, T. Kotaka, N. Hasegawa and A. Usuki, *Polymer* **42:**9633-9640 (2001).

36 P. Liu, K. L. White, H. Sugiyama, J. Xi, T. Higuchi, T. Hoshino, R. Ishige, H. Jinnai, A. Takahara and H.-J. Sue, *Macromolecules* **46:**463-473 (2013).

37 B. P. Grady, F. Pompeo, R. L. Shambaugh and D. E. Resasco, *J Phys Chem B* **106:**5852-5858 (2002).

38 J.-Z. Xu, C. Chen, Y. Wang, H. Tang, Z.-M. Li and B. S. Hsiao, *Macromolecules* **44:**2808-2818 (2011).

39 S. P. Lonkar and R. P. Singh, *Thermochim Acta* **491:**63-70 (2009).

40 Z. Liu, R. Ma, M. Osada, N. Iyi, Y. Ebina, K. Takada and T. Sasaki, *J Am Chem Soc* **128:**4872-4880 (2006).

41 U. Costantino, F. Marmottini, M. Nocchetti and R. Vivani, *Eur J Inorg Chem* **1998:**1439-1446 (1998).

42 V. Nicolosi, M. Chhowalla, M. G. Kanatzidis, M. S. Strano and J. N. Coleman, *Science* **340:**(2013).

43 J. N. Coleman, M. Lotya, A. O'Neill, S. D. Bergin, P. J. King, U. Khan, et al., *Science* **331:**568-571 (2011).

44 Q. Wu, A. Olafsen, O. B. Vistad, J. Roots and P. Norby, *J Mater Chem* **15:**4695-4700 (2005).

45 J. T. Han, J. I. Jang, H. Kim, J. Y. Hwang, H. K. Yoo, J. S. Woo, S. Choi, H. Y. Kim, H. J. Jeong, S. Y. Jeong, K.-J. Baeg, K. Cho and G.-W. Lee, *Sci Rep* **4:**(2014).

46 M. Chhowalla, H. S. Shin, G. Eda, L.-J. Li, K. P. Loh and H. Zhang, *Nat Chem* **5:**263-275 (2013).

47 L. Qiu, W. Chen and B. Qu, *Polym Degrad Stab* **87:**433-440 (2005).

48 Y. Gao, J. Wu, Z. Zhang, R. Jin, X. Zhang, X. Yan, A. Umar, Z. Guo and Q. Wang, *J Mater Chem A* **1:**9928-9934 (2013).

49 A. T. Jones, J. M. Aizlewood and D. R. Beckett, *Makromol Chem* **75:**134-158 (1964).

50 E. B. Gowd, B. Nandan, N. C. Bigall, A. Eychmüller, P. Formanek and M. Stamm, *Polymer* **51:**2661-2667 (2010).

51 K. C. Grabar, K. R. Brown, C. D. Keating, S. J. Stranick, S.-L. Tang and M. J. Natan, *Anal Chem* **69:**471-477 (1997).

52 M. Avrami, *J Chem Phys* **7:**1103-1112 (1939).

53 M. Avrami, *J Chem Phys* **8:**212-224 (1940).

54 Y.-F. Zhang, *J Macromol Sci Part B-Phys* **47:**891-899 (2008).

55 J. Sandler, G. Broza, M. Nolte, K. Schulte, Y. M. Lam and M. S. P. Shaffer, *J Macromol Sci Part B-Phys* **42:**479-488 (2003).

56 B. Chu and B. S. Hsiao, *Chem Rev* **101:**1727-1762 (2001).

Chapter-3

Simultaneous Size Reduction and Delamination of Layered Double Hydroxides: The "Nanosize" Effect of LDH on Hierarchical Structure and Properties of Polypropylene

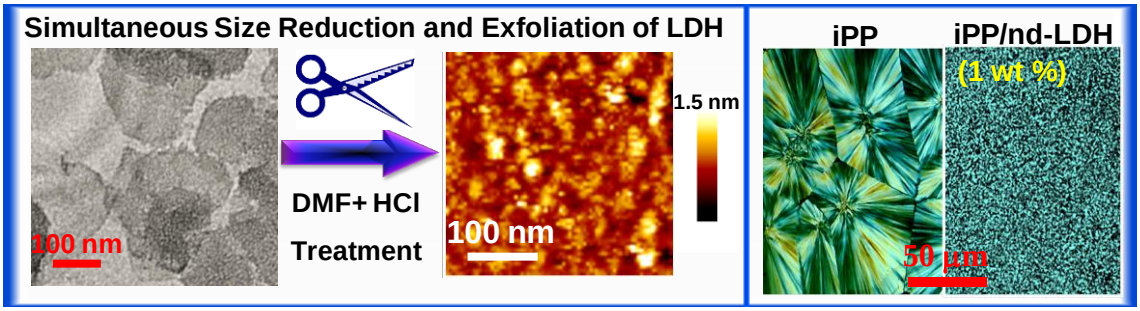

3.1. Abstract

The surface area of nanofillers is a key parameter in determining the properties of polymer nanocomposites. In this work, LDH having different surface areas were synthesized by the co-precipitation method using different bases. A new method has been developed for the simultaneous delamination and the lateral size reduction of LDH in a one-step procedure by treating the as-prepared LDH by dilute acid. This method directly resulted in the delaminated LDH sheets with lateral dimensions as low as 10-30 nm and featured a thickness of ~1 nm with the same chemical composition. The effect of different-sized LDH on the hierarchical structure formation and properties of iPP was systematically investigated. The uniformly dispersed LDH particles have a significant effect on the nucleation ability, thermal stability and mechanical properties of iPP. The incorporation of nanodot LDH showed a remarkable effect on spherulite size, lamellar thickness, crystal structure, crystallization rate and thermal stability of iPP with only 1 wt % loading. Furthermore, the microstructure of the iPP nanocomposites was systematically

investigated at multiple length scales in the presence of different-sized LDH, which is a key to understand the polymer properties.

3.2. Introduction

Engineering thermoplastics in general and polypropylene, in particular, received indispensable attention from the industry, since these are low cost and easily processable polymeric materials used for various applications like fibers, packaging, laboratory equipment, automotive components, electronics etc.[1, 2] The application of polypropylene (iPP) as an engineering plastic is often limited due to its low impact strength and Young's modulus. It has been demonstrated that the addition of the nanofillers to polypropylene can result in the formation of nanocomposites with significantly improved thermomechanical and optical properties.[3-6] Among the numerous nanofillers, two-dimensional sheet like nanostructures such as layered silicates, graphene, and its analogs, and recently LDH have found interest by researchers as multifunctional nanofillers for polymers.[3, 4, 7-9]

The macroscopic properties of semicrystalline polymers are mainly determined by the structure and morphology of the polymers, including the degree of crystallinity, crystallite size, and crystal structure. Hitherto, extensive studies were aimed to clarify the influence of nanosized filler on the crystallization behavior of iPP.[10-14] In most of the cases, the nanofillers act as heterogeneous nucleating agents, enhancing the crystallization kinetics of iPP. When we consider the effect of nanofillers, the particle size, shape, surface modification, the dispersion quality, the interaction with the polymer, etc. play the crucial role in determining the nucleation efficiency of the nanofillers.[12-19] For example, it has been found in several cases that the high degree of dispersion of the nanofillers in polymer matrix increases the rate of crystallization. In some other cases, interactions between the filler surface and the polymer chains determine the nucleation efficiency. Among the commonly used nanofillers, it was showed that carbonaceous nanofillers (carbon nanotubes, graphene, and its analogs) exhibit stronger nucleating abilities for iPP.[13, 20, 21] Using carbon nanotubes, it was demonstrated that the aspect ratio is an important factor influencing the nucleating ability of the nanofillers and the low-aspect-ratio CNTs could provide more nucleating

sites for polymer crystal growth compared with the large-aspect-ratio CNTs.[16] Although some efforts have already been reported to understand the effect of surface modification, the dispersion quality, and shape of the nanofillers, a systematic study by tuning the surface area of the nanofillers is still missing. Specific surface area of the nanofiller plays an important role in reducing the nucleation barrier of the semicrystalline polymers, thereby influencing the crystallization rate of polymers. Compared to other two-dimensional materials, the surface areas of LDH can be easily adjusted during the synthesis or post-modification process.[12, 22]

In our previous chapter, we have tuned the surface area of LDH by ultrasonication and showed that sonicated LDH particles showed better nucleation ability compared to that of the as-synthesized LDH.[12] Herein, we report a method for the simultaneous delamination and the lateral size reduction of LDH in a one-step procedure. This method involves the dilute acid treatment of the as-prepared LDH having the particle sizes ~ 200 nm. The delaminated LDH sheets exhibit lateral dimensions as low as 10-30 nm and feature a thickness of ~1 nm with the same chemical composition. In the present study, we also clarify the effects of three different-sized LDH (having different surface areas) on the various physical properties of the host iPP such as thermal stability, dynamic mechanical behavior and nucleation ability. The remarkable improvements in the physical properties of iPP reported here are with only 1 wt % LDH nanodots. Furthermore, the hierarchical structure of the iPP nanocomposites is investigated using POM, WAXS and SAXS in the presence of different-sized LDH.

3.3. Results and Discussion

3.3.1. Synthesis and Characterization of Different-sized LDH

In our previous chapter, we have reported the synthesis and delamination of Mg-Al LDH using urea as a base.[12] The procedure adopted in that work yielded the LDH with lateral sizes ~ 3-4 μm. By taking the advantage of AMOST method, the hydrophilic LDH was converted into hydrophobic, and it was dispersed effectively in non-polar solvents like xylene.[23] The delaminated LDH (μm-LDH) still retained the hexagonal platelet morphology with the lateral sizes ~3-4 μm. The fragmented LDH having the

lateral sizes ~ 30-100 nm was prepared by the sonication of μm-LDH for longer duration i.e. 4 days. To avoid prolonged sonication of LDH, herein, we used a different reaction environment to prepare the nanometer sized LDH by co-precipitation method. It has been reported that several parameters such as metal ion concentration, reaction temperature, pH, the rate of addition, aging time and mixing efficiency dictate the nucleation and growth process of LDH and as a result the morphology and crystal size.[8, 24-27] In the present case, LDH preparation was carried out using HMT as a base, instead of urea by keeping the reaction conditions same as above except concentration of HMT. Figure 3.1a shows the TEM image of the LDH synthesized using HMT as a base. As evidenced by TEM, the lateral size of the LDH is in the range of 100 – 200 nm, which is several magnitudes lesser than the lateral size of LDH synthesized using urea. Such difference in the lateral size of the LDH might be due to the increase in a number of nucleating sites in the presence of HMT. Compared to urea, HMT is a stronger base, and the ammonia release rate in HMT is faster than that of urea, and as a result, the rapid nucleation occurs in the presence of HMT that resulted in the smaller-sized particles.[27] Another notable difference is the morphology of the platelets, which also occurs due to the difference in the nucleation and growth process in different reaction environments. The energy-dispersive X-ray spectrum (EDS) confirmed the composition of the Mg-Al LDH (Figure 3.1b), and it is in good agreement with the previously reported EDS spectrum of Mg-Al LDH prepared using urea.[12] The morphology and thickness of LDH were evaluated by the AFM. Figure 3.1d shows the typical AFM height image and corresponding height profile of as-synthesized Mg-Al LDH using HMT as a base. It is evident from Figure 3.1d that the as-synthesized sample shows the platelet like-morphology with the lateral size ~200 nm and thickness ~16 nm. The same AMOST method was used to delaminate the LDH, and the TEM image of the delaminated LDH nanosheets (nm-LDH) is shown in Figure 3.1e. Compared to the as-synthesized LDH, the contrast of delaminated LDH (nm-LDH) sheets is weak that indicates the delamination of LDH to single- or few-layer nanosheets.

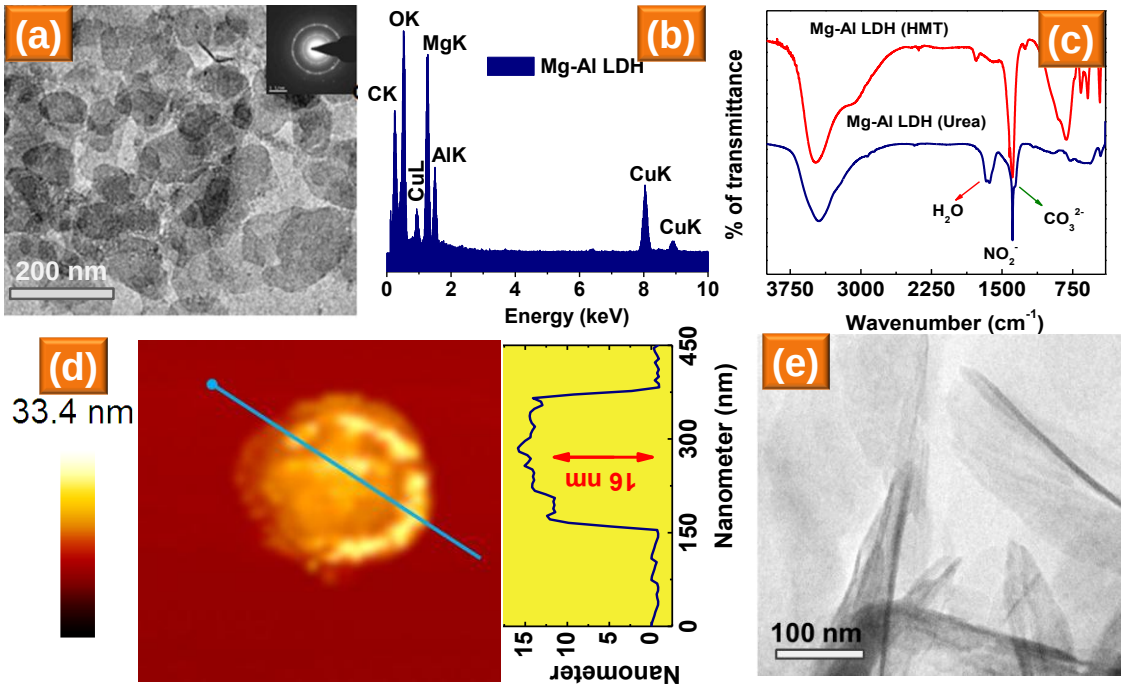

Figure 3.1. Characterization of nm-LDH. (a) TEM, (b) EDS spectrum, (c) FTIR patterns of Mg-Al LDHs prepared in presence different bases (HMT and urea base), (d) AFM image and height profile of as-prepared Mg-Al LDH, and (e) TEM image of delaminated LDH.

The 2D nanodot LDH (nd-LDH) with lateral dimensions of 10-30 nm and thickness ~ 1 nm was prepared by dissolution assisted exfoliation in mixed solvents using the procedure established in the case of other layered materials such as MoS_2.[28] Typically, as-prepared LDH using HMT as base (with ~200 nm lateral size) has been dispersed in a mixture of DMF and HCl (4:1 volume ratio) and sonicated for 2 hours. DMF is a known solvent to swell the Mg-Al LDH and acids can dissolve the LDH.[29-32] Hence the judicious selection of these proper solvents in convenient proportions leads to the cleavage and delamination of the bulk LDH into single layered nanodots without long time energy consuming sonication. The TEM and AFM height images of the nd-LDH are shown in Figure 3.2. It is clear that the lateral size has been reduced drastically to less than 30 nm and the histogram given in the inset of Figure 3.2a shows the lateral size distribution, with the peak maxima at 30 nm. The height of the LDH has been reduced to ~ 1 nm, typical for the single layered sheets (Figure 3.2b),[33] which reveals that these LDH were undergone the process of exfoliation rather than the dissolution of the material. EDS spectrum was documented after the dilute acid treatment, to probe

whether there is any compositional variation and is given in Figure 3.2c. One can notice that the ratio of Mg-Al remains almost same compared to the nm-LDH, which confirms the compositional integrity of nanodots with nano-sized LDH.

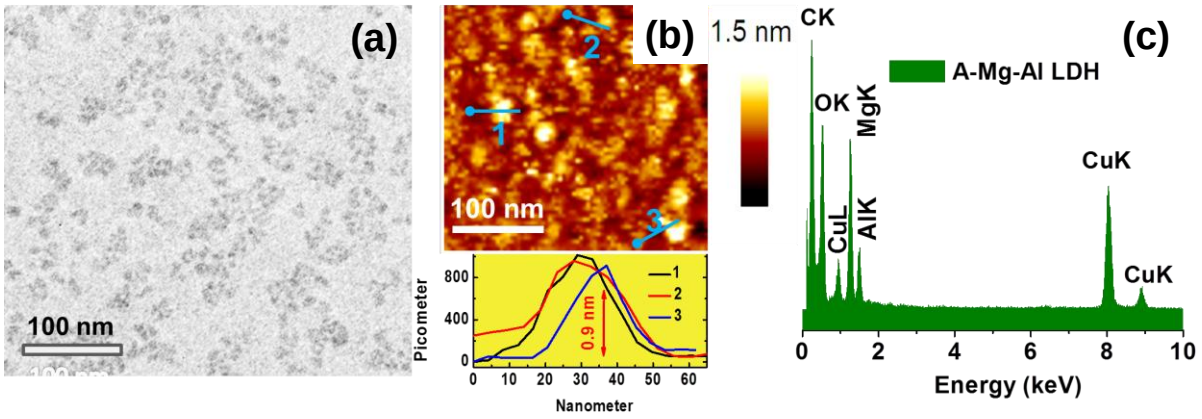

Figure 3.2. Characterization of nd-LDH. (a) TEM, (b) AFM image, and (c) EDS spectrum of nd-LDH obtained by treating the Mg-Al LDH (Figure 3.1a) with mixed solvents (DMF/HCl).

3.3.2. Dispersion of Different-sized Mg-Al LDH in Polypropylene

To investigate the effect of lateral size of LDH on the polymer properties, iPP nanocomposites were prepared using three different sized LDH (μm-LDH, nm-LDH, and nd-LDH), as reported by the previous method.[12] Figure 3.3 depicts the powder X-ray diffraction patterns of iPP nanocomposites containing three different-sized LDH (1 wt%) along with pristine iPP, and LDH prepared using different bases. Both the LDH show the characteristic 00n reflections, confirming the formation of the multilayer LDH structure. The LDH prepared using HMT as a base showed lower 2θ positions of (00n) planes compared to the LDH prepared using urea as a base. This may be due to the presence of different anions within the LDH layers. LDH prepared using HMT as base showed the presence of nitrate anions, whereas both nitrate and carbonate anions are present in the gallery of LDH prepared using urea as a base (Figure 3.1c). Another notable difference observed between these LDH is the change in full-width at half maximum (FWHM) of (00n) planes indicating the different crystal sizes of these LDH. The reflections corresponding to the (00n) planes of LDH are not observed in the X-ray diffraction patterns of iPP nanocomposites containing different-sized LDH that

indicates the fine dispersion of LDH within the iPP matrix without 2D layer stacking. The details about the crystal structure will be discussed in a later section.

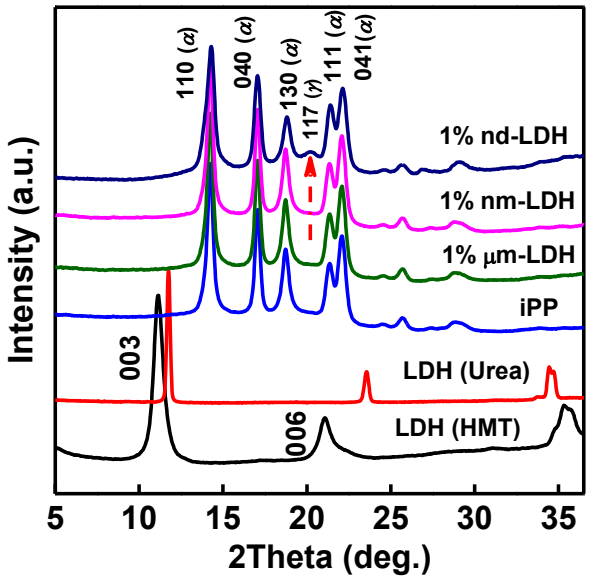

Figure 3.3. Powder X-ray diffraction patterns of iPP and its nanocomposites containing different-sized LDH (for comparison, the powder XRD patterns of LDH prepared by two different bases are shown). Polymer and nanocomposites samples were prepared by cooling the melt at a rate of 10 °C/min in the DSC pan.

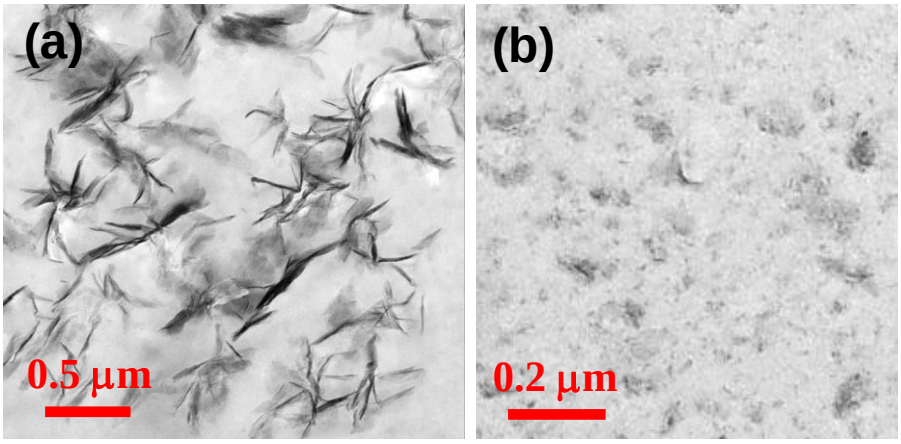

Figure 3.4. Cross-sectional TEM images of the iPP/Mg-Al LDH (5 wt %) nanocomposites prepared using (a) μm-LDH and (b) nm-LDH.

The homogeneous dispersion of μm-LDH and nm-LDH in iPP is further visualized with the help of cryo-TEM using nanocomposites containing 5 wt% of LDH (Figure 3.4). In the case of iPP/μm-LDH nanocomposites, the sheet like morphology of the LDH is preserved in nanocomposite structure. The partially or fully exfoliated LDH

are dispersed in the polymer matrix homogeneously. On the other hand, in iPP/nm-LDH nanocomposites, the dispersion is quite uniform, and the thin transparent sheets retain as such without any aggregation. Visualizing the nd-LDH in iPP matrix is difficult due to their small sizes and the TEM image of the iPP/nd-LDH nanocomposites is not shown here. These results suggest that LDH platelets have been successfully dispersed into the polymer matrix without much agglomeration during solution blending.

3.3.3. Hierarchical Structure of iPP/LDH Nanocomposites

3.3.3.1. Influence of Lateral Size of LDH on the Crystallization Kinetics and Microstructure of iPP

The influence of different-sized Mg-Al LDH on the crystallization rate of iPP was studied using DSC. Quite often, the crystallization temperature (T_{mc}) upon cooling from the melt is used to measure the crystallization rate of the polymer.[34] Higher the T_{mc}, the higher is the crystallization rate of the polymer. Figure 3.5a shows the DSC thermograms of pristine iPP and iPP/LDH nanocomposites containing different-sized LDH (1 wt %) obtained during cooling at a rate of 10 °C/min. It can be seen that the size of the LDH has a significant role in determining the crystallization temperature and the nanocomposite samples showed the higher T_{mc} than pristine iPP, indicating that the addition of LDH accelerates the crystallization rate of iPP. The T_{mc} values measured for various samples are summarized in Table 3.1. The change in T_{mc} values was found to depend upon the lateral size of the LDH used for the preparation of nanocomposites. The incorporation of μm-LDH has a little effect on the T_{mc} (ΔT_{mc} = $T_{mc(nanocomposite)}$-$T_{mc(iPP)}$= 5.2 °C), whereas the incorporation of nm-LDH has a moderate effect on the T_{mc} (ΔT_{mc} = 10.6 °C). On the other hand, the incorporation of nd-LDH dramatically shifted the T_{mc} of iPP to a higher temperature (ΔT_{mc} = 19.5 °C). To the best of our knowledge, the T_{mc} value observed for the iPP containing 1 wt% of nd-LDH is the highest compared to the T_{mc} values reported for iPP/LDH nanocomposites so far. The T_{mc} values reported

Table 3.1. Summary of BET surface area of LDH, crystallization kinetics parameters of iPP and iPP/LDH nanocomposites with different-sized LDH.

Mg-Al LDH		**iPP-Mg-Al LDH nanocomposites**			
Samples	**BET surface area (m^2/g)** (± 5)	**Samples**	$t_{1/2}$ **at 130 °C (min.)** (± 0.2)	**Avrami constant (*n*)** (± 0.01)	T_{mc} **(°C)** (± 0.3)
As-synthesized Mg-Al LDH	115	**iPP**	16.0	2.6	110
μm-LDH	200	**1 wt% μm-LDH**	9.2	2.7	115.2
nm-LDH	393	**1 wt% nm-LDH**	3.8	3.1	120.6
nd-LDH	620	**1 wt% nd-LDH**	0.7	3.5	129.5

In literature for iPP/LDH nanocomposites are summarized in introduction chapter (Table 1.2). To further confirm the influence of different-sized LDH on the crystallization rate of iPP, isothermal crystallization was carried out at 130 °C. Figure 3.5b shows the DSC thermograms of pristine iPP and iPP/LDH nanocomposites containing different-sized LDH (1 wt %) during isothermal crystallization at 130 °C. The crystallization half-time ($t_{1/2}$), which is the time required to complete 50% of the crystallization under isothermal conditions, measured for various samples are summarized in Table 3.1. Compared to the pristine iPP, both the induction time and the $t_{1/2}$ decreased with the incorporation of different-sized LDH and the decrease is drastic in presence of the nd-LDH. The crystallization exotherm observed for the iPP/nd-LDH is very sharp and the $t_{1/2}$ measured is ~0.7 min. It is seen that the lateral size of LDH plays an important role on the crystallization rate of iPP. The incorporation of 1 wt% of μm-LDH, nm-LDH and nd-LDH reduced the $t_{1/2}$ to 42.5%, 76.2% and 95.6%, respectively, of that of the neat iPP at 130 °C. Figure 3.5c illustrates the relationship between the surface area of the LDH and ΔT_{mc} and $\Delta t_{1/2}$ of the nanocomposites. As evident from the graph, a strong correlation was observed between the surface area of the LDH and crystallization kinetics of iPP. In the case of nd-LDH, the effect of LDH loading on the $t_{1/2}$ of the iPP/nd-LDH was investigated using 0.5, 1 and 1.5 wt % loadings. It was found

that 1 wt% of nd-LDH is optimal loading for the effective crystallization of iPP (Figure 3.5d).

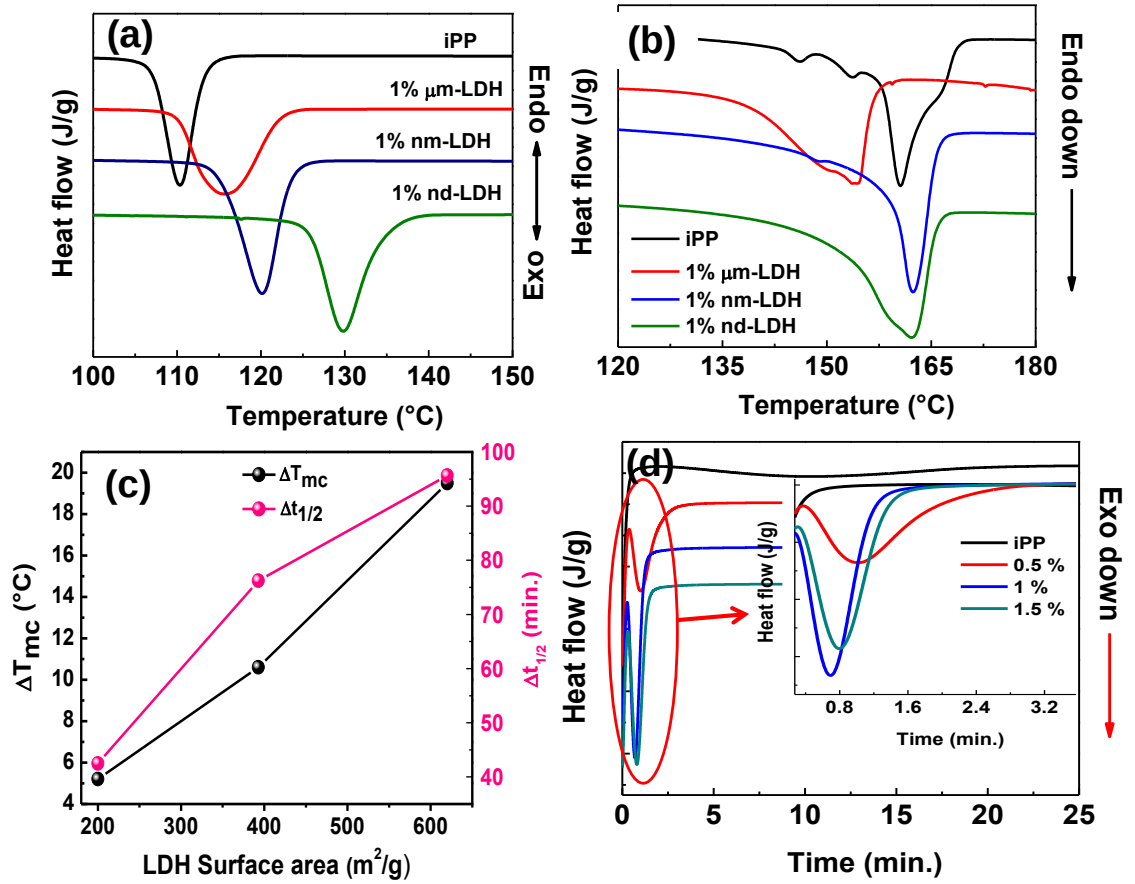

Figure 3.5. DSC thermograms of pristine iPP and iPP/LDH nanocomposites containing different-sized LDH (1 wt %) obtained during (a) cooling from the melt at a rate of 10 °C/min, (b) crystallization isotherms obtained at 130 °C, and (c) surface area of the LDH versus ΔT_{mc} and $\Delta t_{1/2}$ of the nanocomposites, and (d) DSC thermogram shows the isothermal crystallization behavior of the iPP/nd-Mg-Al LDH nanocomposites with different concentration.

Isothermal crystallization kinetics for pure iPP and its nanocomposites containing different-sized LDH were analyzed using Avrami equation as discussed in our previous chapter.[12, 35] Table 3.1 summarizes the Avrami constants estimated for iPP and various nanocomposites crystallized at 130 °C. The *n* values of pure iPP and iPP/μm-LDH were almost similar and this *n* value might be attributed to a heterogeneous nucleation followed by diffusion controlled spherulite growth (mixed two-dimensional (2D) and three-dimensional (3D) crystal growth). On the other hand, *n* value for the

nanocomposites containing nm-LDH and nd-LDH is slightly higher than 3, which is typical for a rapidly nucleating system mostly through heterogeneous nucleation undergoing three-dimensional crystal growth in presence of the tiny LDH particles.

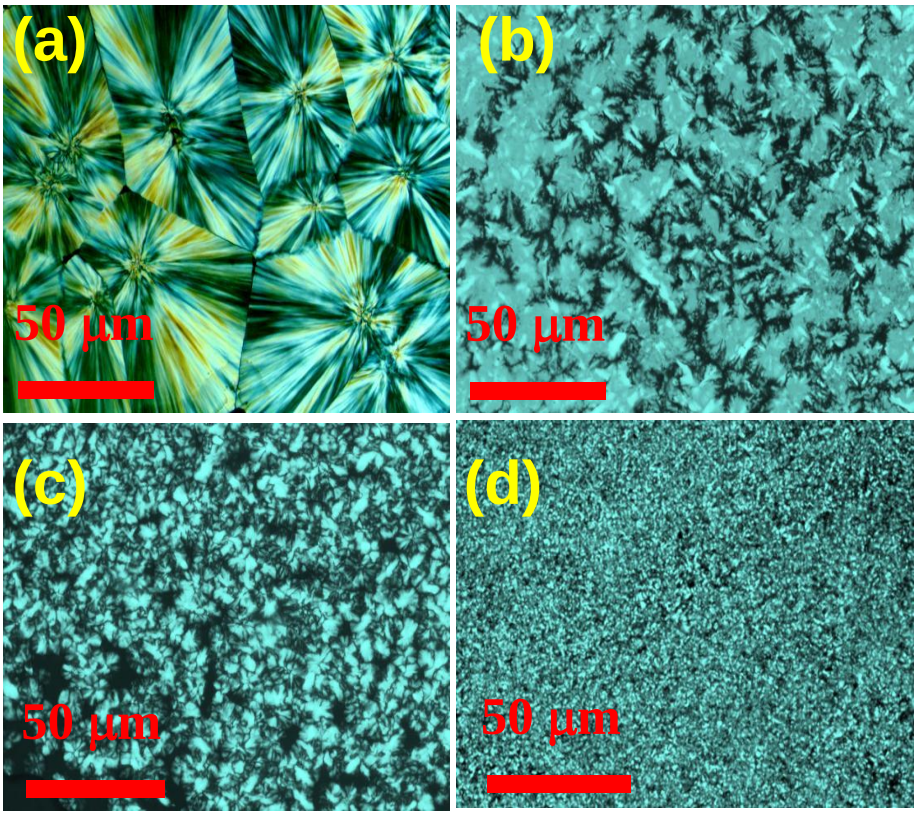

Figure 3.6. POM images of pure iPP and its nanocomposites crystallized isothermally at 130 °C: (a) iPP, (b) iPP/1 wt% *μ*m-LDH, (c) iPP/1 wt% nm-LDH and (d) iPP/1 wt% nd-LDH.

Figure 3.6 shows the POM images of iPP and its nanocomposites prepared using different-sized LDH after isothermal crystallization at 130 °C. The pristine iPP exhibits a characteristic spherulitic structure with well-defined boundaries due to the slow crystallization rate (Figure 3.6a). These spherulites showed negative birefringence (type II) and a Maltese cross extinction pattern is clearly visible.[36-38] In contrast, for the iPP/LDH (1 wt%) nanocomposites, the spherulite size decreases drastically and the individual spherulites are not clearly visible. No evidence of macroscopic aggregation of LDH particles was observed in the nanocomposites. The uniform size of the spherulites in iPP/LDH nanocomposites suggest that the well-dispersed LDH particles act as heterogeneous nucleation sites and barricade iPP spherulite growth. With the decrease in lateral size of the LDH particles, the number of nucleation sites increased

dramatically and higher number of spherulites (or axialites) was observed. By comparing the effect of lateral size of LDH on the crystalline morphology of iPP, it is apparent that nd-LDH provides the largest number of nuclei due to the increased surface area and better dispersion of LDH particles in iPP matrix. By combining the POM results with the aforementioned DSC results, it may be concluded here that nd-LDH particles have the outstanding efficiency on overall crystallization rate of iPP than the larger-sized LDH particles.

3.3.3.2. Influence of Lateral Size of LDH on the Crystal Structure and Lamellar Morphology of iPP

In order to understand the effect of lateral size of LDH on the crystal structure and lamellar morphology of iPP, the samples were prepared with the well-defined thermal history under controlled conditions. All the samples were melted at 200 °C in DSC and cooled to room temperature at a rate of 10 °C/min. The samples recovered from the DSC pans were used to acquire WAXS and SAXS data in transmission mode. The WAXS patterns (Figure 3.3) of iPP, iPP/μm-LDH and iPP/nm-LDH samples showed strong X-ray reflections at 2θ = 14.2°, 17.0°, 18.7°, 20.2°, 21.3°, and 22.1° corresponding to the monoclinic α form.[39] In iPP, the formation of the α form is a kinetically driven process. On the other hand, iPP/nd-LDH nanocomposite sample showed an additional reflection at 2θ = 20.1° and it was assigned to the (117) plane of the γ form.[40] It has been reported that the γ form can be obtained in several manners such as by introducing stereo and regio-irregularities using metallocene catalyst, in the case oligomers having molecular weights between 1000 and 3000 g/mol or at elevated temperature and pressure.[40-43] It was also reported that the formation of the γ form is thermodynamically more favored compared to the α form. Thomann et al. reported that the formation of the γ form is favored under low supercoolings.[40]

As discussed in the preceding section, iPP/nd-LDH nanocomposites were crystallized rapidly at high T_{mc} ~129.5 °C. Presumably, the low degree of supercooling favors the formation of minor fractions of the γ form in iPP/nd-LDH nanocomposite sample. In order to confirm this, pristine iPP was crystallized at 130 °C and the

Table 3.2. Summary of lamellar parameters and degree of crystallinity estimated for iPP and its nanocomposites by different methods.

Samples	Lamellar parameters			Degree of crystallinity		
	L (Å) (± 0.5)	l_c (Å) (± 0.5)	l_a (Å) (± 0.5)	SAXS $(l_c/L)\times100$ (± 0.5)	WAXS* (± 0.5)	DSC** X_c (± 0.5)
iPP	130	76	54	58.4	65.0	58.7
iPP/μm-LDH (1 wt%)	140	81	59	57.8	63.5	55.4
iPP/nm-LDH (1 wt%)	155.5	89.5	66	57.5	64.2	57.0
iPP/nd-LDH (1 wt%)	169	99	70	58.5	65.3	59.9

*$X_c = \frac{I_c}{Ic+Ia} \times 100$, where I_c is area under the crystalline peaks and I_a is area under the amorphous halo.

**$X_c = \frac{\Delta H_m}{\Delta H_m^o} \times 100$, where ΔH_m is the observed melting enthalpies of iPP and its nanocomposites and ΔH_m^o is melting enthalpy of 100% crystalline iPP (177 J/g).[44]

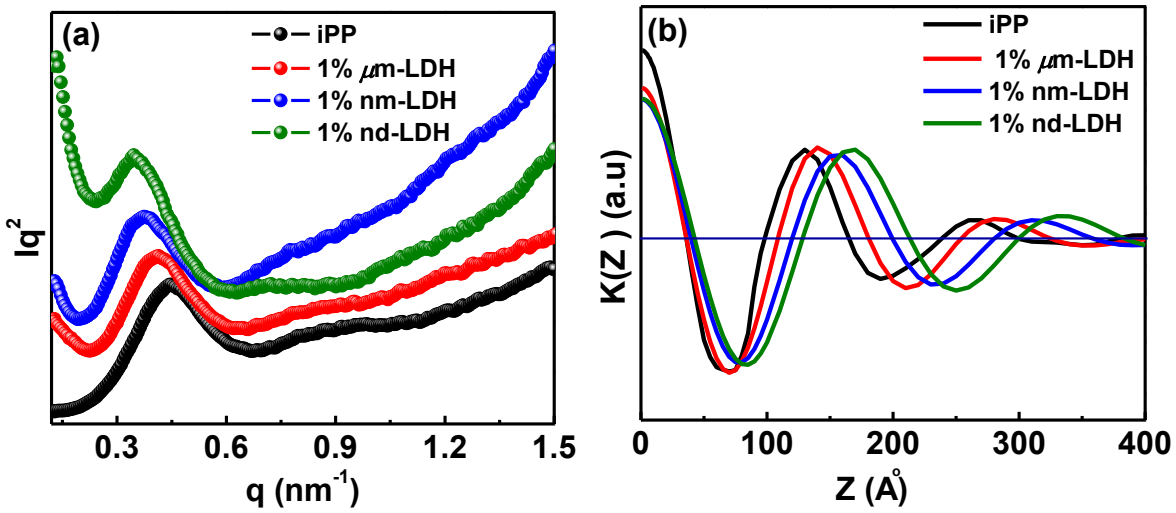

Figure 3.7. (a) Lorentz corrected SAXS patterns of iPP and its nanocomposites with different-sized LDH, (b) corresponding 1D electron density correlation function curves.

Corresponding WAXS pattern (not shown here) showed the presence of minor fractions of the γ form similar to that of the iPP/nd-LDH sample. The degree of

crystallinity was estimated by deconvolution method and the results are summarized in Table 3.2. It is apparent that the degree of crystallinity is not affected much by the addition of different-sized LDH.

To further understand the change in the lamellar thickness, SAXS measurements were carried out on the pristine iPP and its nanocomposites. Figure 3.7a shows the Lorentz-corrected SAXS patterns for both pristine iPP and the nanocomposites prepared using different-sized LDH. Pristine iPP sample shows a peak at ~0.45 nm^{-1} attributed to the alternating crystalline and amorphous microstructure of the lamellae. A broad scattering peak at higher q (~0.9 nm^{-1}) in pristine iPP indicates the formation of ordered periodic lamellar structure. On the other hand, nanocomposite samples containing 1 wt% of different-sized LDH show similar SAXS pattern, albeit the broad scattering intensity at low q, which might be due to the presence of well-dispersed LDH particles within the iPP matrix. The slope of the scattering intensity at low q was found to have correlation with the lateral size of the LDH particles. From the SAXS patterns showed in Figure 3.7a, it is obvious that the presence of different-sized LDH particles do not significantly modify the lamellar structure of iPP other than the morphological parameters such as long period (L), lamellar thickness (l_c) and amorphous thickness (l_a). In order to estimate the morphological parameters, Fourier transformation of the scattering curves was performed based on the method illustrated by Strobl and Schneider as shown in Figure 3.10a to yield the normalized one-dimensional electron density correlation function curves.[45] The lamellar parameters obtained for iPP and its nanocomposites are listed in Table 3.2.

As the crystallinity in these samples is around 60%, based on the earlier reports, we assume that the larger value is crystalline lamellar thickness, l_c, and the smaller value is the amorphous thickness, l_a.[46] These results indicate that the lamellar parameters are strongly influenced by the different-sized LDH. Both L and l_c values were found to increase with the addition of different-sized LDH. It was also found that these values increased with the decrease in the lateral size of the LDH. The L and l_c values of iPP/nd-LDH increased by 39 Å and 23 Å, respectively, with respect to the pristine iPP. In the preceding section, it was showed lateral size of the LDH strongly

influenced the T_{mc} of iPP (Figure 3.5a). In the case of iPP/nd-LDH nanocomposites, the overall crystallization rate of iPP increased significantly and as a result the polymer crystallized at the higher temperature during cooling from the melt. The strong dependence of the crystallization temperature on the lamellar thickness has been reported for some semicrystalline polymers.[47, 48] On the basis of these results, we may say that the lateral size of the particles influences the T_{mc} of iPP under nonisothermal conditions, and that T_{mc} determines the lamellar parameters. The degree of crystallinity ($(l_c/L)\times100$) estimated from the SAXS is in good agreement with the degree of crystallinity calculated from WAXS and DSC. Another noteworthy point to highlight here is that larger LDH particles are not located in the inter-lamellar region of iPP. Nam et al. illustrated the dispersion of clay platelets in the PP matrix in semicrystalline PP nanocomposites.[14] Similar to their case, LDH particles are expected to reside in the amorphous phase outside the stacked lamellar structure.

3.3.4. Performance of iPP/LDH Nanocomposites

3.3.4.1. Thermal Stability of iPP/LDH Nanocomposites

The influence of different-sized LDH (1 wt%) on the thermal stability of iPP was examined by TGA under nitrogen atmosphere (Figure 3.8). The single decomposition observed in all the nanocomposite samples indicates the random scission of polymeric chains is the major decomposition mechanism, quite similar to that of pristine iPP. The 50% weight loss temperature ($T_{0.5}$) for pure iPP is ~ 410 °C and it increases to 436 °C, 448 °C, and 457 °C for 1 wt% loaded iPP/μm-LDH, iPP/nm-LDH, and iPP/nd-LDH nanocomposites, respectively. As the lateral size of LDH decreases, the thermal stability of iPP increases significantly and highest thermal stability was observed in the case of iPP/nd-LDH nanocomposites. It has to be noted that though all the nanocomposite samples are reinforced with same amount of LDH (1 wt%), a significant difference in the thermal stability of iPP was observed with the lateral size of the LDH particles. As reported on our previous chapter, presumably, well dispersed LDH particles capture the radicals that generated during degradation.[12] It is expected that nd-LDH will have relatively large number of dispersed particles in the polymer matrix compared to that of the nm-LDH and μm-LDH. Similar result was observed by O'Hare and co-workers

using 1 wt% LDH loadings in surfactant-modified Mg-Al LDH/PP nanocomposites synthesized by microemulsion method.[49]

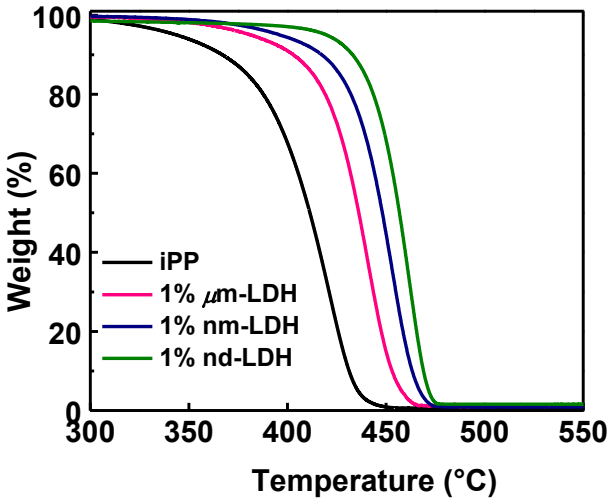

Figure 3. 8. TGA thermograms of iPP and its nanocomposites with different-sized LDH.

3.3.4.2. Dynamic Mechanical Analysis (DMA)

The viscoelastic properties of the iPP and its nanocomposites were analyzed using DMA and the data are given in Figure 3.9. It has to be noted that for viscoelastic properties, nanocomposites were prepared with 5 wt% of different-sized LDH. It is observed that the storage modulus (E') of the nanocomposites is higher than the pristine iPP in the entire temperature range and it decreases with increasing temperature with a plateau region observed near the glass transition temperature (T_g). The sharp reduction of E' in the lower temperature region can be assigned to the amorphous phase relaxation of iPP.[50, 51] It can be seen that the lateral size of the LDH has a significant role on the increase of storage modulus of iPP. Smaller the LDH particle, higher is the storage modulus of iPP. Among the different-sized LDH, nanocomposites having nd-LDH showed higher E' due to the better reinforcing effect of smaller-sized LDH particles in the polymer matrix. These results indicated that higher the surface area of LDH, the stronger is the interfacial strength between iPP and LDH particles.

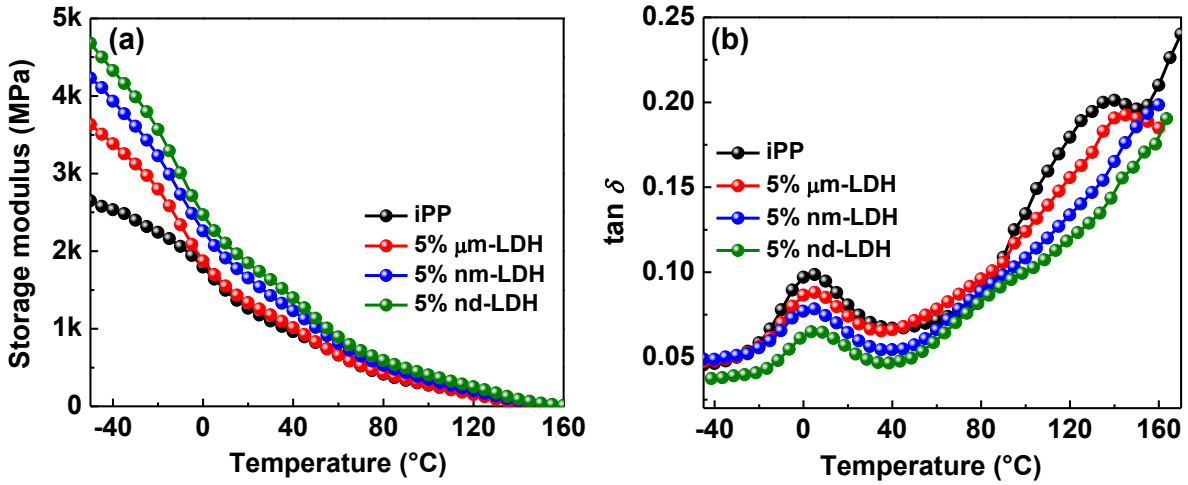

Figure 3.9. Temperature-dependent dynamic mechanical properties of iPP and its nanocomposites containing different-sized LDH: (a) storage modulus (*E'*) and (b) tan *δ*.

The tan δ plot obtained from DMA is given in Figure 3.9b, which gives information about the damping ability of the material. The subtle change in the molecular level motion and the chain relaxations of semicrystalline polymers can be probed from this analysis. In the present case, the peak near ~ 6 °C remains more or less at same temperature in iPP and its nanocomposites, indicating that T_g is not affected by the addition LDH.[14, 50-52] But it should be noted that the intensity of this peak is decreased with the decrease in lateral size of LDH and this might be due to the decreased damping of the stiffer nanocomposites formed with the highly dispersed nd-LDH. In other words, these nd-LDH have more effective interfacial adhesion to the polymer matrix, thereby reducing the molecular chain motions which is indicated by the reduced height of the peak corresponding to T_g. The second broad peak in tan δ lying above 120 °C is arising from the relaxation and reorganization of the crystalline lamella and crystalline-amorphous interface of iPP.[46, 50, 51] It is noticed that storage modulus is decreased and damping of the polymer chains are increased in this temperature regime. It is to be underlined that damping is much lower in the case of nd-LDH composites and no peak is visible in the selected temperature region, possibly due to the fact that presence of smaller-sized LDH favored the lamellar thickening and restricts the free movement and molecular relaxations of amorphous iPP chains due to the increased number of LDH particles.[46, 50-52]

Table 3.3. Summary of DMA analysis of iPP and its nanocomposites containing different-sized LDH.

Samples	Storage modulus (E') MPa at -30 °C (± 0.1)	Storage modulus (E') MPa at 0 °C (± 0.1)	tan δ_{max} (°C) (± 1)
iPP	2.4	1.7	6.1
5 wt% iPP/μm-LDH	3.3	1.9	5.8
5 wt% iPP/nm-LDH	3.9	2.2	5.4
5 wt% iPP/nd-LDH	4.5	2.5	6.7

3.4. Conclusions

Different-sized Mg-Al LDH were prepared by the conventional co-precipitation method, and particularly, a new method was developed to prepare nanodot-LDH by treating the as-prepared LDH with dilute acid. This method provided directly delaminated LDH sheets with lateral dimensions as low as 10-30 nm and feature a thickness of ~1 nm with the same chemical composition. As reported in our previous chapter, highly dispersed iPP nanocomposites were prepared by the solvent mixing method. It was observed that there is a clear dependence of the lateral size of LDH on the physical properties of iPP, and as the lateral size decreases, the properties such as thermal stability and mechanical properties are enhanced significantly. The uniformly dispersed nd-LDH particles have a significant effect on spherulite size, lamellar thickness, and crystal structure of iPP with very low LDH loadings (only 1 wt %). Isothermal and nonisothermal crystallization results revealed that the overall crystallization rate of iPP is faster in the presence of nd-LDH compared to that of the nm-LDH and μm-LDH and it might be due to the presence of the relatively large number of dispersed particles in the polymer matrix with high surface area.

3.5. Experimental Section

Materials: IPP pellets (M_w ~120000, $Đ$ ~4.5) and metal salts like aluminium nitrate ($Al(NO_3)_3 \cdot 9H_2O$), and magnesium nitrate ($Mg(NO_3)_2 \cdot 6H_2O$)) were purchased from Sigma-Aldrich Co. Ltd. Other chemicals such as urea, hexamethylenetetramine (HMT), xylene,

dimethylformamide (DMF), hydrochloric acid (HCl), ethanol, and acetone were received from Merck, India.

Synthesis of LDH: The Mg-Al LDH with different lateral sizes was synthesized using the conventional co-precipitation method as follows.

Micrometer-sized Mg-Al LDH (μm-LDH): Micrometer-sized LDH was synthesized using procedure adopted in the previous chapter.

Nanosized Mg-Al LDH (nm-LDH): The nanosized LDH was synthesized using a strong base HMT.[27] Magnesium nitrate ($Mg(NO_3)_2 \cdot 6H_2O$), aluminium nitrate ($Al(NO_3)_3 \cdot 9H_2O$), and HMT were dissolved in Millipore water in a molar ratio of 2:1:15 which results in a final concentration of 10, 5, 75 mM, respectively. The mixture was refluxed at 100 °C under continuous stirring for 24 hours in inert atmosphere. The precipitate was repeatedly washed with hot Millipore water to remove the unreacted reactants if any and vacuum dried at 60 °C for 24 hours. The lateral sizes of the LDH synthesized by this procedure are ~100-200 nm. Similar to the above, LDH obtained by this method was further washed with acetone and dispersed in xylene to obtain the delaminated LDH nanosheets. Hereafter delaminated nanosized LDH having lateral dimensions ~100-200 nm will be labelled as nm-LDH.

Nanodot Mg-Al LDH (nd-LDH): Nanosized LDH prepared using HMT as base was sonicated in a mixture of DMF and HCl (4:1 volume ratio) for 2 hours to obtain the nanodot Mg-Al LDH. In this procedure, the treatment of LDH with the acid leads to the simultaneous size reduction and the delamination of LDH. The lateral sizes of the nanodot LDH ~10-30 nm. Hereafter these LDH were labelled as nd-LDH.

Preparation of iPP/LDH Nanocomposites: The nanocomposites of iPP/Mg-Al LDH containing three different sized LDH (μm, nm and nd) were prepared using solution blending method as discussed in chapter-2.

3.6. Characterization

XEUSS 2D SAXS/WAXS system with a Genixmicro source from Xenocs was used for the WAXD and SAXS measurements as discussed in chapter-2. Samples crystallized under controlled conditions using a differential scanning calorimeter were used for the X-ray measurements. The two-dimensional SAXS images were azimuthally integrated to obtain 1D scattering intensity profiles as a function of q, where q is the magnitude of scattering vector,

$q = 4\pi \sin \theta/\lambda$, with 2θ being the scattering angle and λ is the X-ray wavelength. The resulting scattering intensity SAXS profiles were corrected for background scattering. To resolve the structure parameters of lamellar structure such as long period (L), lamellar thickness (l_c) and amorphous thickness (l_a), normalized one-dimensional electron density correlation function was derived from the small-angle X-ray scattering curves.

With the assumption of stacked lamellar structure (crystalline and amorphous layers), the normalized one-dimensional electron density correlation function (K(z)) is defined as follows.[45]

$$K(z) = \int_0^\infty q^2 I(q) \cos(qz)\, dq \qquad (3.1)$$

Where z is normal to the layer faces in the lamellar stack, and $I(q)$ is the scattered intensity. The various lamellar structural parameters were calculated from the K(z) curve as shown in Figure 3.10.

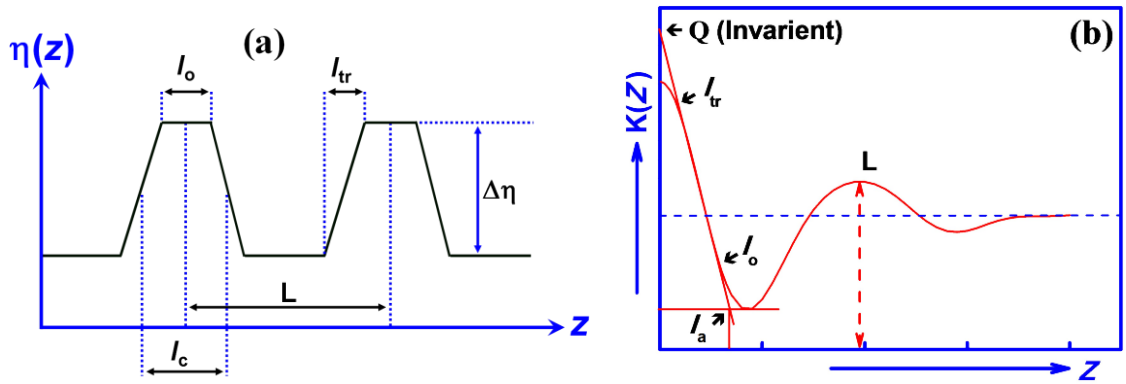

Figure 3.10. Electron density distribution $\eta(z)$ and the one-dimensional electron density correlation function $K(z)$ for the lamellar system. L is the long period and l_a is the amorphous thickness. The mean lamellar thickness (l_c) is obtained by subtracting l_a from the L ($l_c = L - l_a$).

The morphology of various LDH prepared were analyzed with TEM and SEM as discussed in previous chapter. AFM (Digital Instruments, Inc., Santa Barbara with imaging performed using a Dimension 3100 and a CP microscope Park Scientific Instrument, Inc in the tapping mode) was used to probe the dimensions of LDH.

In order to view the polymer nanocomposites, ultrathin sections of the samples (thickness ~ 60 nm) were sliced with a diamond knife (35° knife angle; DIATOME, Switzerland) using ultramicrotome EM UC/FC 6, Leica (Austria) at -140°C. The sections were flooded with a DMSO/water mixture on carbon filmed TEM copper grid. These thin slices of the samples polymer nanocomposites were analyzed using a TEM LIBRA. A

polarized optical microscope (Universal polarizing microscope ZPU01, Carl Zeiss Inc.) equipped with a Linkam hot stage was used to monitor the spherulites. The thin-film specimens were prepared by melting the samples at 200 °C for 1 min and then rapidly cooled to the crystallization temperature. The samples were imaged at the isothermal crystallization temperature of 130 °C.

DSC measurements were performed on a TA Instruments DSC Q2000 model equipped with a refrigerated cooling system under nitrogen gas flow. The crystallization half-time ($t_{1/2}$) was measured to evaluate the crystallization rate of iPP and its nanocomposites. Molten samples were rapidly cooled to the desired crystallization temperature (T_c) (130 °C) at a rate of 100 °C/min, and then the samples were allowed to crystallize at that temperature. The non-isothermal crystallization data were collected while cooling the samples from the melt to room temperature at 10 °C/min. These samples were again reheated to 200 °C to analyze the melting behavior. DMA (TA Instruments Model Q800) was used to study the temperature-dependent dynamic mechanical properties of the samples. The samples with dimensions 25 × 6 × 0.4 mm^3 were prepared using the hot press. All samples were annealed at 130 °C for 5 h. The prepared samples were used to measure the temperature-dependent storage modulus (E') and tan δ at a constant frequency (ω) of 6.28 rad/s with strain amplitude of 0.05%. The measurements were carried out in a temperature range of -50 to 160 °C, with a heating rate of 2 °C/min. Thermal stability of the prepared nanocomposites were analyzed with thermo gravimetric analysis TA Q50 instrument in the heating process at a heating rate of 10 °C/min. All the TGA measurements were carried out under the nitrogen atmosphere (nitrogen gas flow rate of 60 mL/min for the furnace and 40 mL/min for balance).

3.7. References

1 H. Karian, *Handbook of polypropylene and polypropylene composites, revised and expanded*, CRC press (2003).

2 J. Karger-Kocsis, *Polypropylene structure, blends and composites: Volume 3 composites*, Springer Science & Business Media (2012).

3 E. Manias, A. Touny, L. Wu, K. Strawhecker, B. Lu and T. C. Chung, *Chem Mater* **13:**3516-3523 (2001).

4 M. Alexandre and P. Dubois, *Mater. Sci. Eng. R-Rep.* **28:**1-63 (2000).

5 T. Kashiwagi, E. Grulke, J. Hilding, K. Groth, R. Harris, K. Butler, J. Shields, S. Kharchenko and J. Douglas, *Polymer* **45:**4227-4239 (2004).

6 S. Zhang and A. R. Horrocks, *Prog Polym Sci* **28:**1517-1538 (2003).

7 H. Kim, A. A. Abdala and C. W. Macosko, *Macromolecules* **43:**6515-6530 (2010).

8 D.-Y. Wang, A. Das, A. Leuteritz, R. N. Mahaling, D. Jehnichen, U. Wagenknecht and G. Heinrich, *RSC Adv* **2:**3927-3933 (2012).

9 D. Basu, A. Das, K. W. Stöckelhuber, U. Wagenknecht and G. Heinrich, *Prog Polym Sci* **39:**594-626 (2014).

10 T. D. Fornes and D. R. Paul, *Polymer* **44:**3945-3961 (2003).

11 L. Li, C. Y. Li and C. Ni, *J Am Chem Soc* **128:**1692-1699 (2006).

12 B. Nagendra, K. Mohan and E. B. Gowd, *ACS Appl Mater Interfaces* **7:**12399-12410 (2015).

13 J.-Z. Xu, G.-J. Zhong, B. S. Hsiao, Q. Fu and Z.-M. Li, *Prog Polym Sci* **39:**555-593 (2014).

14 P. H. Nam, P. Maiti, M. Okamoto, T. Kotaka, N. Hasegawa and A. Usuki, *Polymer* **42:**9633-9640 (2001).

15 M. D'Haese, F. Langouche and P. Van Puyvelde, *Macromolecules* **46:**3425-3434 (2013).

16 Z. Xu, Y. Niu, Z. Wang, H. Li, L. Yang, J. Qiu and H. Wang, *ACS Appl Mater Interfaces* **3:**3744-3753 (2011).

17 M. Naffakh, A. M. Díez-Pascual, C. Marco, G. J. Ellis and M. A. Gómez-Fatou, *Prog Polym Sci* **38:**1163-1231 (2013).

18 N.-J. Kang, D.-Y. Wang, B. Kutlu, P.-C. Zhao, A. Leuteritz, U. Wagenknecht and G. Heinrich, *ACS Appl Mater Interfaces* **5:**8991-8997 (2013).

19 P. J. Purohit, J. E. Huacuja-Sánchez, D.-Y. Wang, F. Emmerling, A. Thünemann, G. Heinrich and A. Schönhals, *Macromolecules* **44:**4342-4354 (2011).

20 B. P. Grady, F. Pompeo, R. L. Shambaugh and D. E. Resasco, *J Phys Chem B* **106:**5852-5858 (2002).

21 A. R. Bhattacharyya, T. V. Sreekumar, T. Liu, S. Kumar, L. M. Ericson, R. H. Hauge and R. E. Smalley, *Polymer* **44:**2373-2377 (2003).

22 C. Chen, A. Wangriya, J.-C. Buffet and D. O'Hare, *Dalton Trans* **44:**16392-16398 (2015).

23 Q. Wang, X. Zhang, J. Zhu, Z. Guo and D. O'Hare, *Chem Commun* **48:**7450-7452 (2012).

24 D. G. Evans and R. C. T. Slade, Structural Aspects of Layered Double Hydroxides, in *Layered Double Hydroxides*, ed by X. Duan and D. G. Evans. Springer Berlin Heidelberg, Berlin, Heidelberg, pp. 1-87 (2006).

25 Y. Zhao, F. Li, R. Zhang, D. G. Evans and X. Duan, *Chem Mater* **14:**4286-4291 (2002).

26 A. P. Tathod and O. M. Gazit, *Cryst Growth Des* **16:**6709-6713 (2016).

27 K. Okamoto, N. Iyi and T. Sasaki, *Appl Clay Sci* **37:**23-31 (2007).

28 L. Dong, S. Lin, L. Yang, J. Zhang, C. Yang, D. Yang and H. Lu, *Chem Commun* **50:**15936-15939 (2014).

29 Z. Liu, R. Ma, M. Osada, N. Iyi, Y. Ebina, K. Takada and T. Sasaki, *J Am Chem Soc* **128:**4872-4880 (2006).

30 R. Ma, Z. Liu, L. Li, N. Iyi and T. Sasaki, *J Mater Chem* **16:**3809-3813 (2006).

31 M. L. Parello, R. Rojas and C. E. Giacomelli, *J Colloid Interface Sci* **351:**134-139 (2010).

32 F. Leroux, M. Adachi-Pagano, M. Intissar, S. Chauviere, C. Forano and J.-P. Besse, *J Mater Chem* **11:**105-112 (2001).

33 F. Song and X. Hu, *Nat Commun* **5:**4477 (2014).

34 M. R. Mani, R. Chellaswamy, Y. N. Marathe and V. K. Pillai, *Chem Commun* **51:**10026-10029 (2015).

35 M. Avrami, *J Chem Phys* **7:**1103-1112 (1939).

36 B. Lotz and J. C. Wittmann, *J Polym Sci Part B Polym Phys* **24:**1541-1558 (1986).

37 F. Padden Jr and H. Keith, *J Appl Phys* **30:**1479-1484 (1959).

38 P. Maiti, P. H. Nam, M. Okamoto, N. Hasegawa and A. Usuki, *Macromolecules* **35:**2042-2049 (2002).

39 A. T. Jones, J. M. Aizlewood and D. R. Beckett, *Makromol Chem* **75:**134-158 (1964).

40 R. Thomann, C. Wang, J. Kressler and R. Mülhaupt, *Macromolecules* **29:**8425-8434 (1996).

41 R. G. Alamo, M.-H. Kim, M. J. Galante, J. R. Isasi and L. Mandelkern, *Macromolecules* **32:**4050-4064 (1999).

42 B. Lotz, S. Graff, C. Straupé and J. C. Wittmann, *Polymer* **32:**2902-2910 (1991).

43 S. Brückner, P. J. Phillips, K. Mezghani and S. V. Meille, *Macromol Rapid Commun* **18:**1-7 (1997).

44 J. X. Li, W. L. Cheung and D. Jia, *Polymer* **40:**1219-1222 (1999).

45 G. R. Strobl and M. Schneider, *J Polym Scie: Poly Phys Edi* **18:**1343-1359 (1980).

46 P. Liu, K. L. White, H. Sugiyama, J. Xi, T. Higuchi, T. Hoshino, R. Ishige, H. Jinnai, A. Takahara and H.-J. Sue, *Macromolecules* **46:**463-473 (2013).

47 S. Z. D. Cheng, L. Zhu, C. Y. Li, P. S. Honigfort and A. Keller, *Thermochimica Acta* **332:**105-113 (1999).

48 N. S. Murthy, Z.-G. Wang and B. S. Hsiao, *Macromolecules* **32:**5594-5599 (1999).

49 Q. Wang, X. Zhang, C. J. Wang, J. Zhu, Z. Guo and D. O'Hare, *J Mater Chem* **22:**19113-19121 (2012).

50 A. M. Díez-Pascual and M. Naffakh, *ACS Appl Mater Interfaces* **5:**9691-9700 (2013).

51 B. Nagendra, C. V. S. Rosely, A. Leuteritz, U. Reuter and E. B. Gowd, *ACS Omega* **2:**20-31 (2017).

52 M. Naffakh, M. Remskar, C. Marco, M. A. Gomez-Fatou and I. Jimenez, *J Mater Chem* **21:**3574-3578 (2011).

Chapter-4

Polypropylene/Layered Double Hydroxide (LDH) Nanocomposites: Influence of LDH Intralayer Metal Constituents on the Properties of Polypropylene

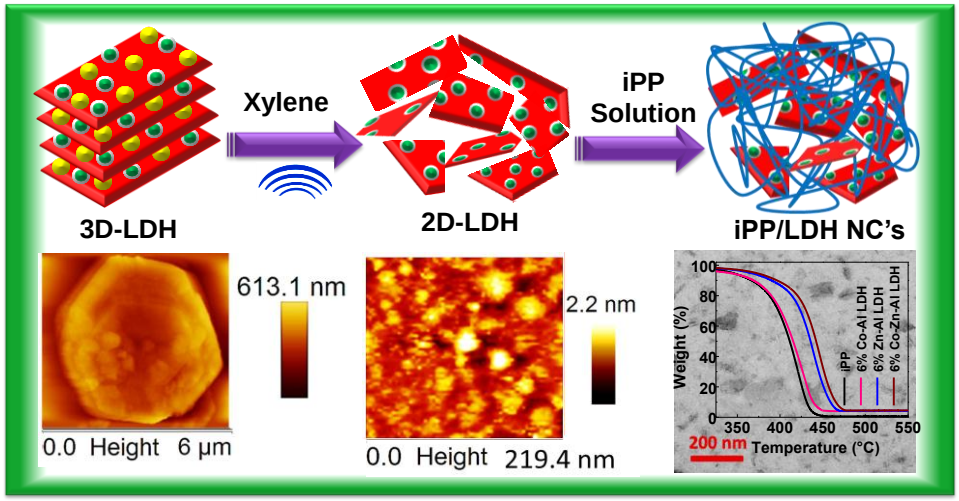

4.1. Abstract

Sonication-assisted delamination of LDH resulted in the smaller sized LDH nanoparticles (~50-200 nm). Such delaminated Co-Al LDH, Zn-Al LDH, and Co-Zn-Al LDH solutions were utilized for the preparation of highly dispersed iPP nanocomposites. TEM and WAXD results revealed that the LDH nanoparticles were well dispersed within the iPP matrix. The intention of the current study is to understand the influence of the intralayer metal composition of LDH on the various properties of iPP/LDH nanocomposites. The sonicated LDH nanoparticles showed a significant increase in the crystallization rate of iPP, however, not much difference in the crystallization rate of iPP was observed in the presence of different types of LDH. The dynamic mechanical analysis results indicated that the storage modulus of iPP was increased significantly with the addition of LDH. The

incorporation of different types of LDH showed no influence on the storage modulus of iPP. But considerable differences were observed in the flame retardancy and thermal stability of iPP with the type of LDH used for the preparation of nanocomposites. The thermal stability (50% weight loss temperature ($T_{0.5}$)) of the iPP nanocomposite containing three-metal-LDH (Co-Zn-Al LDH) is superior to nanocomposites made with the two-metal-LDH (Co-Al LDH and Zn-Al LDH). Preliminary studies on the flame retardant properties of iPP/LDH nanocomposites using the microscale combustion calorimetry showed that the peak heat release rate (HRR) was reduced by 39% in iPP/Co-Zn-Al LDH nanocomposite containing 6 wt% LDH, which is higher than that of two-metal-LDH containing nanocomposites iPP/Co-Al LDH (24%) and iPP/Zn-Al LDH (31%). These results demonstrated that the nanocomposites prepared using three-metal-LDH showed better thermal and flame retardant properties compared to that of the nanocomposites prepared using two-metal-LDH. This difference might be due to the better char formation capability of three-metal LDH compared to that of two-metal-LDH.

4.2. Introduction

Layered materials are an interesting class of compounds, consisting of 2D sheet like structure with strong bindings within the individual layer and weak Van der Waals forces between the layers.[1-4] The weak interaction between these layers allows them to be exfoliated or delaminated into ultrathin 2D nanosheets. These ultrathin nanomaterials have gained significant interest after the discovery of exfoliated graphene from graphite.[5] Dozens of 2D nanomaterials have been reported in the last few years including transition metal oxides, transition metal dichalcogenides, hexagonal boron nitride, synthetic silicate clays, layered metal oxides, LDH, etc.[3, 6-9] Because of the promising applications of these ultrathin 2D nanomaterials, a large number of synthetic methods, such as mechanical cleavage,[5, 10] chemical vapor deposition,[11] ion-intercalation and exfoliation,[2] liquid exfoliation,[3, 6] etc., have been developed.

In recent times, LDH was considered as an emerging class of layered nanofillers for the preparation of polymer nanocomposites.[7, 12-29] Wang et al. converted the hydrophilic LDH layers to hydrophobic by an aqueous miscible organic solvent treatment and prepared the stable dispersions of LDH in nonpolar solvents.[18, 25, 30, 31]

Subsequently, the exfoliated LDH nanosheets were used to prepare polypropylene/LDH nanocomposites by solution blending method.[18, 25] Using this method, it was shown that the PP nanocomposites prepared with Zn_2Al-borate displayed better performance than the nanocomposites prepared with the equivalent Mg_3Al-borate.[25] In another study, Wang and co-workers revealed that the gallery anions resulted in a significant difference in the properties of the polymer/LDH nanocomposites.[32] Synergistic effect of different LDH with the combination of an intumescent flame retardant additive was studied by melt blending method and it was showed that the nanocomposite containing ternary LDH is a better flame retardant additive.[33] Recently, we have reported the highly dispersed iPP/LDH nanocomposites using two different sized (lateral size) LDH and showed that the lateral size of the LDH has a significant influence on the thermal stability and crystallization rate of iPP.[15]

Here, we prepared iPP/LDH nanocomposites filled with three different types of LDH (Co-Al LDH, Zn-Al LDH, and Co-Zn-Al LDH) by solvent mixing method, particularly using the sonicated LDH (fragmented LDH). Both LDH and iPP/LDH nanocomposites were carefully characterized by TEM, AFM, and WAXD. This study aims at unraveling the influence of the intralayer metal constituents of LDH on the crystallization rate, thermal stability, mechanical properties and flamretardancy of iPP nanocomposites. It was found that iPP/LDH nanocomposites containing three-metal-LDH showed better performance in thermal stability and flame retardancy compared to that of iPP/LDH nanocomposites containing two-metal LDH with the same loading.

4.3. Results and Discussion

4.3.1. Synthesis and Characterization of LDH

Both two-metal LDH (Co-Al and Zn-Al LDH) and three-metal LDH (Co-Zn-Al LDH) were synthesized under the similar conditions by co-precipitation method. The powder X-ray diffraction patterns of LDH are displayed in Figure 4.1a. The sharp and symmetric features of the X-ray reflections corresponding to the (00n) planes suggest that the produced LDH have well-organized 2D layer stacking. A slight difference in the peak positions of (00n) planes of different LDH may be due to the presence of either different anions or amount of water molecules within the LDH layer.[32, 34] Several other

reflections assigned to the lattice were observed in the 2θ range 30° – 70° (Figure 4.7c). Overall, the X-ray pattern of the Co-Zn-Al LDH was nearly identical to those of Co-Al LDH and Zn-Al LDH in terms of peak positions and intensities. No peaks other than the typical LDH were detected, indicating the high purity of the obtained products. In literature, similar observation was made in the X-ray patterns of Mg-Al LDH upon the substitution of Mg^{2+} with Co^{2+} to obtain the Mg-Co-Al LDH.[35] Figure 4.1b shows the FTIR spectra of the various LDH studied in this work. All the LDH exhibited the characteristic bands for interlayer carbonate (CO_3^{2-}) and interlayer nitrate (NO_3^-) at 1356 cm^{-1} and 1382 cm^{-1}, respectively. The conditions favored the formation of CO_3^{2-} and NO_3^- was explained in our previous chapter-2.[15] The presence of IR bands at 3440 cm^{-1} (ν(O-H)) and 1632 cm^{-1} ($\delta(H_2O)$) confirmed the presence of interlayer water molecules.

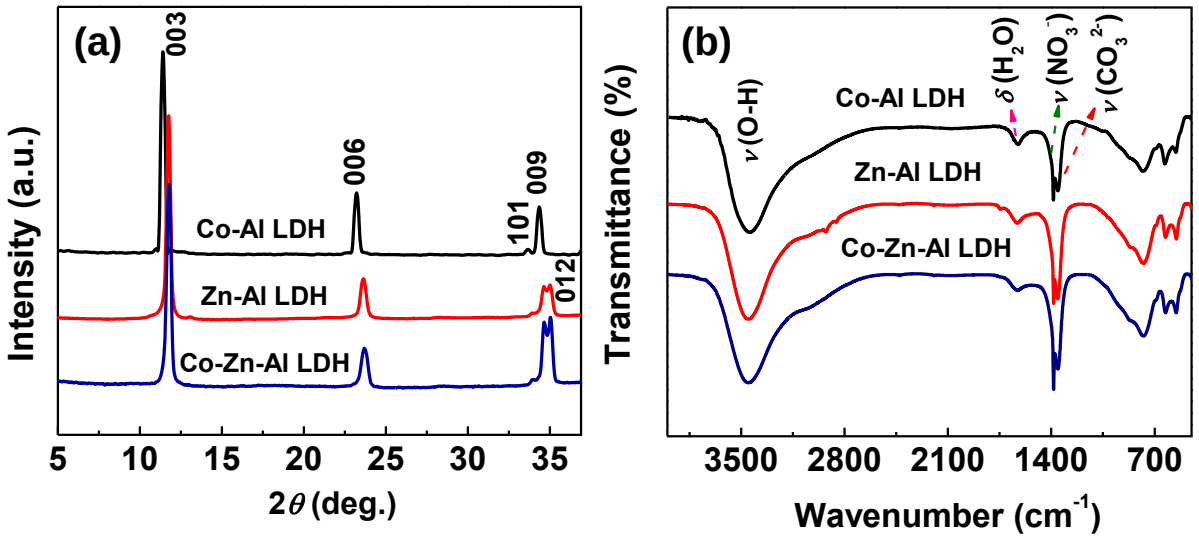

Figure 4.1. (a) Powder X-ray diffraction patterns and (b) FTIR spectra of as-prepared Co-Al LDH, Zn-Al LDH, and Co-Zn-Al LDH.

To obtain the information about the size and shape of the as-synthesized LDH (bulk), the SEM and TEM images were taken and are shown in Figure 4.2. As-prepared LDH platelets displayed the three-dimensional (3D) platelet-like morphology with a dark contrast, indicating the presence of several layers of platelets in a single particle. However, the sizes and shapes of these LDH have found to be different from each other. The Co-Al LDH, Zn-Al LDH, and Co-Zn-Al LDH adopted different morphologies such as circular platelets, hexagonal platelets with rounded edges and hexagonal platelets with

sharp edges, respectively. This difference could be associated with the nucleation and growth mechanism of LDH in different reaction environments (metal salts) and conditions.[36] The chemical compositions of the different LDH were confirmed by energy-dispersive X-ray spectra (EDS) (Figure 4.2). The dominant oxygen peak in EDS of different LDH indicates the presence of water molecules within the layers as well as hydroxyl groups associated with the layers of the as-synthesized LDH platelets.

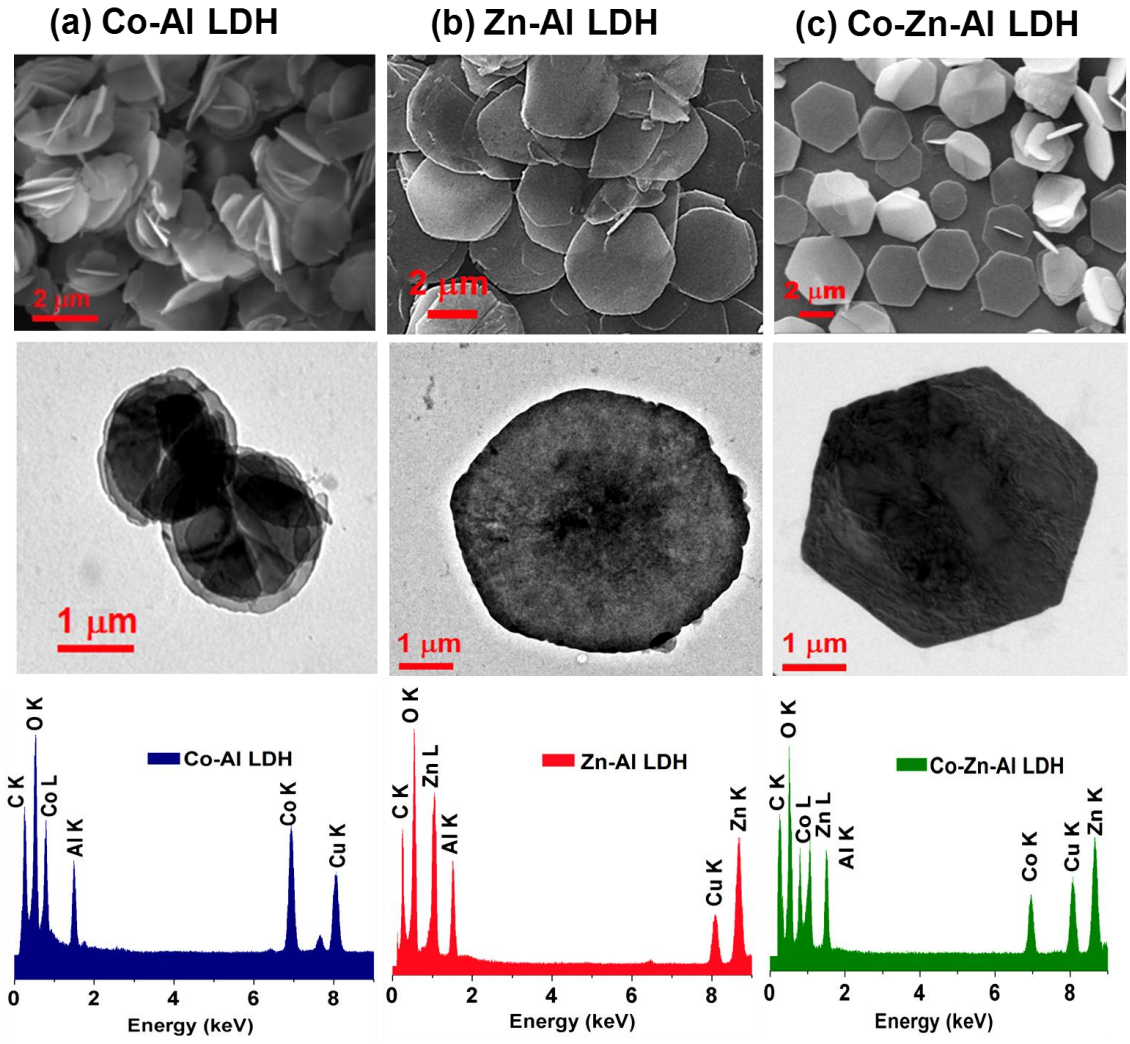

Figure 4.2. SEM, TEM and EDS analysis of as-synthesized LDH (a) Co-Al LDH, (b) Zn-Al LDH and (c) Co Zn Al-LDH.

4.3.2. Sonication Assisted Exfoliation of LDH

O'Hare and co-workers recently reported an AMOST method for the preparation of stable dispersions of LDH in nonpolar solvents.[18, 25] Recently, we have reported a

slightly modified method to obtain highly delaminated sheets of LDH by sonication.[15] The advantage of this sonication process is simultaneous delamination and the lateral fragmentation of LDH. It is also worth mentioning here that, ultrasonic vibration has been extensively used in the liquid exfoliation of two-dimensional layered materials such as graphene, transition metal oxides, and transition metal dichalcogenides.[3, 37-39]

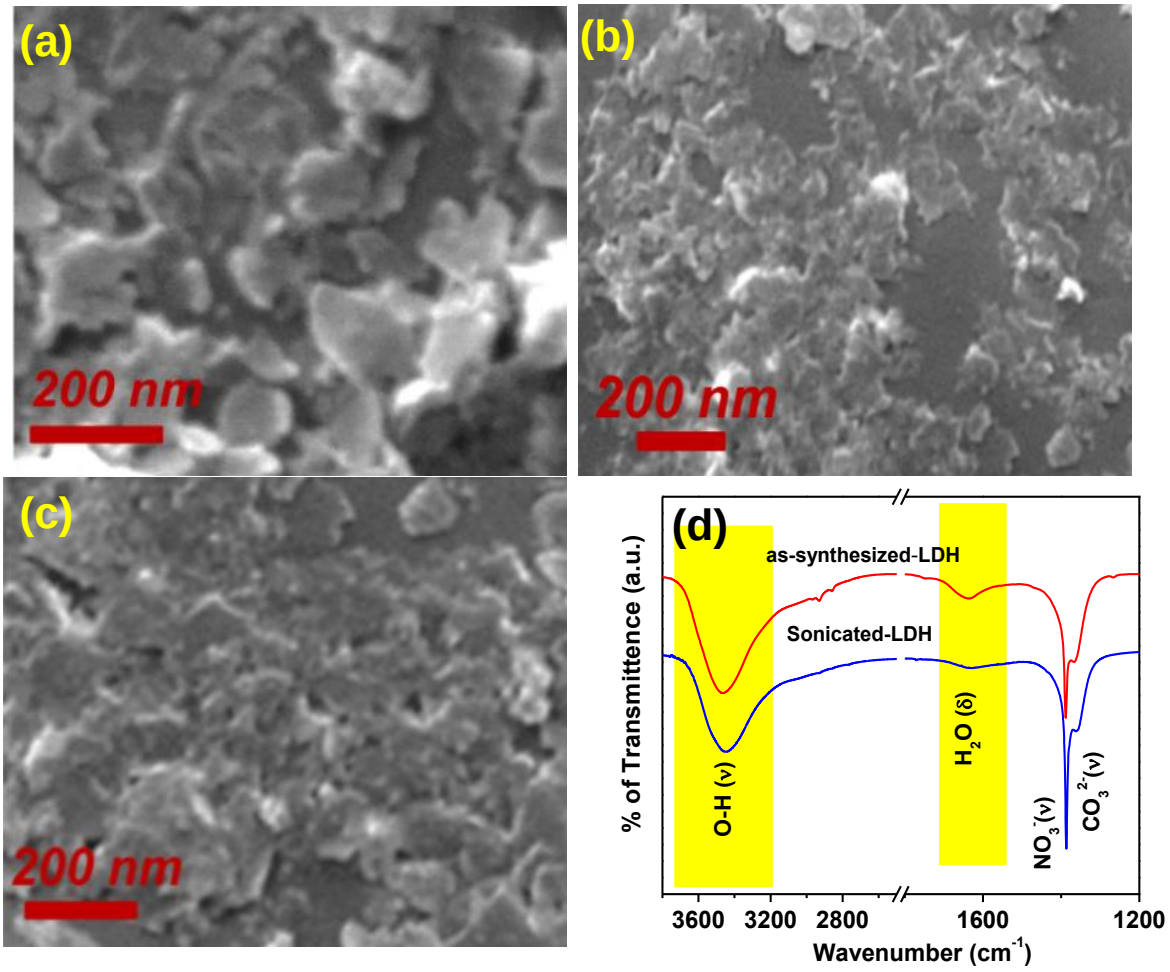

Figure 4.3. SEM images of fragmented LDH nanosheets of (a) Co-Al LDH, (b) Zn-Al LDH, and (c) Co-Zn-Al LDH and (d) FTIR spectra of as-synthesized LDH and sonicated-LDH.

In this study, we used the same process to delaminate the different LDH in xylene. The SEM images of different LDH (Figure 4.3) show the broken platelets in large scale, and the lateral size of LDH reduced to few tens of nanometers. The ultrathin sheets of LDH were directly observed by TEM as shown in Figure 4.4. It is evident that

LDH platelets are broken into small pieces and exhibit a faint contrast compared to their bulk counterparts.

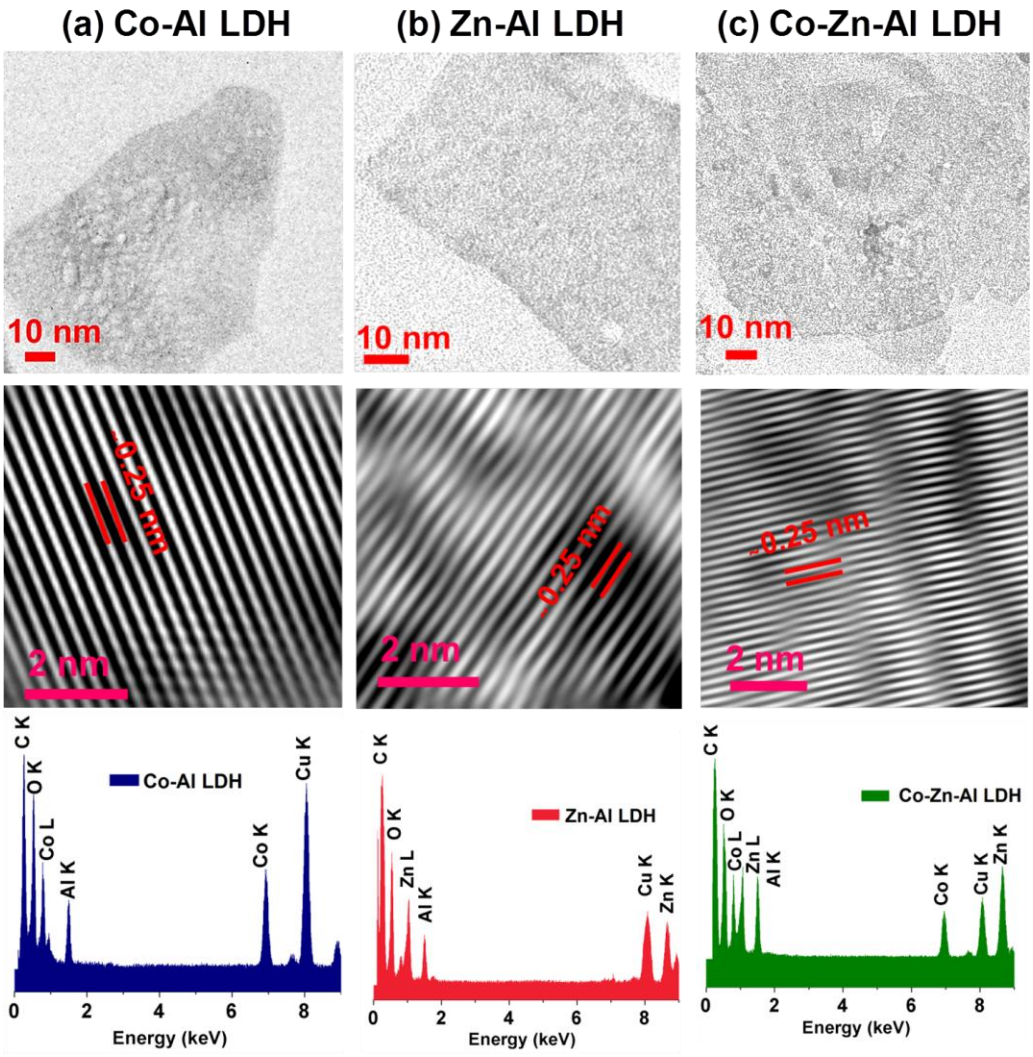

Figure 4.4. Low- and high-resolution TEM images and the corresponding energy dispersive spectra of exfoliated LDH nanosheets (a) Co-Al LDH, (b) Zn-Al LDH, and (c) Co-Zn-Al LDH.

Further, high-resolution TEM was used to obtain more detailed information on the exfoliated LDH (Figure 4.4). These images revealed that the exfoliated LDH sheets are fairly clean and highly crystalline. The uniform atomic orientation and lattice spacing reveal that an individual layer consists of a single crystal domain. The lattice fringes with the same *d*-spacing of ~ 0.25 nm corresponding to the (012) crystal plane were observed in all the LDH samples, and these values are consistent with the *d*-spacing estimated from the XRD results.[40] The EDS spectra of exfoliated LDH

nanosheets are almost comparable to their bulk counterparts other than the oxygen/carbon peak intensity ratio. The intensity of the oxygen peak decreased drastically indicating the removal of water molecules in the exfoliated samples. The removal of water molecules in the exfoliated samples was further confirmed FTIR spectra (Figure 4.3d).

The thickness of Co-Zn-Al LDH (both in bulk and exfoliated form) was evaluated by the AFM. Figure 4.5 shows the typical AFM height images and corresponding height profiles of Co-Zn-Al LDH before and after exfoliation. It is evident from the Figure 4.5a that the as-synthesized sample shows the 3D platelet like-morphology with the lateral size ~ 5 μm and the thickness around few hundreds of nanometers. On the other hand, the exfoliated nanosheets (Figure 4.5b) shows the thickness of fragmented LDH is less than 1.0 nm. This value is in good agreement with the reported value for the single layer of LDH.[2, 34] From these results, we may say that as-synthesized sample contain few hundreds of stacked layers of LDH. The lateral sizes of the exfoliated LDH are ranging from 50 nm to few hundreds of nm and are consistent with the TEM results.

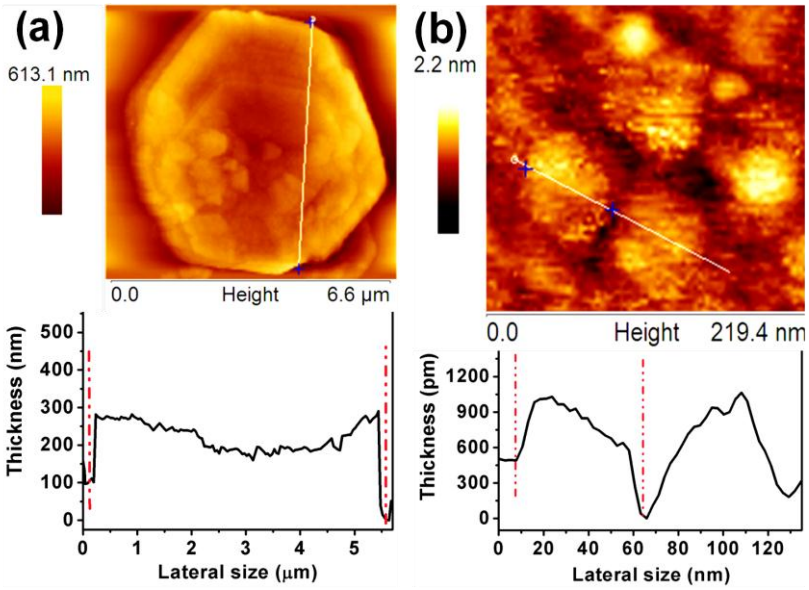

Figure 4.5. AFM images and height profiles of (a) as-synthesized and (b) exfoliated single layer Co-Zn-Al LDH nanosheets.

4.3.3. Synthesis, Structure and Morphology of iPP/LDH Nanocomposites

Schematic representation of the methodology used for the preparation of highly dispersed iPP/LDH nanocomposites is shown in Figure 4.6. As-synthesized LDH was washed with acetone to remove interlayer H_2O molecules from the stacked LDH layers. This process helps in converting the hydrophilic LDH to hydrophobic, and that facilitates the better dispersibility of LDH within the iPP matrix.[22, 25] Subsequently, such washed LDH was sonicated for four days in xylene. The advantage of this step is the simultaneous surface modification and fragmentation of the LDH. Most importantly, this method produces the 2D layered materials with lateral sizes and thickness in the nanometer range. The resulted LDH solution was directly added to the iPP solution to obtain highly dispersed nanocomposites. In the present study, iPP nanocomposites were prepared using three different LDH (Co-Al LDH, Zn-Al LDH, and Co-Zn-Al LDH) by adjusting the amount of LDH to 6 wt %. In addition to this, to understand the influence of LDH loading, in one case iPP/LDH nanocomposites were prepared with 10 wt% of Co-Zn-Al LDH.

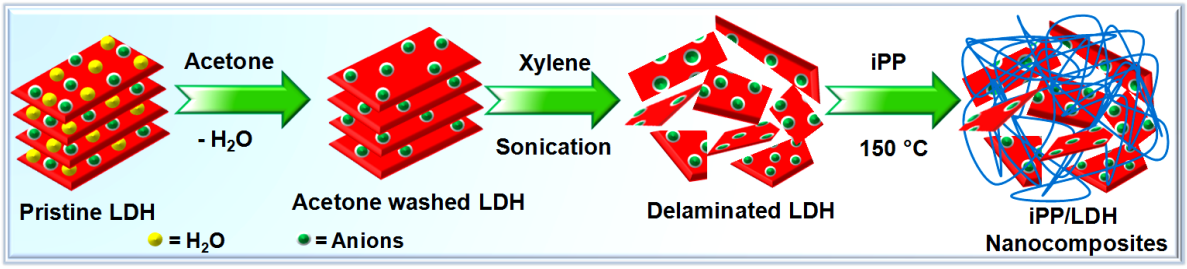

Figure 4.6. Schematic representation of the methodology used for the preparation of highly dispersed polymer nanocomposites based on iPP and LDH.

Such prepared iPP/LDH nanocomposites were crystallized isothermally at 130°C after melting at 200 °C under strictly controlled conditions and analyzed by the X-ray diffraction. Figure 4.7(a, c) shows the X-ray diffraction patterns of various nanocomposites along with the pristine iPP and Co-Zn-Al LDH. The X-ray diffraction patterns of nanocomposites are almost similar to that of the pristine iPP. Both iPP and iPP/LDH nanocomposites show reflections corresponding to the monoclinic α-form.[41] At the same time, no reflections corresponding to the (00n) planes of LDH were observed in nanocomposites indicating the loss of 2D layer stacking of LDH within the

iPP matrix. These results suggest that exfoliated LDH platelets have been successfully dispersed into the polymer matrix without much agglomeration during solution blending. The state of LDH dispersion within the iPP matrix was further confirmed by TEM measurements. Figure 4.7b shows a cross-sectional TEM image of the nanocomposite containing 10 wt % of Co-Zn-Al LDH. The nanosized LDH platelets are homogeneously dispersed in the polymer matrix with sizes ranging from 50 nm to few hundreds of nm. This suggests that the in solution blending method, LDH platelets are successfully transformed from solution to solid state with minimum agglomeration.

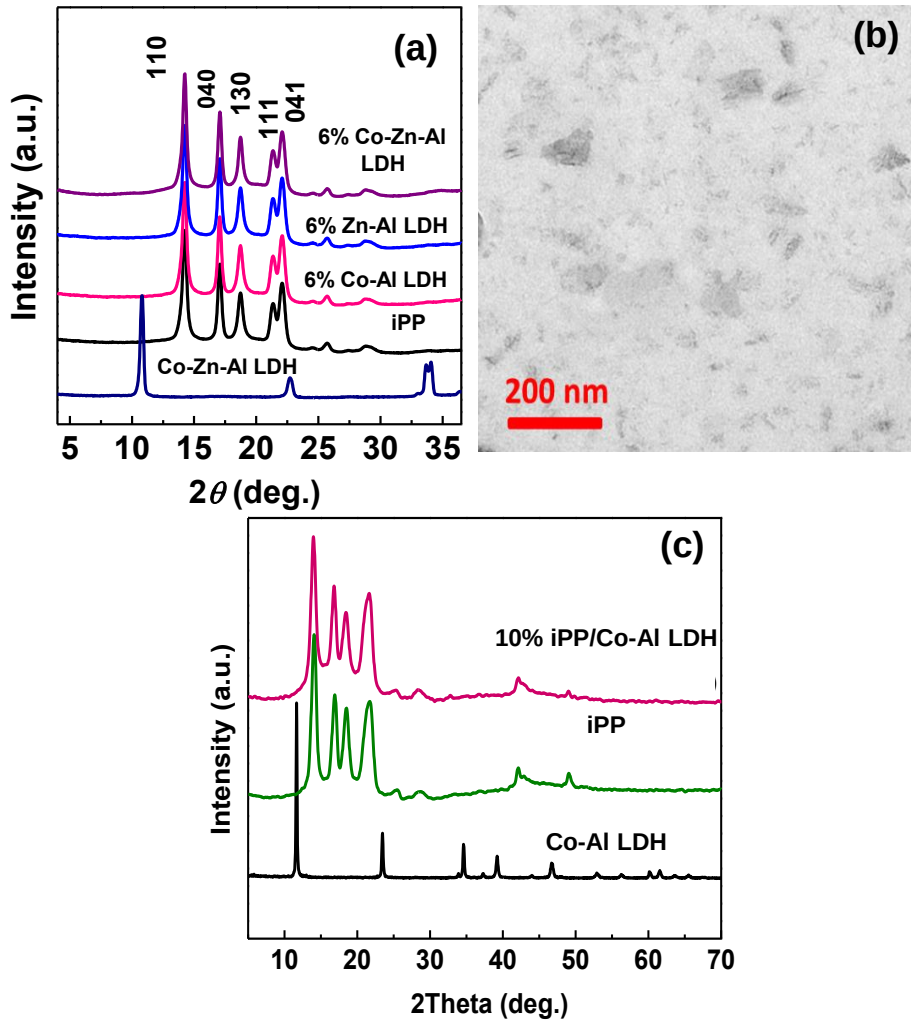

Figure 4.7. (a) Powder X-ray diffractions of iPP and its nanocomposites containing different types of LDH (for the purpose of comparison, powder X-ray diffraction pattern of LDH is shown) (b) cross-sectional TEM image of the iPP/Co-Zn-Al LDH (10 wt%) nanocomposite and (c) Powder X-ray diffraction patterns of Co-Al LDH, iPP and iPP/Co-Al LDH nanocomposite.

4.3.4. Crystallization of iPP/LDH Nanocomposites

Tailoring the crystallinity and crystallization rate of semicrystalline polymers is of great importance to the polymer processing industry. The incorporation of nanofillers in polymer matrices is known to alter the crystallization behavior and the degree of crystallinity of the polymer matrix; which in turn controls the physical properties of the polymers.[15, 42] In order to understand the effect of different LDH on the crystallization rate of iPP, the melt crystallization temperature (T_{mc}) was measured upon cooling the polymer melt. The T_{mc} have been often used to measure of the crystallization rate of the polymer. The higher the T_{mc}, the higher is the crystallization rate of the polymer.[43] Figure 4.8a shows DSC cooling curves of pristine iPP and its nanocomposites at 10 °C/min. The pristine iPP shows a T_{mc} at around 108 °C; however, T_{mc} values shift to 121 ± 1 °C for nanocomposites irrespective of the type of LDH. The higher T_{mc} of the nanocomposites compared to that of iPP clearly indicates the faster crystallization of iPP in the presence of LDH; however, no change in the crystallization rate was observed with the type of LDH used for the preparation of nanocomposites.

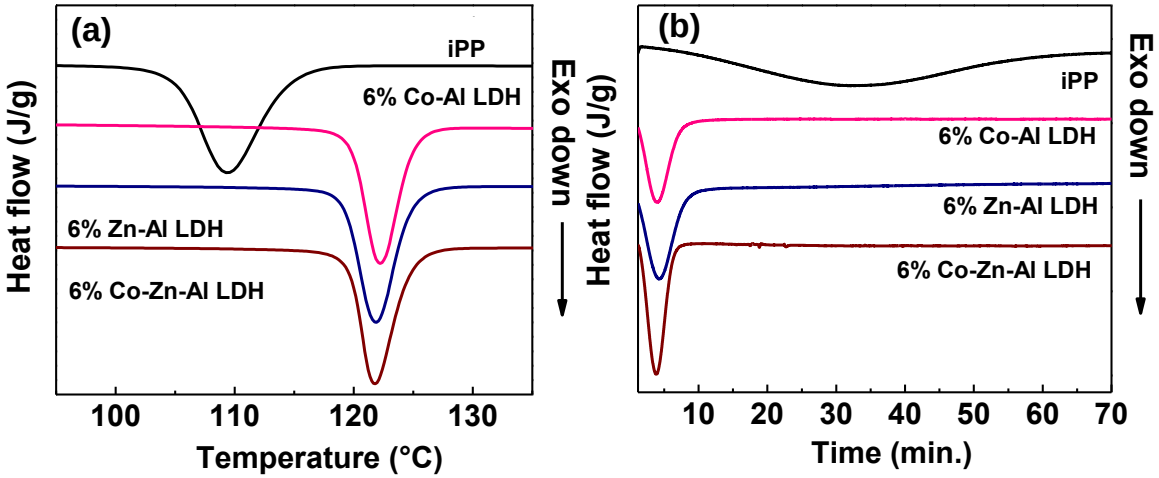

Figure 4.8. (a) DSC cooling thermograms of pristine iPP and its nanocomposites crystallized non-isothermally after melting at temperature 190 °C for 1 min (b) Crystallization isotherms obtained at 132 °C for pristine iPP and its nanocomposites.

To further confirm the effect of different types of LDH on the crystallization rate of iPP, the crystallization half time ($t_{1/2}$) was obtained at an isothermal crystallization temperature (T_c). The $t_{1/2}$ is usually defined as the time at which 50% of the

crystallinity is developed. Figure 4.8b shows the representative DSC isothermal curves of pristine iPP and various nanocomposites crystallized at 132 °C. The $t_{1/2}$ of pristine iPP was 33.3 min and it decreased significantly for all the nanocomposites irrespective of the type of LDH ($t_{1/2}$~ 4 ± 0.2 min). Usually, the crystallization rate G is reciprocal of $t_{1/2}$ i.e. $G = 1/t_{1/2}$. Figure 4.9 shows the temperature dependence of $1/t_{1/2}$ for pristine iPP and nanocomposites containing different type of LDH. It is observed that the crystallization rate decreases with increasing T_c for all the samples, suggesting that the overall isothermal crystallization rate decreases with increasing T_c, because of the low degree of supercooling ($\Delta T = T_m° - T_c$, where $T_m°$ is the equilibrium melting temperature) at higher T_c.[44] It was also observed that the crystallization rate of nanocomposites (0.53 – 0.05 min^{-1}) is higher than that of the pristine polymer (0.17 – 0.01 min^{-1}). These results suggested that the presence of LDH enhanced the crystallization process of iPP significantly, indicating that the fragmented LDH are effective nucleating agents for iPP. In our previous work, detailed crystallization kinetics has been carried out using different sized LDH particles and showed that the lateral size of the LDH particles has a significant role in controlling the crystallization rate of iPP.[15] This study revealed that the type of LDH does not affect the crystallization rate of iPP.

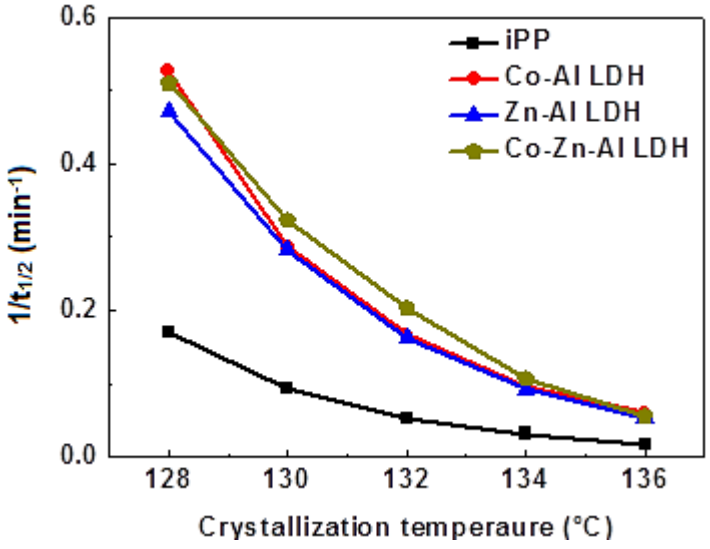

Figure 4.9. Temperature dependence of crystallization rate ($G = 1/t_{1/2}$) for pristine iPP and its nanocomposites using different types of LDH.

4.3.5. Dynamic Mechanical Analysis

The inorganic fillers dispersed in the polymer matrix are known to influence the viscoelastic properties of the polymer.[45-47] The effect of the different types of LDH particles on the dynamic mechanical performance of iPP/LDH nanocomposites was investigated by DMA. Figure 4.10 shows the temperature dependence of storage modulus (E') and loss tangent (tan δ) of iPP and its nanocomposites containing different types and amounts of LDH. Table 4.1 summarizes the DMA data extracted from Figure 4.10 for various samples. The storage modulus of the pristine iPP is 2.5GPa at -30 °C, and it decreases over the whole temperature range. The plateau region observed in the temperature range of -10 to 40 °C is associated with the relaxation of the amorphous region. The tan δ curve, which measures the energy dissipation (damping) ability of the material, shows peaks at 9.7 °C and another broad peak around ~112 °C for the pristine iPP. The first peak at 9.7 °C is corresponding to the glass transition temperature (T_g) and the second one is attributed to the damping within the crystalline lamellae.[45-47] Around 150 °C, a sharp decrease in the storage modulus and the sudden increase in the tan δ are due to the onset of melting of iPP crystals.

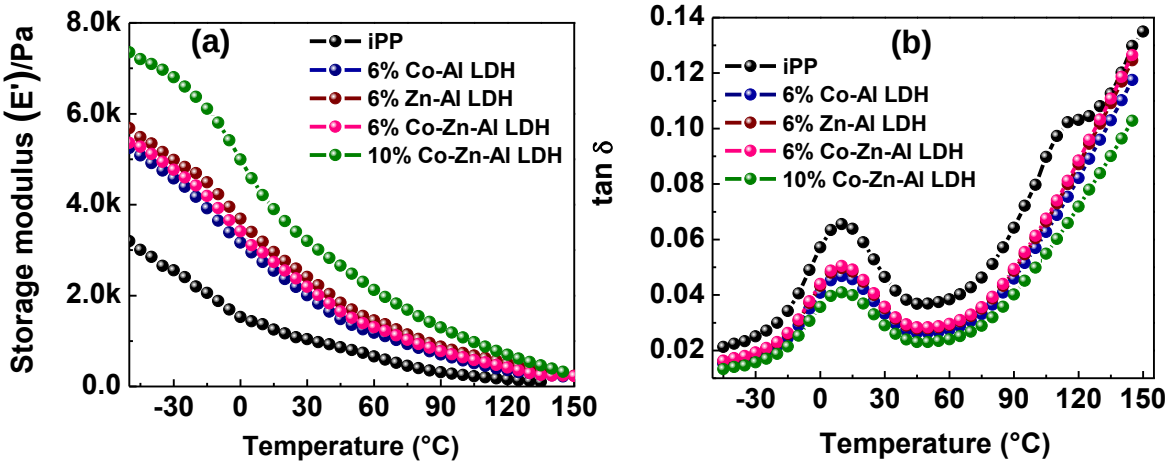

Figure 4.10. Temperature-dependent (a) storage modulus (E') and (b) loss factor (tan δ) measured in the heating process for iPP and its nanocomposites containing different LDH.

On addition of 6 wt% of different types of LDH, the storage modulus at -30 °C increased to 4.5, 4.6 and 4.65 GPa for nanocomposites containing Co-Al LDH, Zn-Al LDH, and Co-Zn-Al LDH, respectively, which is almost 1.8 fold increment compared to that of pristine iPP. The iPP/LDH nanocomposites exhibit the higher storage modulus across

the measured temperature range. The average storage modulus measured at room temperature is almost two-fold higher for nanocomposites than that of the pristine iPP. Increasing the LDH content to 10 wt% further increases the storage modulus to 6.6 and 3.2 GPa at -30 °C and room temperature, respectively for iPP/Co-Zn-Al LDH nanocomposites. Generally, the increase in the storage modulus could be due to the increase in the percent crystallinity; however, in the present study, the percent of crystallinity (see Table 4.1) measured for various samples using the WAXD data shown in Figure 4.7 were almost the same for pristine iPP and iPP/LDH nanocomposites. Moreover, it is clearly observed that the increase in the LDH content increases the storage modulus of iPP. Based on these observations, the increase in the storage modulus could be attributed to the reinforcing effect of LDH, i.e. the homogeneous dispersion of LDH within the polymer matrix without agglomerates. It has to be noted that a little or no difference in the storage modulus was observed with the type of LDH chosen (6 wt% loading) for the preparation of nanocomposites. The addition of LDH caused no change in the peak position of the tan δ curve near 9.5 °C, indicating that the T_g of iPP did not change in the presence of the LDH particles. It is worth mentioning here that the T_g of iPP is in the range of -10 to 10 °C, depending on the grade and molecular weight.[45, 48-50] However, the height of the tan δ peak decreases with the addition of LDH, which indicates the good wettability between the LDH and iPP.[45] In few reports, it has been reported that the T_g of the polymer was reduced, where the organically modified fillers were used for the preparation of nanocomposites due to the plasticization effect.[51] In some other cases, the T_g of the polymer was increased due to the restricted mobility of the polymer chains in the presence of fillers.[45] However, in the present study, no change in the T_g of iPP was observed in the presence of surfactant-free LDH particles. The magnitude of the broad peak around ~112 °C, which was attributed to the damping within the crystalline lamellae decreased for the nanocomposites. In nanocomposites, the LDH particles are expected to accumulate within the amorphous region of the polymer matrix. These particles are influencing the relaxation of iPP chains within the crystalline lamellae and crystalline-amorphous interfaces.

Table 4.1. Summary of the degree of crystallinity measured from WAXD and temperature-dependent dynamic mechanical properties.

Samples	X_c (%)* (± 1)	E' at -30 °C (GPa) (± 0.1)	E' at 30 °C (GPa) (± 0.1)	E' at 100 °C (GPa) (± 0.1)	tan δ_{max}(°C) (± 1)
iPP	65.1	2.5	1.04	0.25	9.7
iPP/Co-Al LDH (6 wt%)	65.8	4.5	2.02	0.57	9.2
iPP/Zn-Al LDH (6 wt%)	65.8	4.6	2.46	0.70	9.6
iPP/Co-Zn-Al LDH (6 wt%)	64.6	4.65	2.2	0.64	10.3
iPP/Co-Zn-Al LDH (10 wt%)	63.3	6.580	3.25	1.08	9.8

*The degree of crystallinity (X_c) was calculated as the ratio of the area under the crystalline peaks to the total area under the X-ray scattering curve

4.3.6. Flammability and Thermal Properties

Microscale combustion calorimetry (MCC) is a relatively new technique used for the evaluation of flammability of materials using small quantities of the sample, and this works on the principle of oxygen combustion. This technique was successfully used as a preliminary test for the evaluation of flame retardant properties of polymer/LDH nanocomposites.[16, 26-28] The heat release rate (HRR) is considered to be the most important parameter to estimate the flammability behavior of the polymer materials. Figure 4.11 presents the HRR plots for pristine iPP and its nanocomposites using different types and quantities of LDH. Several parameters, such as specific heat release rate (HRR), heat release capacity (HRC), and total heat release (THR) are summarized in Table 4.2 along with the 50% degradation temperature estimated from TGA. Unlike the crystallization rate and storage modulus, the nanocomposites containing different types of LDH showed different HRR values. For the pristine iPP, the HRR value is around 1435 W/g. With the addition of 6 wt% of different types of LDH, the HRR values were reduced to 1080, 990 and 880 W/g for Co-Al LDH, Zn-Al LDH, and Co-Zn-Al LDH, respectively. These results clearly suggested that different LDH have different flame retardant efficiency. Three-metal-LDH showed 38% reduction in HRR value, which is better than the other two-metal-LDH with the same LDH loadings.

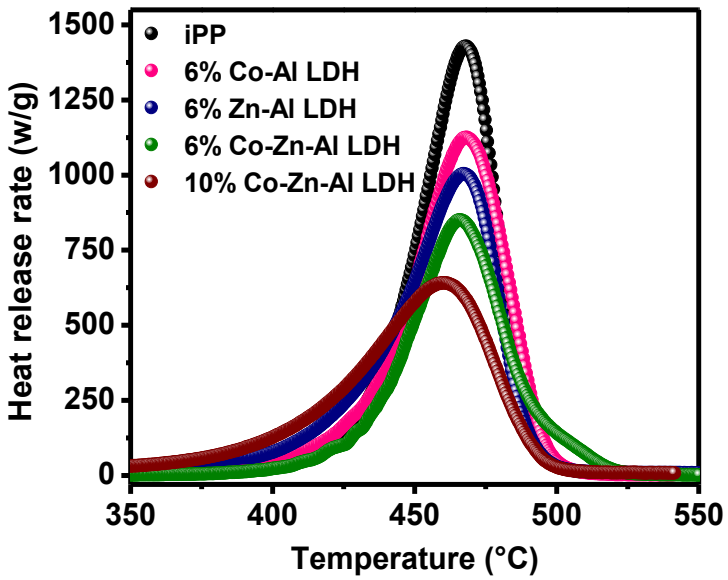

Figure 4.11. The HRR versus temperature curves for pristine iPP and its nanocomposites containing Co-Al LDH (6 wt%), Zn-Al LDH (6 wt%) and Co-Zn-Al LDH (6 wt% and 10 wt%).

Matusinovic et al. showed that the dispersion of LDH in the polymer matrix is one of the key parameters in achieving the good flame retardancy.[52] As discussed in the preceding section, highly dispersed nanocomposites were obtained using all types of LDH, so the dispersion of LDH may not be the key reason for the difference in the flame retardant behavior. It was also demonstrated that different gallery anions have different flame retardant efficiency.[26, 53, 54] However, in the present study, the different LDH used have the same anions (both CO_3^{2-} and NO_3^-) because of the same protocol used for the synthesis of different LDH. It has been shown that the char formation can slow down the HRR upon the Ignition of polymers and it can inhibit the flame spreading.[19, 33, 55, 56] To understand the difference in the flame retardant efficiency of different LDH, the amount of char formed upon the degradation of polymer matrix was analyzed by TGA. Figure 4.12a shows the TGA thermograms of pristine iPP and its nanocomposites containing 6 wt% of different types of LDH. Thermal stability of the polymer will be discussed in the later section. As seen from Figure 4.12a, the pristine polymer shows almost no char, whereas the samples containing different types of LDH show different char amounts ranging from 4.1 to 4.6 wt%. To further understand the reason for the difference in the char yield, TGA thermograms of different LDH were taken and are shown in Figure 4.12b. By considering the char yields of different LDH,

the expected char residues was estimated for the nanocomposites prepared using different types of LDH and are shown in Table 4.3. It is quite clear that different LDH gives different char yields, which follows the order of Co-Zn-Al LDH > Zn-Al LDH > Co-Al LDH. Similar to char yields, the HRR also follows the same order. Based on these results, the lowest HRR value of the nanocomposite prepared using three-metal-LDH (Co-Zn-Al LDH) can probably attribute to the better char formation of three-metal-LDH, which reduces the heat and mass transfer between the gas and condensed phases. It is worth mentioning here that LDH acts like both endothermic flame retardant and char forming flame retardant.[56] Under fire conditions, the LDH filler endothermically decomposes into water, carbon dioxide, metal hydroxides and other gases depending on the gallery anions. Further, the decomposition products of the LDH are non-flammable, and so the residue left behind by the thermal decomposition (usually a metal oxide) dilutes the total amount of polymer fuel availability (condensed phase).[19] This process promotes the formation of char and protects the bulk polymer exposure to air. This char helps in reducing the HRR during the combustion and suppresses the smoke production. From the TGA results of LDH, it is clear that the char formation is effective in three-metal-LDH compared to that of two-metal-LDH.

To further verify the effect of LDH loading, 10 wt % of Co-Zn-Al LDH was added to iPP and it was observed that the HRR value was further reduced by 55%. Wang and co-workers showed the reduction in the HRR value by 54% using four times higher LDH loadings (i.e. 40 wt%) in high-density polyethylene/LDH nanocomposites using MCC.[26] The heat release capacity (HRC) values estimated from the HRR curve (see Table 4.2) also shows similar trend like the HRR values, indicates that the three-metal-LDH are efficient flame retardant fillers compared to that of the two-metal-LDH.

The total heat release (THR) calculated from the area under the HRR curve is an important parameter to understand the fire hazards of the material.[26, 27] It has been shown that for efficient flame retardant filler, the THR value should reduce effectively when it is incorporated into the polymer.[26, 27] It is obvious from the Table 4.2 that the THR value is considerably reduced with the addition of 6 wt% of LDH and further reduced with increasing the LDH loading to 10 wt%. A small difference in the THR

values was observed with the type of LDH used for the preparation of nanocomposites. Three-metal-LDH showed the lower THR value compared to that of the other two-metal-LDH indicating that the three-metal-LDH is better flame retardant nano-filler for the iPP.

Table 4.2. Summary of thermal and flammability properties for iPP and its nanocomposites.

Samples	HRR (w/g) (± 5)	HRR reduction (%)	THR (kJ/g) (± 1)	HRC ($Jg^{-1}K^{-1}$) (± 5)	$T_{0.5}$ (°C) (± 2)
iPP	1435	-	54.0	1460	410
iPP/Co-Al LDH (6 wt%)	1080	25	49.9	1050	420
iPP/Zn-Al LDH (6 wt%)	990	31	48.7	985	430
iPP/Co-Zn-Al LDH (6 wt%)	880	38	48.17	905	443
iPP/Co-Zn-Al LDH (10 wt%)	640	55	43.9	690	435

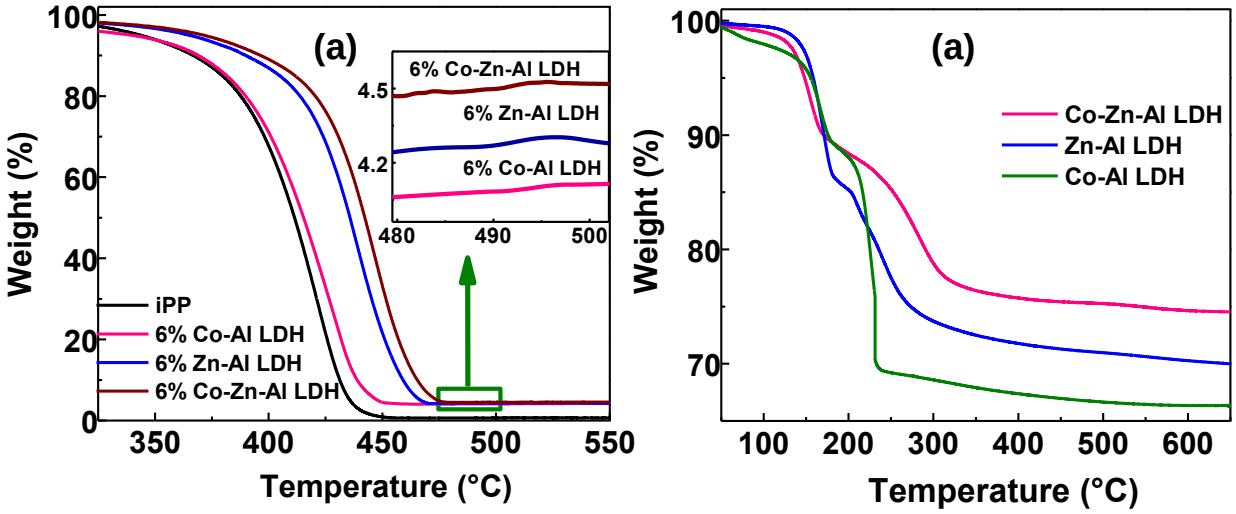

Figure 4.12. TGA thermograms for (a) pristine iPP and its nanocomposites containing 6 wt% of Co-Al LDH, Zn-Al LDH and Co-Zn-Al LDH (b) pure LDH powders.

The relative thermal stability of iPP was evaluated in the presence of different types of LDH. The 50% weight loss temperature ($T_{0.5}$) measured for various samples from Figure 4.12a are summarized in Table 4.2. It can be seen that the pristine iPP degraded completely with the $T_{0.5}$ at 410 °C. The thermal decomposition temperature of

iPP containing different types of LDH shifted to higher temperatures compared to pristine iPP. However, significant differences are seen in thermal stability of nanocomposites containing different types of LDH. The $T_{0.5}$ values of iPP containing Co-Al LDH (6 wt%), Zn-Al LDH (6 wt%) and Co-Zn-Al LDH (6 wt%) increased to 420, 430 and 443 °C, respectively. It has been shown that the enhanced thermal stability is due to the homogeneous dispersion of the nanosized LDH in the iPP matrix, where the dispersed nanoparticles act as trapping sites for the radicals generated during the degradation of the polymer.[15, 18, 20] However, in the present study, the dispersion of the LDH particles in the iPP matrix is more or less same in different nanocomposites. One of the possibilities for the difference in the degradation temperature is the catalytic ability of the metal constituents used for the preparation of LDH. Typically, cobalt is known for the catalytic degradation of polyolefins.[57] However, in the present study, the cobalt containing three-metal-LDH (Co-Zn-Al LDH) showed the better thermal stability than the other two LDH. Based on the present results, we are speculating that the difference in the thermal stability of iPP containing different types of LDH might be due to the thermally stable char formed by the degradation of LDH, which prevents the further degradation of iPP. As mentioned in the preceding section, the char formation in different LDH follows the order of Co-Zn-Al LDH > Zn-Al LDH >Co-Al LDH. Similar to this, the thermal stability and flame retardancy of the nanocomposites also follows the same order. On the other hand, the nanocomposite with 10 wt% of Co-Zn-Al LDH shows $T_{0.5}$ value ~ 435 °C (data not shown here), which is less than the $T_{0.5}$ value of nanocomposite containing 6 wt% of Co-Zn-Al LDH. This might be due to the agglomeration of LDH in higher loadings. Similar kinds of observations were reported in the literature.[15, 20, 25] It was shown that 2.5 wt% of sonicated LDH was the optimal loading for the effective thermal stability of iPP due to its better dispersion in iPP matrix.[15] In this way, the intralayer metal constituents of LDH play an important role in determining the properties of the nanocomposites.

Table 4.3. Summary of char yields of as-synthesized LDH and its nanocomposites.

Samples	Pristine LDH char yields (%)	Samples	iPP/LDH nanocomposites char yields (%)	
			Expected	Observed
-	-	iPP	0	0
Co-Al LDH	66.7	iPP/Co-Al LDH (6 wt%)	4.00	4.23
Zn-Al LDH	71.0	iPP/Zn-Al LDH (6 wt%)	4.26	4.37
Co-Zn-Al LDH	75.3	iPP/Co-Zn-Al LDH (6 wt%)	4.52	4.58

4.4. Conclusions

Two-metal-LDH and three-metal-LDH were successfully synthesized by co-precipitation method and delaminated by ultrasonication in xylene. The sonication step resulted in both delamination and fragmentation of LDH. TEM and AFM analysis confirmed the delamination of LDH. Subsequently, highly dispersed iPP/LDH nanocomposites were prepared by solution blending method. The dispersion of LDH within the iPP matrix was further confirmed by TEM and WAXD. We have found that the incorporation of either two-metal-LDH or three-metal-LDH dramatically improves the crystallization rate and storage modulus of iPP. However, not much difference is observed in these properties with the type of LDH used for the preparation of nanocomposites. On the other hand, the kind of LDH could influence the thermal stability and flame retardant properties of iPP. Keeping the filler loading at 6 wt%, the 50% weight loss temperature ($T_{0.5}$) of the iPP nanocomposite containing three-metal-LDH (Co-Zn-Al LDH) is higher than the corresponding nanocomposites prepared using the two-metal-LDH (Co-Al LDH and Zn-Al LDH). Preliminary data on the flame retardant properties showed the better reduction in HRR value compared to that of two-metal-LDH containing nanocomposites. These differences might be due to the better char formation capability of three-metal-LDH compared to that of two-metal-LDH. These results demonstrated that the proper selection of metal constituents of LDH

is imperative in the preparation of polymer/LDH nanocomposites with desirable properties.

4.5. Experimental section

Materials: IPP pellets (M_w ~120000, $Đ$ ~4.5) were kindly supplied by Sumitomo chemicals Co. Ltd., Japan. Metal salts like $Al(NO_3)_3 \cdot 9H_2O$, $Co(NO_3)_2 \cdot 6H_2O$ and $Zn(NO_3)_2 \cdot 6H_2O$ were purchased from Sigma-Aldrich Co. Ltd. Other chemicals such as urea, xylene, ethanol, and acetone were obtained from Merck, India.

Synthesis of LDH: Different types of LDH used in this study were synthesized by a conventional co-precipitation method using urea as the base. Three-metal-LDH (Co-Zn-Al LDH) was prepared by dissolving three metal salts ($Co(NO_3)_2 \cdot 6H_2O$, $Zn(NO_3)_2 \cdot 6H_2O$, and $Al(NO_3)_3 \cdot 9H_2O$), and urea in Millipore water with the ratio of 1:1:1:7. The total mixture was then heated to the refluxing temperature (about 100 °C) under continuous stirring for 24 h in the ambient atmospheric environment. The resultant light pink color precipitate was rapidly quenched in cold water and filtered, and then the precipitate was repeatedly washed with hot Millipore water to remove the unreacted reactants if any. Such obtained LDH powder was repeatedly washed with acetone. The end product was dispersed in xylene and sonicated for 4 days in an ultrasonication bath at room temperature. The resulting suspension was stable at room temperature for a few hours. Two-metal LDH (Co-Al LDH and Zn-Al LDH) were synthesized in the same way, with the exception that the Co^{2+} and Al^{3+}, Zn^{2+} and Al^{3+} metal nitrates were taken in 2:1 ratio.

Preparation of iPP/LDH Nanocomposites: Three different LDH (Co-Zn-Al LDH, Co-Al LDH, and Zn-Al LDH) were used as reinforcement fillers for the preparation of iPP nanocomposites. The synthetic procedure is same as used in chapter-2. The type and amount of LDH were adjusted to prepare different nanocomposites with various LDH loadings (0, 6 and 10%). The actual loading of the LDH in iPP was estimated using TGA and the details are given in Table 4.3.

4.6. Characterization

Synthesized LDH was thoroughly characterized using WAXD, TEM, SEM, AFM and FTIR as discussed in previous chapters.

Thermogravimetric Analysis (TGA) – TGA thermograms were collected in the heating process at 10 °C/min using TA Q50. All the measurements were carried under the nitrogen atmosphere (nitrogen gas flow rate of 60 mL/min for the furnace and 40 mL/min for balance).

Differential Scanning Calorimetry (DSC) – DSC measurements were performed on a Perkin Elmer Pyris 6 DSC apparatus under nitrogen gas flow. The temperature and heat flow were calibrated using a high purity indium. The crystallization half-time ($t_{1/2}$) was measured to evaluate the crystallization rate of iPP and its nanocomposites. Molten samples were rapidly cooled to the desired crystallization temperature (T_c) (132 °C) at a rate of 100 °C/min, and the samples were allowed to crystallize at that temperature. These samples were reheated to 190 °C to measure the melting temperature.

Microscale combustion calorimetry (MCC): The microscale combustion calorimetry (MCC-1, FTT) was used as a preliminary test to evaluate the combustion behavior of iPP and iPP/LDH nanocomposites. In MCC system, approximately 5 mg of sample was heated to 700 °C at a heating rate of 1 °C/s in the stream of N_2 flow at 80 cm^3/min. The resulting volatile anaerobic thermal degradation products in the nitrogen gas stream are mixed with 80 cm^3/min carrying gas (nitrogen of 80 mL min^{-1}; oxygen of 20 mL min^{-1}) and subsequently burned at 900 °C in a combustion furnace. The flame retardant parameters have been measured from this test, and are the heat release rate (HRR) in $W.g^{-1}$, % of the reduction in HRR, total heat release rate (THR) in $KJ.g^{-1}$, temperature maxima (T_{-max}) in °C and heat release capacity (HRC) in $J.g^{-1}.K^{-1}$.

Dynamic Mechanical Analysis (DMA): The DMA (TA Instruments Model Q800) was used to study the temperature-dependent dynamic mechanical properties of the samples as discussed in chapter-3.

4.7. References

1 A. K. Geim, *Science* **324:**1530-1534 (2009).

2 Z. Liu, R. Ma, M. Osada, N. Iyi, Y. Ebina, K. Takada and T. Sasaki, *J Am Chem Soc* **128:**4872-4880 (2006).

3 J. N. Coleman, M. Lotya, A. O'Neill, S. D. Bergin, P. J. King, U. Khan, K et al., *Science* **331:**568-571 (2011).

4 V. V. Naik, T. N. Ramesh and S. Vasudevan, *J Phys Chem Lett* **2:**1193-1198 (2011).

5 K. S. Novoselov, A. K. Geim, S. V. Morozov, D. Jiang, Y. Zhang, S. V. Dubonos, I. V. Grigorieva and A. A. Firsov, *Science* **306:**666-669 (2004).

6 V. Nicolosi, M. Chhowalla, M. G. Kanatzidis, M. S. Strano and J. N. Coleman, *Science* **340:**(2013).

7 D.-Y. Wang, A. Das, A. Leuteritz, R. N. Mahaling, D. Jehnichen, U. Wagenknecht and G. Heinrich, *RSC Adv* **2:**3927-3933 (2012).

8 M. Alexandre and P. Dubois, *Mater. Sci. Eng. R-Rep.* **28:**1-63 (2000).

9 W.-L. Song, P. Wang, L. Cao, A. Anderson, M. J. Meziani, A. J. Farr and Y.-P. Sun, *Angew. Chem. Int. Ed.* **51:**6498-6501 (2012).

10 K. S. Novoselov, D. Jiang, F. Schedin, T. J. Booth, V. V. Khotkevich, S. V. Morozov and A. K. Geim, *Proc Natl Acad Sci U S A* **102:**10451-10453 (2005).

11 Y. Zhang, L. Zhang and C. Zhou, *Acc Chem Res* **46:**2329-2339 (2013).

12 F. Leroux and J.-P. Besse, *Chem Mater***13:**3507-3515 (2001).

13 Y. Gao, J. Wu, Q. Wang, C. A. Wilkie and D. O'Hare, *J Mater Chem A* **2:**10996-11016 (2014).

14 D. Basu, A. Das, K. W. Stöckelhuber, U. Wagenknecht and G. Heinrich, *Prog Polym Sci* **39:**594-626 (2014).

15 B. Nagendra, K. Mohan and E. B. Gowd, *ACS Appl Mater Interfaces* **7:**12399-12410 (2015).

16 B. Nagendra, A. Das, A. Leuteritz and E. B. Gowd, *Polym Int* **65:**299-307 (2016).

17 W. Chen and B. Qu, *J Mater Chem* **14:**1705-1710 (2004).

18 Q. Wang, X. Zhang, J. Zhu, Z. Guo and D. O'Hare, *Chem Commun* **48:**7450-7452 (2012).

19 Z. Matusinovic and C. A. Wilkie, *J Mater Chem* **22:**18701-18704 (2012).

20 Q. Wang, X. Zhang, C. J. Wang, J. Zhu, Z. Guo and D. O'Hare, *J Mater Chem* **22:**19113-19121 (2012).

21 J.-H. Yang, W. Zhang, H. Ryu, J.-H. Lee, D.-H. Park, J. Y. Choi, A. Vinu, A. A. Elzatahry and J.-H. Choy, *J Mater Chem A* **3:**22730-22738 (2015).

22 S. O'Leary, D. O'Hare and G. Seeley, *Chem Commun* 1506-1507 (2002).

23 W. Chen and B. Qu, *Chem Mater* **15:**3208-3213 (2003).

24 W. Chen, L. Feng and B. Qu, *Chem Mater* **16:**368-370 (2004).

25 Q. Wang, J. P. Undrell, Y. Gao, G. Cai, J.-C. Buffet, C. A. Wilkie and D. O'Hare, *Macromolecules* **46:**6145-6150 (2013).

26 Y. Gao, Q. Wang, J. Wang, L. Huang, X. Yan, X. Zhang, Q. He, Z. Xing and Z. Guo, *ACS Appl Mater Interfaces* **6:**5094-5104 (2014).

27 D.-Y. Wang, A. Das, F. R. Costa, A. Leuteritz, Y.-Z. Wang, U. Wagenknecht and G. Heinrich, *Langmuir* **26:**14162-14169 (2010).

28 N.-J. Kang, D.-Y. Wang, B. Kutlu, P.-C. Zhao, A. Leuteritz, U. Wagenknecht and G. Heinrich, *ACS Appl Mater Interfaces* **5:**8991-8997 (2013).

29 P. J. Purohit, J. E. Huacuja-Sánchez, D.-Y. Wang, F. Emmerling, A. Thünemann, G. Heinrich and A. Schönhals, *Macromolecules* **44:**4342-4354 (2011).

30 Q. Wang and D. O'Hare, *Chem Commun* **49:**6301-6303 (2013).

31 L. Qiu, Y. Gao, X. Yan, J. Guo, A. Umar, Z. Guo and Q. Wang, *RSC Adv* **5:**51900-51911 (2015).

32 Y. Gao, J. Wu, Z. Zhang, R. Jin, X. Zhang, X. Yan, A. Umar, Z. Guo and Q. Wang, *J Mater Chem A* **1:**9928-9934 (2013).

33 X. Wang, Y. Sporer, A. Leuteritz, I. Kuehnert, U. Wagenknecht, G. Heinrich and D.-Y. Wang, *RSC Adv* **5:**78979-78985 (2015).

34 F. Song and X. Hu, *Nat Commun* **5:**4477 (2014).

35 T.-H. Kim, W.-J. Lee, J.-Y. Lee, S.-M. Paek and J.-M. Oh, *Dalton Trans* **43:**10430-10437 (2014).

36 T. Yokoi, K. Tsukada, S. Terasaka, M. Kamitakahara and H. Matsubara, *J Asian Ceram Soc* **3:**230-233 (2015).

37 A. Ciesielski and P. Samori, *Chem Soc Rev* **43:**381-398 (2014).

38 J. T. Han, J. I. Jang, H. Kim, J. Y. Hwang, H. K. Yoo, J. S. Woo, S. Choi, H. Y. Kim, H. J. Jeong, S. Y. Jeong, K.-J. Baeg, K. Cho and G.-W. Lee, *Sci Rep* **4:**5133 (2014).

39 M. Chhowalla, H. S. Shin, G. Eda, L.-J. Li, K. P. Loh and H. Zhang, *Nat Chem* **5:**263-275 (2013).

40 Y. Zhao, G. Chen, T. Bian, C. Zhou, G. I. N. Waterhouse, L.-Z. Wu, C.-H. Tung, L. J. Smith, D. O'Hare and T. Zhang, *Adv Mater* **27:**7824-7831 (2015).

41 A. T. Jones, J. M. Aizlewood and D. R. Beckett, *Makromol Chem* **75:**134-158 (1964).

42 T. D. Fornes and D. R. Paul, *Polymer* **44:**3945-3961 (2003).

43 M. R. Mani, R. Chellaswamy, Y. N. Marathe and V. K. Pillai, *Chem Commun* **51:**10026-10029 (2015).

44 Z. Qiu and Z. Li, *Ind Eng Chem Res* **50:**12299-12303 (2011).

45 A. M. Díez-Pascual and M. Naffakh, *ACS Appl Mater Interfaces* **5:**9691-9700 (2013).

46 P. Liu, K. L. White, H. Sugiyama, J. Xi, T. Higuchi, T. Hoshino, R. Ishige, H. Jinnai, A. Takahara and H.-J. Sue, *Macromolecules* **46:**463-473 (2013).

47 P. Maiti, P. H. Nam, M. Okamoto, N. Hasegawa and A. Usuki, *Macromolecules* **35:**2042-2049 (2002).

48 M. Naffakh, M. Remskar, C. Marco, M. A. Gomez-Fatou and I. Jimenez, *J Mater Chem* **21:**3574-3578 (2011).

49 P. H. Nam, P. Maiti, M. Okamoto, T. Kotaka, N. Hasegawa and A. Usuki, *Polymer* **42:**9633-9640 (2001).

50 W. Leelapornpisit, M.-T. Ton-That, F. Perrin-Sarazin, K. C. Cole, J. Denault and B. Simard, *J Polym Sci, Part B: Polym Phys* **43:**2445-2453 (2005).

51 K. Wang, S. Liang, J. Deng, H. Yang, Q. Zhang, Q. Fu, X. Dong, D. Wang and C. C. Han, *Polymer* **47:**7131-7144 (2006).

52 Z. Matusinovic, J. Feng and C. A. Wilkie, *Polym Degrad Stab* **98:**1515-1525 (2013).

53 C. Nyambo, P. Songtipya, E. Manias, M. M. Jimenez-Gasco and C. A. Wilkie, *J Mater Chem* **18:**4827-4838 (2008).

54 C. Li, J. Wan, E. N. Kalali, H. Fan and D.-Y. Wang, *J Mater Chem A* **3:**3471-3479 (2015).

55 X. Wang, S. Zhou, W. Xing, B. Yu, X. Feng, L. Song and Y. Hu, *J Mater Chem A* **1:**4383-4390 (2013).

56 A. B. Morgan and J. W. Gilman, *Fire Mater* **37:**259-279 (2013).

57 A. J. Sipinen and D. R. Rutherford, *J Environm Polym Degrad* **1:**193-202 (1993).

Chapter-5

Synergistic Effect of Layered Double Hydroxides and Multi-walled Carbon Nanotubes on the Properties of Polypropylene Nanocomposites

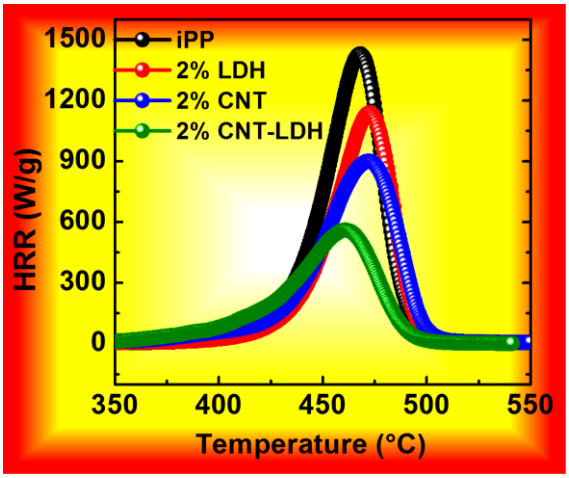

5.1. Abstract

Hybrid materials of multiwall carbon nanotubes (CNT) and Co-Zn-Al LDH were synthesized and used as nanofillers for the preparation of iPP nanocomposites. For the purpose of comparison, iPP/CNT and iPP/CNT-Co-Zn-Al LDH nanocomposites were also prepared. The main objective of the current study is to understand synergistic effect CNT/LDH hybrid on the structure, crystallization, mechanical, thermal degradation and flammability features of iPP. The incorporation of CNT has accelerated the overall crystallization rate of the iPP and temperature-dependent viscoelastic behavior, over the LDH and CNT-LDH filled nanocomposites. On the other hand, nanocomposites prepared using hybrid materials (CNT-LDH) showed better flame-retardant and thermal stability

compared to the nanocomposites containing CNT and LDH. With addition of the 2 wt% CNT-LDH hybrid filler, the PHRR values was significantly reduced from the 1400 W/g for neat iPP to 580 W/g (59 %), and it is larger than the CNT (980 W/g (30 %)) and LDH (1160 W/g (19%)) reinforced nanocomposites. The 50 % weight loss temperature ($T_{0.5}$) of the nanocomposites was shifted towards higher temperatures; larger improvement was observed for the 2 wt% iPP/CNT-LDH nanocomposites (~44 °C). Synergetic flame-retardancy and thermal degradation stability of the iPP/CNT-LDH nanocomposites might be influenced by many factors such as catalytically charring effect, jammed network, filler thermal stability and their residual char behavior, poor thermal conductivity, which yields the efficient flame-retardant and thermally resisting nanocomposites.

5.2. Introduction

The unification of one-dimensional and two-dimensional nanomaterials lead to the new hybrid materials that can take the constructive advantages of individual nanomaterials and enhance the multiple properties of commercial low-cost polymers when used as fillers to prepare nanocomposites.[1-6] Carbon nanotubes (CNTs) are the most established one- dimensional nanomaterial, thanks to their unparalleled electrical, mechanical and thermal properties.[7, 8] CNTs have been widely employed to strengthen the polymers, to enhance the electrical and thermal conductivities of the host matrix.[1, 9-15] These tubular structures are also found to increase the flame retardancy of the polymers very effectively resulting from the formation of structured networks.[3, 11, 12, 14-16]

Synergistic effects of CNTs have been explored with a variety of two dimensional materials, among which graphene has been studied for many applications including the thermal management, supercapacitors, flame retardant polymers, etc.[13, 17-19] LDH are another set of two-dimensional structures, which are known to impart better properties to the polymers, like increase in the crystallization rate, improved mechanical and thermal stability and superior flame retardant properties.[18-22] It is possible to design LDH with desired shape, size, and metal content to prepare polymer/LDH nanocomposites with excellent properties.[19, 21, 23-27]

The incorporation of LDH based flame retardant additives to polymer is well documented in the literature, which indicates the commercial importance of these materials.[18, 21, 28] However, in most cases, the filler loading is very high, which makes the processing of the polymer extremely difficult due to the drastic enhancement of complex viscosity.[18, 28] In our previous work, we showed that well-dispersed LDH are good flame retardant agents and better nucleating agents for iPP, even at lower loadings.[29] Recent reports based on graphene/LDH, CNT/clay, CNT/MoS_2, nanosilica/LDH, and fullerene/CNT reinforced nanocomposites exhibited exceptional flame retardancy, and mechanical properties over its individual filler reinforced nanocomposites.[6, 30-36] The flame retardant mechanism is different in carbon based materials and LDH. The hybrids of these are expected to show better performance in terms of flame retardancy.[17, 32, 37]

In this work, hierarchical CNT-LDH was synthesized by ultrasound assisted exfoliation of the layered assembly of LDH nanosheets on the surface of CNT tubes, and this hybrid filler was further used for the preparation of polymer nanocomposites. Here we adopted the solvent mixing method for the preparation of highly dispersive iPP/LDH, iPP/CNT and iPP/CNT-LDH nanocomposites. The influence of filler type on the crystallization kinetics, dynamic mechanical behavior, flame-retardancy and thermal stability of iPP was systematically carried out. It was found that, iPP/CNT-LDH nanocomposites showed better flame retardancy and thermal stability with same loading, whereas, iPP/CNT nanocomposites showed better dynamic mechanical behavior and faster crystallization rate compared to the iPP/LDH and iPP/CNT-LDH nanocomposites.

5.3. Results and Discussion

5.3.1. Synthesis and Morphology of Co-Zn-Al LDH

Figure 5.1a shows typical SEM image of the Co-Zn-Al LDH, synthesized by co-precipitation method in the presence of urea. From the Figure it is clear that the formed LDH platelets showed a well-defined hexagonal morphology with the mean lateral size of 2-4 μm. The dark contrast of the TEM image (Figure 5.1b) confirms that the as-synthesized LDH comprises of multilayered hexagonal platelets. The presence of

three-metal constituents in the LDH (Co, Zn and Al) was confirmed by energy-dispersive X-ray spectrum (EDS) (Figure 5.1c). The structural feature was further analyzed by powder X-ray diffraction patterns (XRD). It exhibited symmetric sharp reflections with narrow full width and half maximum (FWHM) values corresponding to the (00n) planes of the LDH, which indicates the high crystalline nature (Figure 5.3a). The presence of anions in LDH was confirmed from the FTIR spectrum (Figure 5.1d). The strong bands at 1352 and 786 cm^{-1} are assigned to the stretching and bending vibration of CO_3^{2-} anions, respectively.[38] Another sharp peak located at 1380 cm^{-1} (N–O stretching vibration) indicated the presence of nitrate anion (NO_3^-). Here it is important to point out that as prepared LDH consists of a mixture of carbonate and nitrate as gallery anions. A broad band centered at 3420 cm^{-1} is owing to the O-H (ν) stretching vibration of the metal hydroxide layer and interlayer H_2O molecules. Another weak band centered at 1610 cm^{-1} is attributable to the O–H bending vibration (δ) of the gallery water molecule. [38]

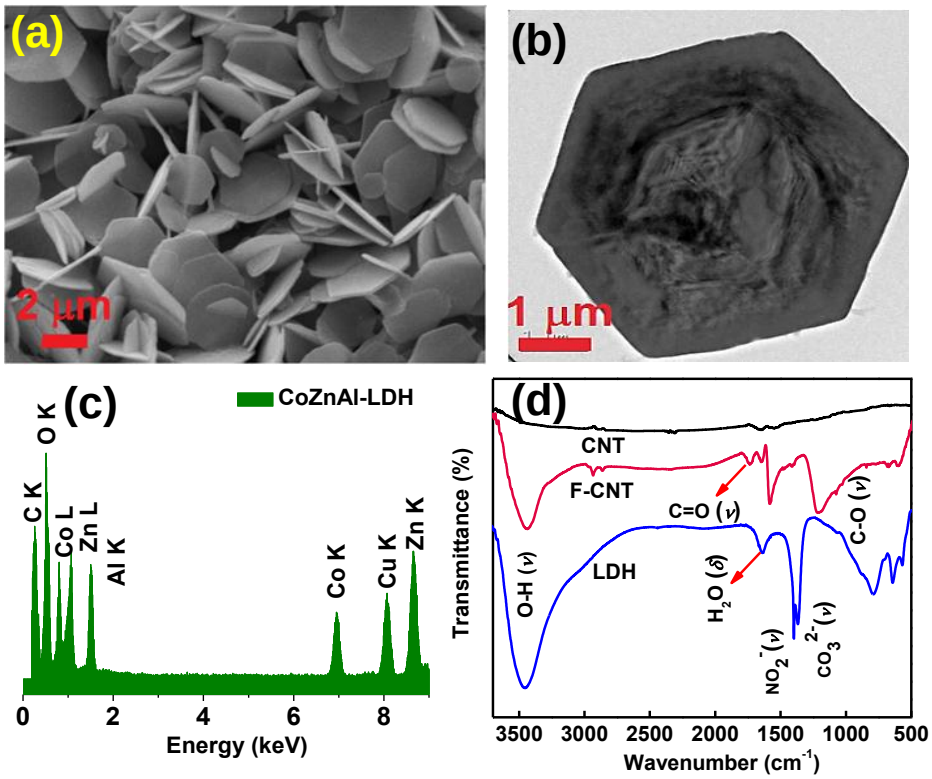

Figure 5.1. (a) SEM, (b) TEM image, and (c) EDS for as synthesized Co-Zn-Al LDH. (d) FTIR spectrum for the as synthesized LDH, pristine CNT, and functionalised CNT.

5.3.2. CNT Functionalization and CNT-LDH Hybrid Preparation

Since the hydrophobic surface of CNT obstructs its interaction with the hydrophilic LDH, the CNT surface was initially functionalized by the modified Hummers process to make it hydrophilic. Figure 5.1d shows the FTIR spectra of the pristine CNT and the functionalized CNT. It is obvious that the modified CNT shows two characteristic absorption peaks at 3440 and 1730 cm^{-1}, corresponding to the hydroxy (O-H) and carbonyl (C=O) stretching vibrations, respectively, which demonstrates the successful introduction of the hydrophilic functional (O-H, -COOH) groups on to the CNT surface.[39] Raman spectroscopy was used further to understand the functionalization of the CNT (Figure 5.2a). As expected, the pristine CNT exhibited a prominent G-band at 1588 cm^{-1} assigned to the tangential C-C stretching vibrations, both longitudinally and transversally on the nanotube axis.[39] Another less intensive band was located at 1345 cm^{-1}, corresponding to D-band. Generally, this band occurs due to the vibration of carbon atoms with dangling bonds in the plane termination of disordered graphite carbon, and intensity of the D-band depends on the disordered nature.[39] However, the CNT functionalized using modified Hummer's method displays a different scattering pattern compared to pristine CNT. The D-band appears more intensive than the G-band for the functionalized CNT, which indicates the defects and disordered crystal structure of the CNT due to the oxidation process. Moreover, it is quiet clear from the TEM analysis (Figure 5.2b) that the CNT surface appear like an irregular nanoribbon instead of the nanotube morphology. This result confirms the formation of the defected nanotubes, which is accredited to the oxidative functionalization of the CNT.[39]

The CNT-LDH hybrids were prepared by solvent mixing method followed by sonication. Major advantage of the sonication in hydrophobic solvent is that the surface modification and fragmentation of the LDH platelets happen simultaneously, and that results in the formation of hierarchical CNT-LDH morphology. The hierarchical morphology is confirmed using the TEM analysis (Figure 5.2c), where the broken LDH nanosheets adhered over the functionalised CNT surface. The hierarchical co-assembly between the CNT and LDH is mainly driven by strong electrostatic interaction forces, induced by the LDH and CNT surfaces.[17, 40] Interactions between the CNT and

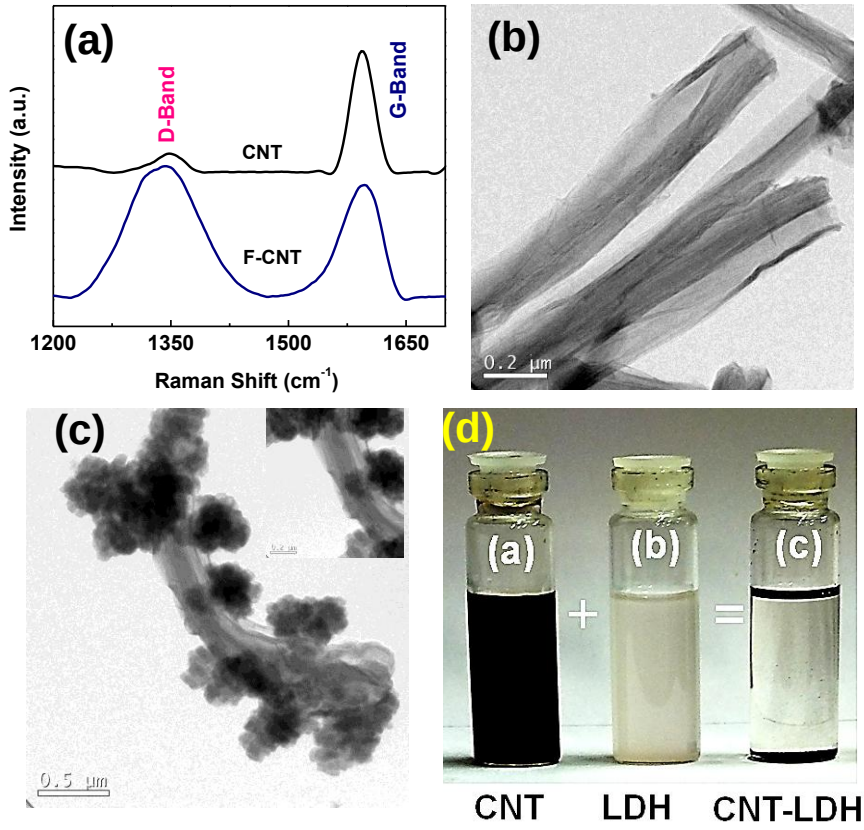

Figure 5.2. (a) Raman spectrum for pristine CNT and functionalized CNT, (b) TEM image of functionalized CNT. (c) TEM image of hierarchical hybrids of CNT-LDH, and (d) Photograph shows the CNT, LDH and CNT-LDH dispersion in the xylene solvent, taken after keeping it aside for 10 min (1 mg/ml concentration).

LDH can be easily observed from the sedimentation process.[40] Figure 5.2d displays the photograph of the sonicated dispersions of CNT, LDH, and CNT-LDH in xylene, which was kept aside for 10 min after the sonication. The functionalized CNT and LDH containing solutions were found to be stable for a shorter duration. On the other hand, the CNT-LDH hybrid showed a rapid sedimentation, demonstrating the strong electrostatic interaction between them.[30]

5.3.3. Synthesis of iPP/CNT-LDH Nanocomposites

The uniformly dispersed hybrid iPP/CNT-LDH nanocomposites were prepared by solvent mixing method, which initially modifies the filler surface into hydrophobic. The surface modification will help in the better dispersion of the inorganic fillers into the non-polar polypropylene matrix. Figure 5.3a displays the

WAXS patterns of the neat iPP and its nanocomposites (2 wt% LDH, 2 wt% CNT and 2 wt% CNT-LDH), which were prepared by following a strict thermal program as discussed in the experimental section. The WAXS patterns reveal that the peaks corresponding to the LDH and CNT are completely extinct in the nanocomposites, and only the polypropylene crystalline peaks are detected, which indicates the uniform distribution of the filler in the polymer matrix. To support the WAXS analysis, the nanocomposite morphology was further examined by TEM analysis. Figure 5.3b shows a cross-sectional TEM image of the nanocomposite containing 5 wt% CNT-LDH. It is clear that the LDH and CNT hybrids mixtures still retain their hierarchical morphology within the polymer matrix, without phase separation. They have also maintained an isolated morphology without any aggregation. LDH platelets are completely delaminated and distributed homogenously, the 00n planes remained silent (Figure 5.3a).

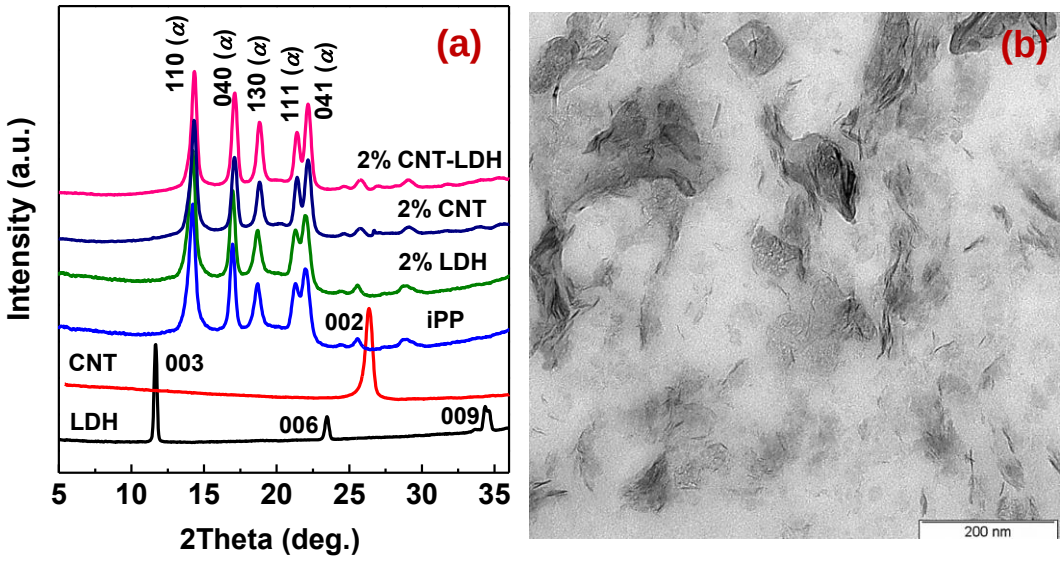

Figure 5.3. (a) WAXS patterns of neat LDH, CNT, iPP and their nanocomposites obtained by solution blending method and (b) cross-sectional TEM image of the iPP/CNT-LDH nanocomposite (5 wt% CNT-LDH).

We investigated the influence of the LDH, CNT, and CNT-LDH on the polymorphism of iPP. The XRD patterns (Figure 5.3a) indicated that both neat iPP and nanocomposites possess similar diffraction pattern. The Miller indices (hkl) are 110 (14.2°), 040 (17.0°), 130 (18.7°), 111 (21.3°), and 041 (22.1°), which represents the

monoclinic crystalline phase (α-crystal form). These results demonstrated that the dispersed additives do not have any influence on the polymorphic behavior of iPP.[41]

5.3.3.1. Crystallization and Melting Behavior of iPP Nanocomposites

The melt crystallization behavior of iPP with different fillers has been investigated under non-isothermal and isothermal conditions. Figure 5.4a shows the DSC thermograms of non-isothermally crystallized samples at a rate of 10 °C/min. The results are summarized in Table 5.1. As discussed in previous chapters, pristine polymer shows poor crystallization rate, with the melt crystallization temperature (T_{mc}) at ~109 °C. On the other hand, upon addition of 2 wt% fillers, the T_{mc} of the polymer shifted towards higher temperature. The T_{mc} shifted to 122 °C, 130.5 °C, and 127 °C for nanocomposites containing 2 wt% of LDH, CNT, and CNT-LDH, respectively. These results indicated that the dispersed inorganic additives accelerated the overall crystallization rate of iPP. However, the nanocomposites containing CNT showed higher crystallization rate due to the better nucleation efficiency of 1-dimensional nanofillers. The isothermal crystallization behavior was also investigated at 130 °C (Figure 5.4c). The crystallization half time ($t_{1/2}$) values obtained for different samples are listed in Table 5.1. The nanocomposites showed the shorter crystallization half-time compared to the pristine iPP and $t_{1/2}$ values follows the order of CNT> LDH-CNT> LDH. Both the non-isothermal and isothermal crystallization studies revealed that the nucleation efficiency of CNT is superior to the LDH-CNT, which is followed by LDH. Dispersed additives are known to facilitate the crystallization process in semicrystalline polymers by virtue of their larger specific surface area and non-covalent interaction forces.[5, 42, 43] However, the CNT containing nanocomposites show prominent nucleation effect compared to the LDH and CNT-LDH containing nanocomposites. It is owing to the better interaction of the methyl groups of the iPP with CNT surface compared to the CNT-LDH and LDH surface through non-covalent force.[5, 42] These filler surfaces act as a template for the generation of the nucleation centers that would prompt the overall crystallization rate of the iPP.[5, 42, 44] In the previous chapters, it has been showed that the lateral sizes of LDH has a strong influence on the nucleation efficiency and the overall crystallization rate.

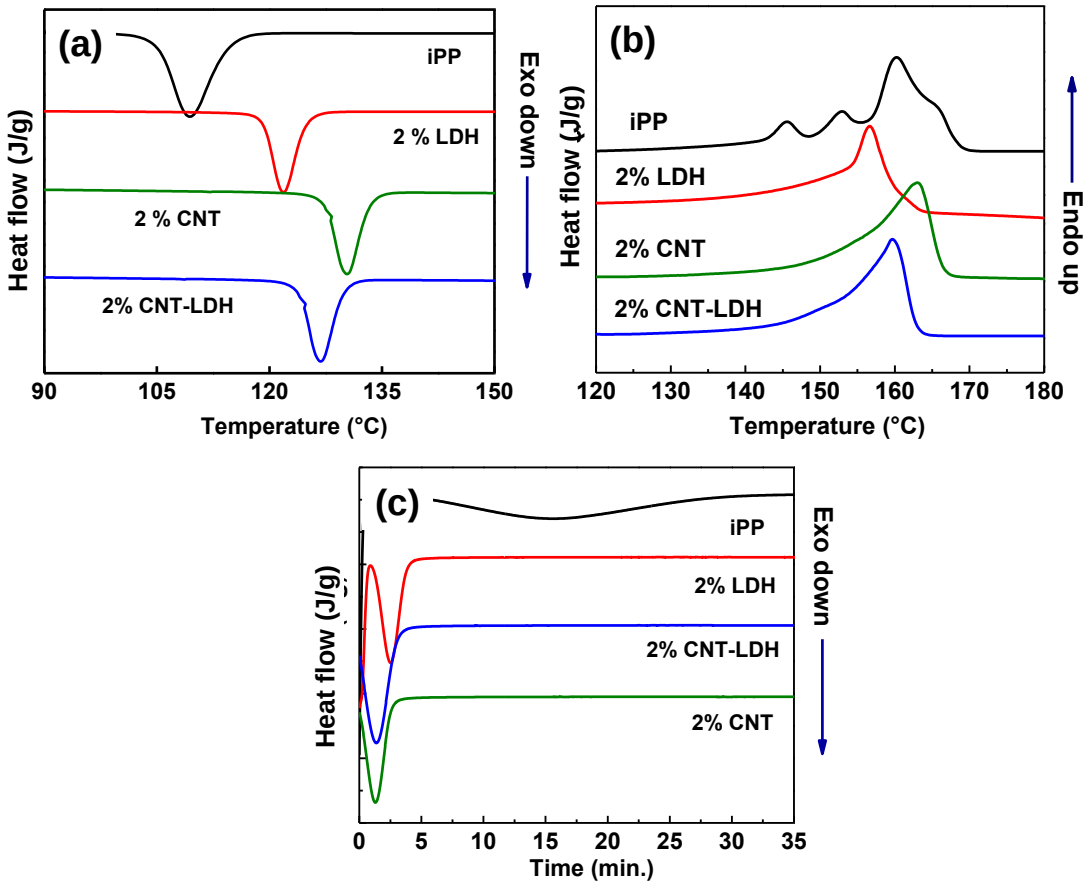

Figure 5.4. DSC curves of neat iPP and its nanocomposites (a) non-isothermal melt crystallization (T_{mc}), (b) subsquent melting behavior at a rate of 10 °C/min, and (c) isothermal crystallization behavior at 130 °C.

The melting behavior of semicrystalline polymers is significantly influenced by many factors including polymorphism, molecular weight, thermal program (heating and cooling rates) used for the sample preparation, the recrystallization phenomena, etc.[5, 9, 45] Figure 5.4b shows the DSC reheating curves of the non-isothermally crystallized samples, at rate of 10 °C/min. Under the strict thermal condition, neat iPP and nanocomposites exhibited significantly different melting behavior from one another, but with almost similar melting enthalpy (Table 5.1). The neat iPP showed multiple melting peaks, whereas the nanocomposites exhibited different melting behavior. This can be related to the recrystallization phenomena.[5, 9, 46] Impact of other parameters (polymorphism, molecular weight, tactility and thermal program) can be overlooked since we followed more or less similar procedures in both the systems using the same polymer. According to Alamo and co-workers, under larger

cooling rates, polymer will not get enough time to form perfect crystallites (lamellae), instead, they form multiple disordered crystallites with different sizes.[47, 48] Then it can reorganize (melting followed by recrystallization) into perfect and stable crystallites during the reheating process, which is the main reason for the multiple melting peaks. Here it is important to mention that the disappearance of the multiple endothermic peaks in the nanocomposites is probably due to the fact that, in the presence of the fillers, polymer chains can rapidly grow into more uniform and perfect stable crystallites, even under larger cooling rate.[5, 44]

Table 5.1. Summary of the crystallization, melting behavior and temperature-dependent dynamic mechanical properties of the nanocomposites.

Sample	T_{mc} (°C) (± 1)	$t_{1/2}$ at 130 °C min. (± 0.2)	ΔHm (J/g) (±2)	E' (GPa) at 30°C (±0.3)	tan δ_{max} (°C) (±1)
iPP	109	16	104	2.4	6.2
2 wt% iPP/LDH	122	2.3	102.4	2.9	7.6
2 wt% iPP/CNT	130.5	0.9	106	4.9	6.6
2 wt% iPP/CNT-LDH	127	1.3	100.6	4.45	5.5

5.3.3.2. Temperature-dependent Dynamic Mechanical Properties

Dispersed inorganic rigid phase inside the polymer matrix is known to alter the viscoelastic properties of the polymer.[9, 10, 49, 50] The viscoelastic properties of polypropylene nanocomposites containing different fillers were evaluated by temperature-dependent dynamic mechanical analysis (DMA). Figure 5.5a shows the plot of storage modulus (E') as a function of temperature, and the results are summarized in Table 5.1. Both the systems show a progressive reduction in E' over the whole observed temperature region. Especially, the reduction was more prominent in -10 to 40 °C temperature region associated with the glass phase relaxation (T_g),[9, 51, 52] whereas the decrease is only marginal in the high-temperature region, i.e., above 50 °C. At 30 °C, the comparison point, the pristine polymer showed a E' value about 2.4 MPa, whereas the nanocomposites exhibited an improved viscoelastic behavior. E' was

increased from 2.4 MPa for the reference polymer to 2.8 and 4.9 MPa for the nanocomposites containing 2 wt% of LDH and CNT fillers, respectively. On the other hand, the 2 wt% iPP/CNT-LDH nanocomposites showed E' value about 4.45 MPa, which is lower than that of 2 wt% iPP/CNT-LDH nanocomposites. The improved E' of the nanocomposites is mainly attributed to the reinforcing effect of the homogenously dispersed rigid filler, and enhanced % of crystallinity. The change in the melting enthalpy (ΔH_m) between the polymer and nanocomposites (Table 5.1.) was considerably small, and hence the effect of the percentage of crystallinity can be neglected. Thus the reinforcing effect of fillers helps only in improving the E' of the iPP. Here it is important to point out that the nanocomposites exhibited different E' values, although filler amount was similar. Among the fillers used, the CNT was found to alter the viscoelastic properties considerably, which is followed by CNT-LDH and LDH. These differences in the E' among the nanocomposites are possibly due to the variation in the specific surface area of the filler and the interaction forces between the matrix and the filler.[42, 44]

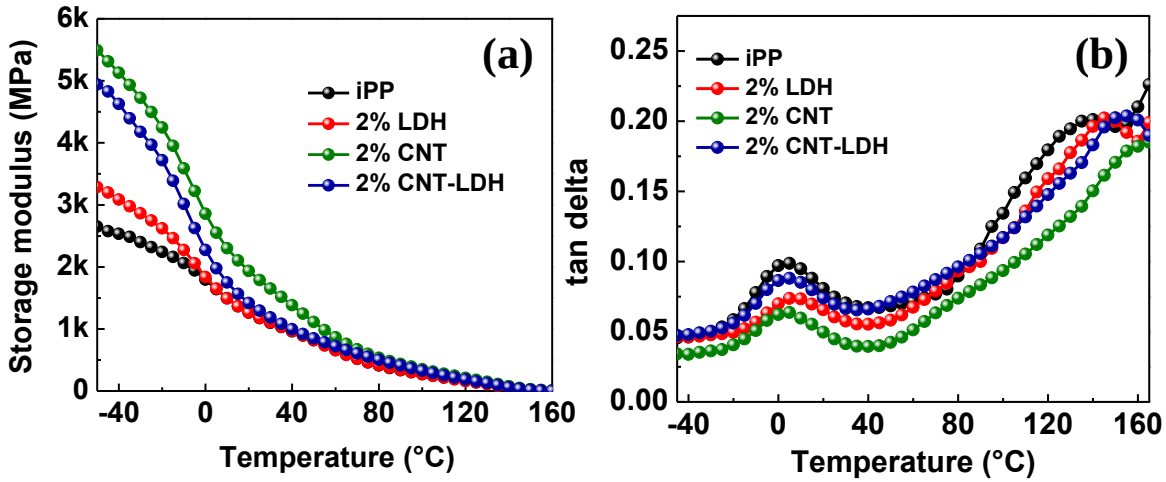

Figure 5.5. Temperature-dependent dynamic mechanical properties (a) storage modulus (E') and (b) tan δ curves for the polymer nanocomposites containing different fillers.

Temperature-dependent tan δ curves are shown in Figure 5.5b, which can give the information about the damping ability and molecular relaxations in the semicrystalline polymers. We detected two major molecular relaxations in the temperature range -50 to 160 °C. The lower temperature maximum in the tan δ curve is

corresponding to the amorphous phase relaxation, that is T_g of the polymer. Both the neat polymer and nanocomposites exhibit T_g in the range 5.5-7.5 °C (Table 5.1.). The difference in the T_g among the samples is considerably small or negligible. It indicates that the incorporated filler did not modify the T_g of the polypropylene. Another molecular relaxation was noticed slightly above the T_g, which appears as a broad mechanical relaxation extending from 80 to 140 °C. The higher temperature second order relaxation in PP matrix is generally ascribed to the damping within the crystalline lamellae. Normally, the height and area of the tan δ curve represent both reinforcing and filler-matrix interactions strength. Nanocomposites exhibit less intense tan δ curve compared to the pristine polymer, which might be due to the interfacial interactions between the matrix and filler. The dispersed rigid fillers completely restrict the polymer chain motion, leading to the lowering of the damping characteristics.

5.3.3.3. Thermal and Flammability Properties

The TGA measurements were performed under nitrogen atmosphere to understand the thermal stability and residual charring behavior of iPP, in the presence of CNT, LDH and CNT-LDH filler. Figure 5.6 shows the TGA thermograms obtained for various samples. The 50% mass loss temperatures ($T_{0.5}$) are presented in Table 5.2. The $T_{0.5}$ value obtained for the neat polymer was around 410 °C. However, upon incorporation of fillers, the thermal stability of the nanocomposites has been found to improve, irrespective of the filler type. Different fillers used in this study showed different $T_{0.5}$ values, although the filler loadings are same. The $T_{0.5}$ values obtained for neat iPP, iPP/2 wt% CNT and iPP/2 wt% LDH nanocomposites are 410 °C, 432 °C, and 442 °C, respectively. On the other hand, the nanocomposites with 2 wt% hierarchical CNT-LDH filler showed an improved $T_{0.5}$ value of around 454 °C.

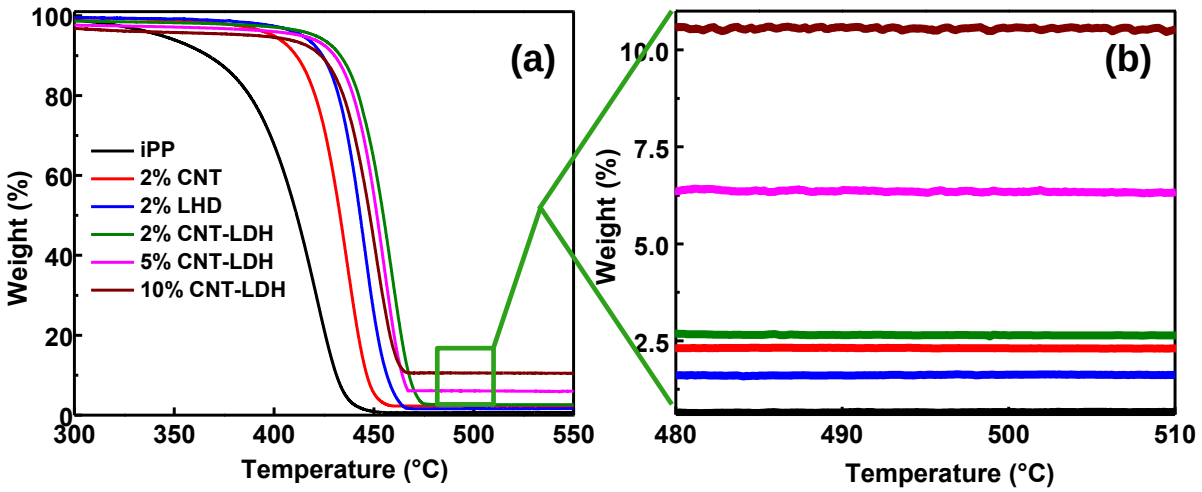

Figure 5.6. (a) TGA thermograms of iPP and its nanocomposites containing different fillers and filler loadings and (b) the enlarged thermograms in the high-temperature region (480-510 °C).

Table 5.2. Summary of the thermal stability ($T_{0.5}$), residual char (expected and observed) and LOI of the nanocomposites containing different fillers and filler loadings.

Samples	$T_{0.5}$ in °C (±3)	Residual char yields (%)		LOI (%) (±1)
		Expected	Observed (± 0.2)	
iPP	410	0	0	16.5
2 wt% iPP/LDH	442	1.5	1.62	17.0
2 wt% iPP/CNT	432	1.34	2.25	20.0
2 wt% iPP/LDH-CNT	454	1.6	2.66	20.0
5 wt% iPP/LDH-CNT	451	4	6.0	23.0
10 wt% iPP/LDH-CNT	448	8	10.6	26.0

However, not much further enhancement in the $T_{0.5}$ value was observed on increasing the filler loadings (5 wt% and 10 wt%). The improved thermal stability of the nanocomposites is mainly attributed to physical barrier effect of the filler, which restricts the polymer chain mobility and delays the rapid transfer of the gaseous products.[16, 43, 53, 54] Residual charring behavior of the nanocomposites and filler will be discussed in the later section.

The relative combustion behavior of nanocomposites was examined by microscale combustion calorimetry (MCC). The extracted parameters from the HRR curve (Figure 5.7.) are given in Table 5.3.[18, 37, 55-57] As expected, the neat iPP was found to show maximum PHRR, 1435 W/g. It is considered that larger PHRR value directs that the neat iPP is highly flammable in nature. However, after the incorporation of a small amount of filler, the PHRR values are considerably reduced, which again decreases with the increase in the filler loadings. At 1 wt% filler loading, the PHRR was reduced from 1435 W/g to 1322 and 900 W/g for the LDH (7.8 %) and CNT (37.28 %) nanocomposites, respectively. On the other hand, the composite containing 1 wt% hierarchical CNT-LDH showed the least PHRR value, i.e., 776 W/g (45.9%). The HRR value of iPP can be decreased further by increasing the amount of the filler. Nevertheless, unpredictable flame-retardancy behavior was noticed with the CNT incorporated nanocomposites. The PHRR of 2 wt% CNT nanocomposites was slightly increased from 900 W/g (37.28 %) for 1 wt% CNT nanocomposites to 988 W/g (30.45 %). Inconsistent flammability behaviors were observed only in the case of iPP/CNT nanocomposites with larger CNT loading, which can be ascribed to the rapid increase in thermal conductivity (Figure 5.8b.).[3, 16, 54] Kashiwagi et al. also observed similar flammability behavior, which they explained based on the relation between the flammability behavior and thermal conductivity of a series of nanocomposites containing different carbon nanomaterials.[3, 16, 53] Where in case of LDH and CNT-LDH reinforced nanocomposites as follows with respect to the filler concentration, which was shown 1160 w/g (19.16 %) and 580 w/g (59.58 %) reduction in PHRR for 2 wt% LDH and 2 wt% CNT-LDH nanocomposites, respectively. The larger PHRR reduction was observed in the presence of the CNT-LDH hybrids. Other flammability parameters such as HRC, THR, HRC, and T_{-max} were also measured (Table 5.3), which followed the similar trend like the PHRR results.

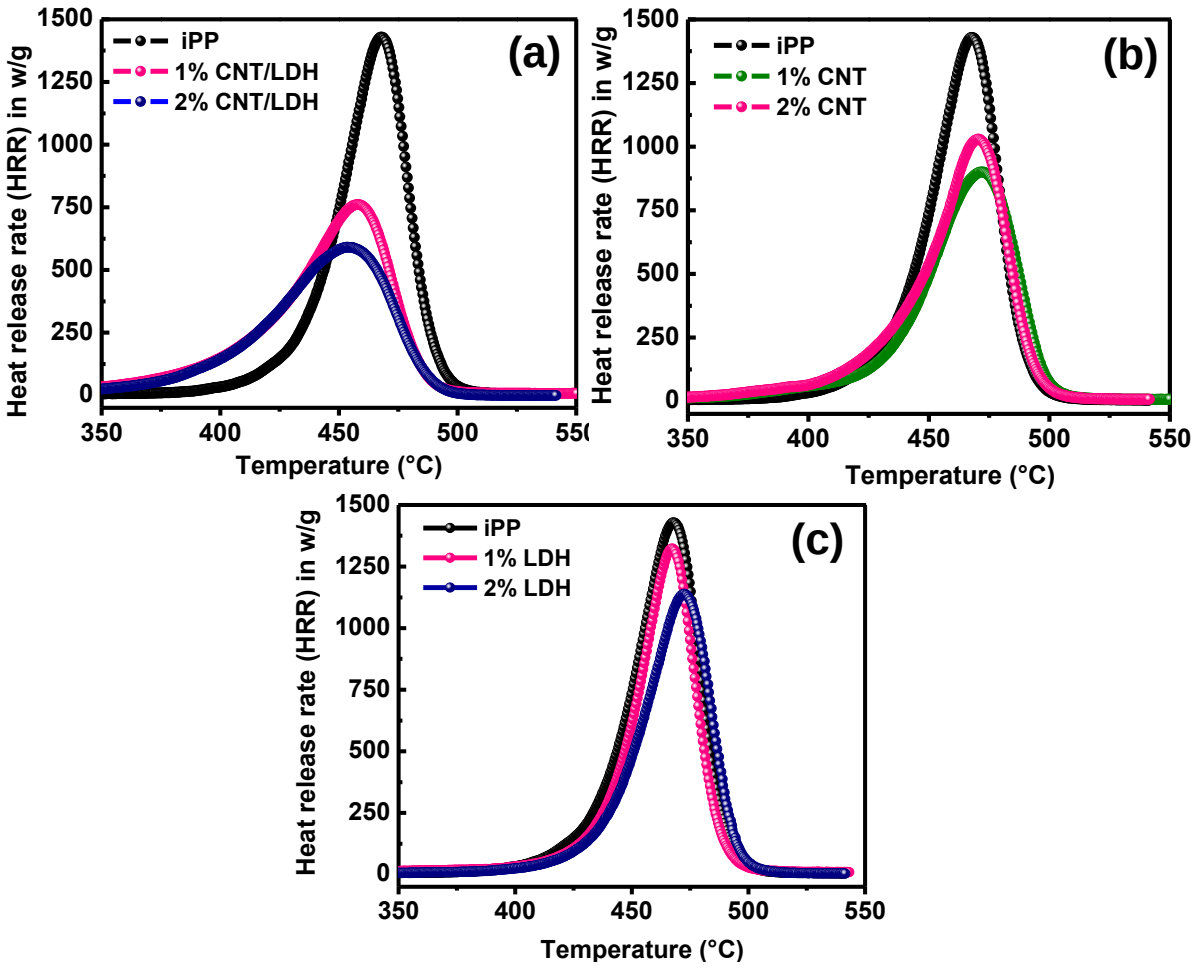

Figure 5.7. Heat release rate curves obtained for (a) iPP/CNT-LDH (b) iPP/CNT and (c) iPP/LDH nanocomposites with different filler concentration.

The standard LOI test was performed further to understand the flame-retardancy of the nanocomposites. It is a widely used technique to estimate the fire-hazardous nature of the polymer in bulk scale.[18, 23, 24, 58, 59] The obtained LOI values are presented in Table 5.2. The reference iPP sample exhibited the lowest value ~ 16.5 %, and hence it comes under the highly flammable material.[60, 61 53] On the other hand, the nanocomposites showed an improved LOI, and the largest value was observed for the 10 wt% CNT-LDH reinforced nanocomposites (~26 %). The improved LOI is mainly ascribed to the enhanced flame-retardancy of the nanocomposites, which is in good agreement with the MCC experimental data.

5.3.3.4. Flame-Retardant Mechanism

Flame-retardant behavior of the nanocomposites is mainly explained by three different mechanisms; the gas phase, endothermic, and char induced (intumescent) flame-retardancy.[18, 21, 28] The endothermic and char induced flame-retardancy mechanisms are applicable mainly in the condensed phase, and are the important mechanisms taking place in numerous flame-retardant nanofillers, such as CNT, graphene, layered silicate, LDH, and polyhedral silsesquioxanes (POSS).[3, 21, 28, 36, 53, 62]

Table 5.3. Flammability parameters of iPP and its nanocomposites obtained from MCC test.

Sample	PHRR in (W/g) (±20)	% of reduction in HRR	THR in kJ/g (± 0. 5)	T_{-max} in (°C) (±2)	HRC in (J/g.k) (±20)
iPP	1435	-	54.0	468	1460
1 wt% iPP/LDH	1322	7.8	53.1	467.5	1356
2 wt% iPP/LDH	1160	19.16	51.36	472.5	1146
1 wt% iPP/CNT	900	37.28	46.52	472	923
2 wt% iPP/CNT	988	30.45	47.77	470.5	969
1 wt% iPP/CNT-LDH	776	45.92	45.48	464	803
2 wt% iPP/CNT-LDH	580	59.58	43.62	461	616

The LDH and CNT fillers come under the endothermic and intumescent flame-retardant material, respectively.[18, 28, 37] In the current investigation, although the filler loadings are same, significant difference in the flame-retardancy order was observed. The hierarchical CNT-LDH containing nanocomposites showed the better flame-retardancy even with a small filler loading (2 wt%). The residual charring behavior and physical barrier effect are some of the key aspects of an efficient flame-retardant nanocomposite.[3, 18, 28, 37, 63] In addition, other supporting parameters including filler network and dispersion state in the polymer matrix, filler thermal stability and poor thermal conductivity are also important in a low fire hazardous polymer nanocomposites.[3, 16, 18, 29, 30, 64] In the present work, the residual charring behavior of the nanocomposites was investigated (Table 5.2). The estimated char yields were

calculated by considering the residual char yield of neat filler (Figure 5.8a), and the observed values were directly obtained from the TGA thermogram of the nanocomposites (Figure 5.6b). From Table 5.2, it is clear that the no residue was left for the reference iPP, whereas their corresponding nanocomposite yielded residual char. The observed residual char amounts were larger than the expected one, on the basis of the filler loading.

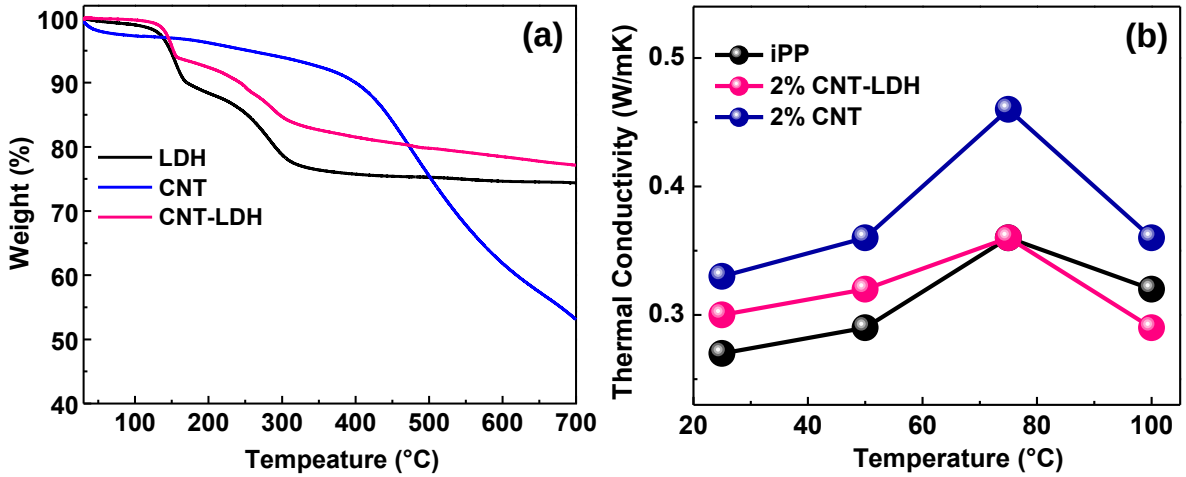

Figure 5.8. (a) TGA thermogram for neat fillers and (b) thermal conductivity results obtained for iPP and its nanocomposites.

The char yield was found to increase with the increase in the filler concentration and can be attributed to the dispersed filler jammed network structure (Figure 5.3b), which mainly initiates the residual carbon char formation during the combustion process.[3, 53, 54] Here it is important to note that with same amounts of filler loading (2 wt%), the nanocomposites with different filler exhibited different char yields. The hierarchical CNT-LDH filler containing nanocomposites showed the larger residual char compared to the iPP/CNT, which is followed by iPP/LDH nanocomposites. The formation of residual char followed the same order (iPP/CNT-LDH>iPP/CNT>iPP/LDH>iPP nanocomposites) as that of the flame-retardancy and thermal stability. Therefore, residual charring behavior is the key parameter to reduce the flammability of the nanocomposites, and the flame-retardancy efficiency differs with respect to the char amounts or residual char yield of the filler.[3, 18, 30, 36, 37, 63] In the combustion process the residual char act as a thin protective layer over the sample surface and hinders the rapid transfer of heat, flammable gases and oxygen, which

reduces the flammability of the nanocomposites.[3, 18, 28, 30, 53] In addition to the residual charring behavior, other supporting parameters (Figure 5.8) such as filler thermal history, poor thermal conductivity and filler distribution states cooperatively helped the hierarchical iPP/CNT-LDH nanocomposites to attain better flame-retardant properties compared to the individual filler reinforced nanocomposites (iPP/CNT and iPP/LDH). This whole process followed the condensed phase flame-retardancy mechanism.[3, 28]

5.4. Conclusions

In summary, LDH, CNT and CNT-LDH were incorporated with iPP using a solution blending method to prepare highly dispersed polymer nanocomposites. Through a systematic examination, we found that the CNT dispersed nanocomposites exhibited superior nucleation and temperature-dependent viscoelastic behavior, over the LDH and CNT-LDH filled nanocomposites. Unlike those two physical characteristics (nucleation and dynamic mechanical performance), the hierarchical CNT-LDH filled polymer nanocomposites showed improved flame-retardancy and thermal degradation behavior, even with a small fraction the filler. Upon addition of the 2 wt% CNT-LDH filler, thermal degradation stability (44 °C) and flame-retardancy (59%) of the iPP has been improved considerably compared to the CNT and LDH reinforced nanocomposites. The LOI values also enhanced significantly, and the maximum improvement was observed for the 10 wt% iPP/CNT-LDH nanocomposites (~26 %). The synergistic effect of CNT and LDH helps in improving the thermal stability and flame-retardancy of the hierarchical iPP/CNT-LDH nanocomposites. The formed hierarchical CNT-LDH jammed networks in polymer matrix act like an effective catalyst to generate larger amounts of residual carbon char and it forms a protecting layer over the surface. This protecting layer helps in delaying the heat and flammable gas release and thus makes the iPP/CNT-LDH nanocomposite a potential flame-retardant and thermally stable material.

5.5. Experimental Description

Materials: IPP (M_w ~120000, $Đ$ ~4.5) used in the current study was kindly supplied by Idemitsu Petrochemical Co., Ltd. Japan. $Al(NO_3)_3 \cdot 9H_2O$, $Co(NO_3)_2 \cdot 6H_2O$, $Zn(NO_3)_2 \cdot 6H_2O$ metal salts and multiwall carbon nanotubes (MWCNT) were obtained from Sigma Aldrich Co. Ltd. Other chemicals (reagents and solvents) such as nitric acid (HNO_3), sulfuric acid (H_2SO_4), potassium permanganate ($KMnO_4$), urea, xylene, ethanol, and acetone were purchased from Merck Co., Ltd. India.

Synthesis of Co-Zn-Al LDH: The Co-Zn-Al LDH with the metal ratio 1:1:1 was synthesized using the procedure adopted in chapter-4.

Functionalization of MWCNT: Modified Hummers method was used for the functionalization of MWCNTs.[39] In this method, 15 g of the MWCNTs and 12 ml of concentrated H_2SO_4 was added to a 250 ml round-bottom flask. The resulting mixture was stirred continuously for 24 h at room temperature, after that the solution temperature was raised to 40 °C. During the addition of 175 mg of $NaNO_3$ and 0.5 g of $KMnO_4$, the reaction temperature was maintained below 45 °C. Later the solution temperature was raised to 40 °C and kept for 30 min with continuous stirring. Subsequently, 40 ml of water was added slowly to the flask using a dropper. After 15 minutes, the flask was removed from the oil bath, and 70 ml of water and 5 ml of 30% H_2O_2 were added at the end of the reaction. The functionalized MWCNT was collected by passing through a nylon membrane and the resultant functionalized MWCNT were repeatedly washed with 5% HCl solution and distilled water. Finally, sample was collected and dried in vacuum oven at 80 °C for 24 h.

Synthesis of Nanocomposites: The polypropylene nanocomposite with different filler concentration was prepared by solution blending approach. For 2 wt% iPP/LDH-CNT nanocomposites, initially, 0.02 g of acetone washed 0.01g LDH, and 0.01g MWCNT was taken into a two necked round bottom flask consisting of 100 ml xylene solvent and subsequently sonicated for four days in a bath sonicator. To the sonicated solution 0.9800 g of iPP was added and then refluxed at 150 °C for 24 h. Finally, the polymer solution was reprecipitated from ethanol. The precipitate was collected by vacuum filtration and dried under vacuum at 100 °C for 24 h. The remaining nanocomposites (2

wt% iPP/LDH and 2 wt% iPP/CNT) and the pure polymer were also prepared by following the same process.

5.6. Characterization

The morphology of prepared LDH and CNT were analyzed using TEM (JEOL 2010 operating at 300 kV) and SEM as discussed in the previous chapters.

DSC measurements were performed using a TA Q2000 DSC apparatus. All the measurements were carried out under the nitrogen atmosphere. For measuring the crystallization half-time ($t_{1/2}$), the molten samples were rapidly cooled from the melt to the desired crystallization temperature (130 °C) at a faster cooling rate of 100 °C/min, and the samples allowed to crystallize at that temperature. The non-isothermal crystallization data were collected while cooling the samples from the melt to room temperature at 10 °C/min cooling rate. Those samples were again reheated to 200 °C for understanding the melting behavior. DMA (TA Instruments Model Q800) was used to study the temperature-dependent dynamic mechanical properties of the samples as discussed in the previous chapter. Thermal stability of the prepared nanocomposites were analyzed with the help of thermo gravimetric analysis TA Q50 instrument.

Microscale combustion calorimetry (MCC-1, FTT) experiments were performed using the same procedure as explained in chapter 4.

The limiting oxygen index (LOI) values were measured by digital oxygen index analyzer (Fire Testing Technology, UK) according to ASTM D2863-97. The specimens with the dimension 10 cm × 1 cm × 0.2 cm were used for the test.

5.7. References

1 N. G. Sahoo, S. Rana, J. W. Cho, L. Li and S. H. Chan, *Prog Polym Sci* **35:**837-867 (2010).

2 H. Kim, A. A. Abdala and C. W. Macosko, *Macromolecules* **43:**6515-6530 (2010).

3 T. Kashiwagi, F. Du, J. F. Douglas, K. I. Winey, R. H. Harris and J. R. Shields, *Nat Mater* **4:**928-933 (2005).

4 J. N. Coleman, M. Lotya, A. O'Neill, S. D. Bergin, P. J. King, U. Khan, et al., *Science* **331:**568-571 (2011).

5 J.-Z. Xu, G.-J. Zhong, B. S. Hsiao, Q. Fu and Z.-M. Li, *Prog Polym Sci* **39:**555-593 (2014).

6 W. D. Zhang, I. Y. Phang and T. X. Liu, *Adv Mater (Weinheim, Ger)* **18:**73-77 (2006).

7 S. Iijima, *Nature* **354:**56-58 (1991).

8 S. Iijima and T. Ichihashi, *Nature* **363:**603-605 (1993).

9 M. Naffakh, A. M. Díez-Pascual, C. Marco, G. J. Ellis and M. A. Gómez-Fatou, *Prog Polym Sci* **38:**1163-1231 (2013).

10 S. K. Kumar, B. C. Benicewicz, R. A. Vaia and K. I. Winey, *Macromolecules* **50:**714-731 (2017).

11 Y.-H. Chen, G.-J. Zhong, J. Lei, Z.-M. Li and B. S. Hsiao, *Macromolecules* **44:**8080-8092 (2011).

12 S. B. Kharchenko, J. F. Douglas, J. Obrzut, E. A. Grulke and K. B. Migler, *Nat Mater* **3:**564-568 (2004).

13 M.-Q. Zhao, Q. Zhang, X.-L. Jia, J.-Q. Huang, Y.-H. Zhang and F. Wei, *Adv Funct Mater* **20:**677-685 (2010).

14 M. C. García-Gutiérrez, J. J. Hernández, A. Nogales, P. Panine, D. R. Rueda and T. A. Ezquerra, *Macromolecules* **41:**844-851 (2008).

15 P. Liu, K. L. White, H. Sugiyama, J. Xi, T. Higuchi, T. Hoshino, R. Ishige, H. Jinnai, A. Takahara and H.-J. Sue, *Macromolecules* **46:**463-473 (2013).

16 T. Kashiwagi, E. Grulke, J. Hilding, K. Groth, R. Harris, K. Butler, J. Shields, S. Kharchenko and J. Douglas, *Polymer* **45:**4227-4239 (2004).

17 D. Baoxian and F. Zhengping, *Nanotechnology* **21:**315603 (2010).

18 Y. Gao, J. Wu, Q. Wang, C. A. Wilkie and D. O'Hare, *J Mater Chem A* **2:**10996-11016 (2014).

19 D.-Y. Wang, A. Das, A. Leuteritz, R. N. Mahaling, D. Jehnichen, U. Wagenknecht and G. Heinrich, *RSC Adv* **2:**3927-3933 (2012).

20 F. Leroux, M. Adachi-Pagano, M. Intissar, S. Chauviere, C. Forano and J.-P. Besse, *J Mater Chem* **11:**105-112 (2001).

21 Z. Matusinovic and C. A. Wilkie, *J Mater Chem* **22:**18701-18704 (2012).

22 D. Basu, A. Das, K. W. Stöckelhuber, U. Wagenknecht and G. Heinrich, *Prog Polym Sci* **39:**594-626 (2014).

23 X. Wang, Y. Sporer, A. Leuteritz, I. Kuehnert, U. Wagenknecht, G. Heinrich and D.-Y. Wang, *RSC Adv* **5:**78979-78985 (2015).

24 E. N. Kalali, X. Wang and D.-Y. Wang, *J Mater Chem A* **3:**6819-6826 (2015).

25 J.-H. Yang, W. Zhang, H. Ryu, J.-H. Lee, D.-H. Park, J. Y. Choi, A. Vinu, A. A. Elzatahry and J.-H. Choy, *J Mater Chem A* **3:**22730-22738 (2015).

26 L. Qiu, Y. Gao, X. Yan, J. Guo, A. Umar, Z. Guo and Q. Wang, *RSC Adv* **5:**51900-51911 (2015).

27 Q. Wang, X. Zhang, J. Zhu, Z. Guo and D. O'Hare, *Chem Commun* **48:**7450-7452 (2012).

28 A. B. Morgan and J. W. Gilman, *Fire Mater* **37:**259-279 (2013).

29 B. Nagendra, C. V. S. Rosely, A. Leuteritz, U. Reuter and E. B. Gowd, *ACS Omega* **2:**20-31 (2017).

30 X. Wang, S. Zhou, W. Xing, B. Yu, X. Feng, L. Song and Y. Hu, *J Mater Chem A* **1:**4383-4390 (2013).

31 S. Pack, T. Kashiwagi, D. Stemp, J. Koo, M. Si, J. C. Sokolov and M. H. Rafailovich, *Macromolecules* **42:**6698-6709 (2009).

32 A. Edenharter, P. Feicht, B. Diar-Bakerly, G. Beyer and J. Breu, *Polymer* **91:**41-49 (2016).

33 S.-D. Jiang, Z.-M. Bai, G. Tang, L. Song, A. A. Stec, T. R. Hull, Y. Hu and W.-Z. Hu, *ACS Appl Mater Interfaces* **6:**14076-14086 (2014).

34 C. Zhang, W. W. Tjiu, T. Liu, W. Y. Lui, I. Y. Phang and W.-D. Zhang, *J Phys Chem B* **115:**3392-3399 (2011).

35 S. Peeterbroeck, M. Alexandre, J. B. Nagy, C. Pirlot, A. Fonseca, N. Moreau, G. Philippin, J. Delhalle, Z. Mekhalif, R. Sporken, G. Beyer and P. Dubois, *Compos Sci Technol* **64:**2317-2323 (2004).

36 G. Beyer, *Fire Mater* **29:**61-69 (2005).

37 Y. Gao, Y. Zhang, G. R. Williams, D. O'Hare and Q. Wang**6:**35502 (2016).

38 B. Nagendra, K. Mohan and E. Bhoje Gowd, *ACS Appl Mater Interfaces* **7:**12399-12410 (2015).

39 D. C. Marcano, D. V. Kosynkin, J. M. Berlin, A. Sinitskii, Z. Sun, A. Slesarev, L. B. Alemany, W. Lu and J. M. Tour, *ACS Nano* **4:**4806-4814 (2010).

40 S. Huang, H. Peng, W. W. Tjiu, Z. Yang, H. Zhu, T. Tang and T. Liu, *J Phys Chem B* **114:**16766-16772 (2010).

41 A. T. Jones, J. M. Aizlewood and D. R. Beckett, *Makromol Chem* **75:**134-158 (1964).

42 H. E. Miltner, N. Grossiord, K. Lu, J. Loos, C. E. Koning and B. Van Mele, *Macromolecules* **41:**5753-5762 (2008).

43 B. Nagendra, K. Mohan and E. B. Gowd, *ACS Appl Mater Interfaces* **7:**12399-12410 (2015).

44 J.-Z. Xu, C. Chen, Y. Wang, H. Tang, Z.-M. Li and B. S. Hsiao, *Macromolecules* **44:**2808-2818 (2011).

45 M. Naffakh, C. Marco and G. Ellis, *J Phys Chem B* **115:**10836-10843 (2011).

46 E. Piorkowska and G. C. Rutledge, *Handbook of Polymer Crystallization*, Wiley (2013).

47 P. S. Dai, P. Cebe, M. Capel, R. G. Alamo and L. Mandelkern, *Macromolecules* **36:**4042-4050 (2003).

48 R. G. Alamo, B. D. Viers and L. Mandelkern, *Macromolecules* **28:**3205-3213 (1995).

49 M. Gahleitner, *Prog Polym Sci* **26:**895-944 (2001).

50 B. Chen, J. R. G. Evans, H. C. Greenwell, P. Boulet, P. V. Coveney, A. A. Bowden and A. Whiting, *Chem Soc Rev* **37:**568-594 (2008).

51 A. M. Díez-Pascual and M. Naffakh, *ACS Appl Mater Interfaces* **5:**9691-9700 (2013).

52 M. Naffakh, M. Remskar, C. Marco, M. A. Gomez-Fatou and I. Jimenez, *J Mater Chem* **21:**3574-3578 (2011).

53 X. Wang, E. N. Kalali, J.-T. Wan and D.-Y. Wang, *Prog Polym Sci* **69:**22-46 (2017).

54 T. Kashiwagi, E. Grulke, J. Hilding, R. Harris, W. Awad and J. Douglas, *Macromol Rapid Commun* **23:**761-765 (2002).

55 D.-Y. Wang, A. Das, F. R. Costa, A. Leuteritz, Y.-Z. Wang, U. Wagenknecht and G. Heinrich, *Langmuir* **26:**14162-14169 (2010).

56 Y. Gao, Q. Wang, J. Wang, L. Huang, X. Yan, X. Zhang, Q. He, Z. Xing and Z. Guo, *ACS Appl Mater Interfaces* **6:**5094-5104 (2014).

57 P.-J. Wang, X.-P. Hu, D.-J. Liao, Y. Wen, T. R. Hull, F. Miao and Q.-T. Zhang, *Ind Eng Chem Res* **56:**920-932 (2017).

58 C. Huggett, *Fire Mater* **4:**61-65 (1980).

59 M. L. Janssens, *Fire Technology* **27:**234-249 (1991).

60 S. Zhang and A. R. Horrocks, *Prog Polym Sci* **28:**1517-1538 (2003).

61 A. Dasari, Z.-Z. Yu, G.-P. Cai and Y.-W. Mai, *Prog Polym Sci* **38:**1357-1387 (2013).

62 P. Kiliaris and C. D. Papaspyrides, *Prog Polym Sci* **35:**902-958 (2010).

63 J. Zhang, Q. Kong, L. Yang and D.-Y. Wang, *Green Chem* **18:**3066-3074 (2016).

64 S. Jiang, Z. Gui, G. Chen, D. Liang and J. Alam, *ACS Appl Mater Interfaces* **7:**14603-14613 (2015).

Chapter-6

Conclusions and Future Perspectives

The following general questions were addressed to understand the relationship between structure, morphology, and physical characteristics of the polymer nanocomposites. What are the thermodynamic driving forces that direct intercalation/exfoliation of LDH? How would lateral dimensions of the fillers affect the properties of the resultant polymer nanocomposites? Do the intralayer metal constituents of LDH modify the composite's properties? We tried to address some of these questions with the support of experimental evidence in this thesis.

The key findings and conclusions of the present thesis are summarized below.

In order to understand the thermodynamic driving forces that direct intercalation/exfoliation of LDH, we have developed two different methods for the delamination and the lateral size reduction of LDH. In the first method, we used sonication-assisted delamination of LDH to prepare stable dispersions of smaller-sized LDH nanoparticles in non-polar solvents (~50–200 nm). In the second method, we developed a new approach to obtain the nanodots of delaminated LDH sheets without the aid of longer sonication. To the best of our knowledge, it is for the first time, the delaminated LDH with lateral dimensions as low as 10-30 nm and featured a thickness of ~1 nm were obtained. In both these methods, the solvents used for the dispersion of LDH played a crucial role in removing the intercalated water molecules and in the second case, the anion exchange was also taken place. This has resulted in the weakening of the strong electrostatic interactions between the LDH layers to obtain the delaminated sheets. LDH sheets thus obtained were used for synthesizing highly dispersed iPP nanocomposites with different loadings from 1 to 10 wt % using a modified solvent mixing method. Furthermore, we systematically compared the influence of the lateral size of LDH on the hierarchical structure and properties of iPP.

Conclusions:

In chapters 2 & 3, we systematically investigated how the lateral size of LDH particles would affect the properties of the polypropylene. In the first study, highly exfoliated iPP nanocomposites were synthesized by the modified solvent mixing method using two different sized Mg-Al LDH (nano and μm-sized LDH) nanoparticles. It was observed that sonicated LDH nanoparticles (nano LDH: ~50–200 nm) dramatically improve the thermal stability, nucleation ability and crystallization rate of iPP at very low LDH loadings compared to that of nanocomposites with larger LDH (μm-sized LDH) particles with the same concentration. This might be due to the high surface area of the smaller LDH nanoparticles and its better dispersibility within the polymer matrix. However, it was observed that the incorporation of LDH nanoparticles did not change the crystallization growth mechanism and crystal structure of iPP. Longer sonication of LDH is not economically viable, and it is difficult to obtain large quantities of exfoliated LDH by this method. To overcome this, a simple and single step approach has been developed for the simultaneous delamination and the lateral size reduction of LDH. Treatment of the as-prepared LDH with dilute acid led to the formation of delaminated LDH sheets with lateral dimensions as low as 10-30 nm (nanodot LDH) and featured a thickness of ~1 nm, with the same chemical composition. The effect of three different lateral-sized LDH (micro, nano and nanodot LDH) on the hierarchical structure and properties of iPP was systematically investigated. It was observed that the different-sized LDH particles have a significant effect on the nucleation ability, thermal stability and mechanical properties of iPP. Especially the incorporation of nanodot LDH showed a remarkable effect on spherulite size, lamellar thickness, crystal structure, crystallization rate, thermal stability, and mechanical behavior of iPP. The nucleation ability of iPP in the presence of nanodot LDH is the best compared to other iPP nanocomposites reported using LDH as fillers in the literature. Based on these two chapters, we may say that the surface area of nanofillers and dispersion state are key factors in determining the properties of polymer nanocomposites.

Another important feature of LDH is its flexibility in tuning the composition of inorganic layers. Influence of the intralayer metal composition on polymer properties was not systematically investigated in the literature. For that purpose, we prepared two-metal-LDH (Co-Al LDH and Zn-Al LDH) and three-metal-LDH (Co-Zn-Al LDH) and used them as nanofillers to prepare highly dispersed iPP nanocomposites using the same solution blending method. It was found that the incorporation of either two-metal-LDH or three-metal-LDH dramatically improves the crystallization rate and storage modulus of iPP. However, not much difference is observed in these properties with the type of LDH used for the preparation of nanocomposites. On the other hand, the kind of LDH could influence the thermal stability and flame retardant properties of iPP. When the filler loading was ~6 wt%, the $T_{0.5}$ and HRR values of the iPP nanocomposites containing three-metal-LDH (Co-Zn-Al LDH) were found to be significantly higher than that of the corresponding nanocomposites prepared using the two-metal-LDH (Co-Al LDH and Zn-Al LDH). This difference might be due to the better char formation capability of three-metal LDH compared to that of two-metal-LDH.

Carbon nanotubes are known to enhance the physical properties of polymers. An attempt was made here to study the effect of CNT/LDH hybrid filler on the physical properties of iPP and compared these results with iPP/LDH and iPP/CNT nanocomposites. We found that the CNT dispersed nanocomposites exhibited superior nucleation and temperature-dependent viscoelastic behavior, over the LDH and CNT-LDH filled nanocomposites. However, unlike those two physical characteristics (nucleation and dynamic mechanical performance), the hierarchical CNT-LDH filled polymer nanocomposites showed improved flame-retardancy and thermal degradation behavior, even with the addition of a small fraction of the filler. Upon adding 2 wt% CNT-LDH filler, thermal degradation stability (44 °C) and flame-retardancy (59%) of the iPP has been improved considerably compared to the CNT and LDH reinforced nanocomposites. The LOI values also enhanced significantly, and the maximum improvement was observed for the 10 wt% iPP/CNT-LDH nanocomposites (~26 %). The synergistic effect of CNT and LDH helps in improving

the thermal stability and flame-retardancy of the hierarchical iPP/CNT-LDH nanocomposites. The hierarchical CNT-LDH jammed networks formed in the polymer matrix act as an effective catalyst to generate larger amounts of residual carbon char and it forms a protecting layer over the surface. This protecting layer helps in delaying the heat and flammable gas release and thus makes the iPP/CNT-LDH nanocomposite a potential flame-retardant and thermally stable material.

Future Perspectives

The results obtained in this study provide an excellent scope for the further studies as discussed below.

- The prime focus of the current thesis was the investigation of the effect of different lateral sized LDH on some of the properties of iPP, such as crystallization and mechanical behavior. However, the effect of lateral size on the flame retardant behavior of iPP was not investigated. Prospectively, the influence of the different lateral sized LDH on flame retardancy would be interesting to investigate.
- In the present work, iPP nanocomposites were prepared using as-synthesized LDH and demonstrated that three-metal LDH showed better flame retardant behavior compared to the two-metal LDH. There is a large scope to investigate the synergistic effect of three-metal LDH with suitable organic species, which may help in improving the flame-retardancy of engineering plastics.
- Hybrids containing 2D layered materials within polymeric matrices have a great potential as functional nanocomposites for gas separation technologies. It will be interesting to investigate the barrier properties of the developed nanocomposite films.

PUBLICATIONS

(From Thesis)

1) **Baku Nagendra**, C.V.S. Rosely, A. Leuteritz, U. Reuter and E. Bhoje Gowd*- Polypropylene/Layered Double Hydroxide Nanocomposites: Influence of LDH Intralayer Metal Constituents on the Properties of Polypropylene.
   ACS Omega, 2, 20-31 (2017)
2) **Baku Nagendra**, A. Das, A. Leuteritz and E. Bhoje Gowd*. Structure and Crystallization behaviour of Syndiotactic Polystyrene/Layered Double Hydroxide Nanocomposites.
   Polymer International, 65, 299-307 (2016)
3) **Baku Nagendra**, K. Mohan and E. Bhoje Gowd* - Polypropylene/Layered Double Hydroxide (LDH) Nanocomposites: Influence of LDH Particle Size on the Crystallization Behavior of Polypropylene.
   ACS Applied Materials and Interfaces, 7, 12399-12410 (2015)
4) **Baku Nagendra**, A. M. Joseph and E. Bhoje Gowd*. Simultaneous Size Reduction and Delamination of Layered Double Hydroxides: The "Nanosize" Effect of LDH on Hierarchical Structure and Properties of Polypropylene. **(Under Submission)**
5) **Baku Nagendra**, A. M. Joseph and E. Bhoje Gowd*. Synergistic Effect of Layered Double Hydroxides and Multi-walled Carbon Nanotubes on the Properties of Polypropylene Nanocomposites. **(Under preparation)**
6) **Baku Nagendra** and E. Bhoje Gowd*. Biodegradable Polymer/Nano Layered Double Hydroxides (LDH) Hybrid Nanocomposites. **(Under preparation)**

List of Related Publications

7) A. M. Joseph, **Baku Nagendra**, E. Bhoje Gowd* and K.P. Surendran* - Screen-Printable Electronic Ink of Ultrathin Boron Nitride Nanosheets. ***(A.M.J. and B.N. contributed equally)***

ACS Omega, 1, 1220-1228 (2016)

8) A. M. Joseph, **Baku Nagendra**, K.P. Surendran* and E. Bhoje Gowd* - Syndiotactic Polystyrene/Hybrid Silica Spheres of POSS Siloxane Composites Exhibiting Ultralow Dielectric Constant.

ACS Applied Materials and Interfaces, 7, 19474-19483 (2015)

9) R.C. Jose, P. Shaiju, **Baku Nagendra** and E. Bhoje Gowd* – Influence of host preparation method on the structural phase transitions of syndiotactic polystyrene upon the guest exchange with *n*-alkanes.

Polymer 54, 6617-6627 (2013)

BEST POSTER AWARDS

1) **Baku Nagendra** and E. Bhoje Gowd – **National Seminar on Frontiers of Polymers and Advanced Materials (FPAM-2014)**, Department of Chemistry, University of Kerala, Thiruvananthapuram, India, November 05-07, 2014.
2) **Baku Nagendra** and E. Bhoje Gowd – **International Conference on Advanced Functional Materials (ICAFM-2014)**, CSIR-NIIST, Thiruvananthapuram, India, February 19-21, 2014.
3) **Baku Nagendra,** Sijla Rosely and E. Bhoje Gowd **- Polymer Conference for Young Researchers (PCYR-2015)**, Society for Polymer Science India, Thiruvananthapuram Chapter, Thiruvananthapuram, India, December 18, 2015.
4) Sijla Rosely, **Baku Nagendra** and E. Bhoje Gowd **– MRSI North East Symposium on Advanced Materials for Sustainable Applications,** Jorhat, India, February 18-20, 2016.